The Thesis Committee for Cody Jay Bills certifies that this is the approved version of the following thesis:

Deletions in SARS-CoV-2 nsp6 enhance antagonism of type-I interferon signaling

Committee:

Pei-Yong Shi, Ph.D. Supervisor

Andrew L. Routh, Ph.D. Chair

Petr G. Leiman, Ph.D.

Michelle Ward, Ph.D.

Jeffrey Wilusz, Ph.D.

Deletions in SARS-CoV-2 nsp6 enhance antagonism of type-I interferon signaling

by

Cody Jay Bills, B.S.

Thesis

Presented to the Faculty of the Graduate School of

The University of Texas Medical Branch

in Partial Fulfillment

of the Requirements

for the Degree of

Doctor of Philosophy

The University of Texas Medical Branch

March, 2023

Dedication

Dedicated to my incredible wife and children, for their love and support.

Acknowledgements

I would like to express tremendous gratitude to Pei-yong Shi for giving me a chance in his lab, for his patience as I learned, and for always being willing to discuss science with me; to Hongjie Xia for his technical expertise and assistance with difficult experiments; to Xuping Xie for supporting me with the HAE and animal experiments and working through the Nanostring data and especially for helpful discussions regarding interpretations of data and feasible follow-up experiments; to Jing Zou for her kindness, and Chaitanya Kurhade for discussions and insights on the data and conversations about career possibilities. Thank you to John Chen and Birte Kalveram for their tremendous efforts with animal experiments. Thank you to my committee for discussions and guiding me through the process. Thank you to my parents for teaching me good work ethic, dedication, and determination. Thank you most of all to my loving wife and daughters for their love, support, and patience as I spent countless hours away from home.

Deletions in SARS-CoV-2 nsp6 enhance antagonism of type-I interferon signaling

Publication No._____

Cody Jay Bills, B.S.

The University of Texas Medical Branch, 2023

Supervisor: Pei-Yong Shi

Severe acute respiratory syndrome coronavirus 2 (SARS-CoV-2) continues to evolve and adapt long after it first emerged in 2019. As the causative agent of the coronavirus disease 2019 (COVID-19), a tremendous effort has been made to understand the molecular pathogenesis of SARS-CoV-2. Recent research has identified nonstructural protein 6 (nsp6) as a major contributor to SARS-CoV-2 replication through the formation of replication organelles, antagonism of interferon type I (IFN-I) responses, and NLRP3 inflammasome activation, a major factor of severe COVID-19. Here, I review the most recent published findings regarding the multiple roles of nsp6 in promoting SARS-CoV-2 replication and investigate further the effect of variant nsp6 mutations in molecular pathogenesis of SARS-CoV-2, specifically the antagonism of IFN-I pathways. I demonstrate that a mutant SARS-CoV-2 USA/WA1-2020 (WA1) containing a nsp6 mutation (ΔSGF-WA1) seen in the Alpha (B.1.1.7) and Omicron sublineages (BA.2, BA.4, BA.5) is less susceptible to IFN-α treatment in African green monkey kidney epithelial cells expressing the human co-factor TMPRSS2 (Vero E6-TMPRSS2) compared to full-length WA1. Nsp6 mutations ΔSGF and ΔLSG, a similar deletion found in BA.1 nsp6, augment the ability of nsp6 to block phosphorylation of

STAT1 and STAT2 *in vitro* compared to WA1 nsp6, thereby suppressing the IFN-I signaling pathway. Furthermore, ΔSGF-WA1 infection of primary airway cultures secretes similar levels of infectious virus and viral RNA than WA1-infected cells but produces higher levels of intracellular viral RNA than WA1 and outcompetes parental WA1 in a competition experiment. Lastly, ΔSGF-WA1 infected mice have higher levels of viral RNA than WA1-infected mice and experience lower survival rates with a longer disease period. These data suggest that variants containing ΔSGF or ΔLSG mutations are more virulent and may cause more severe disease in COVID-19 patients.

TABLE OF CONTENTS

List of Figures

List of Abbreviations

ACE2	Angiotensin-converting enzyme 2
COVID-19	Coronavirus disease 2019
CPE	Cytopathic effect
CST	Cell Signaling Technology
CTD	C-terminal domain
DFCP1	Double FYVE-containing protein 1
DMEM	Dulbecco's modified Eagle's medium
DMVs	Double-membrane vesicles
Dpi	Days post-infection
ER	Endoplasmic reticulum
ERGIC	ER-to-Golgi intermediate compartment
FBS	Fetal bovine syndrome
GSBS	University of Texas Medical Branch
HEK293T	Human epithelial kidney cells 293T
hpi	Hours post-infection
HyPAS	Hybrid pre-autophagosomal structures
IFNAR	IFN alpha receptor
IFN-I	Interferon type-I
IL-1b	Interleukin-1 beta
IL-18	Interleukin-18
IRF3	Interferon regulatory factor 3
IRF9	Interferon regulatory factor 9
ISGs	Interferon stimulated genes
ISRE	Interferon stimulated regulatory element
JAK1	Janus kinase 1
LDs	Lipid droplets
M	Membrane
MHV	Mouse hepatitis virus
N	Nucleocapsid
NEB	New England Biolabs
NLRP3	NLR Family Pyrin Domain Containing 3
nsp6	Nonstructural protein 6
nsps	Nonstructural proteins
ORFs	Open reading frames
PI3K	Class III phosphatidylinositol 3-kinase
PI3P	Phosphatidylinositol 3-phosphate
P/S	Penicillin/streptomycin

PRRs	Pathogen recognition receptors
RNA	Ribonucleic acid
S	Spike
SARS-CoV	Severe Acute Respiratory Syndrome coronavirus
SARS-CoV-2	Severe Acute Respiratory Syndrome coronavirus 2
SIGMAR1	Sigma-1 receptor
STAT1 and STAT2	Signal transducer and activator of transcription proteins 1
TBK1	Tank-binding kinase 1
TDC	Thesis and Dissertation Coordinator
TMEM41B	Transmembrane Protein 41B)
TMPRSS2	Transmembrane protease, serine 2
TYK2	Tyrosine kinase 2
UTMB	University of Texas Medical Branch
VMP1	Vacuole Membrane Protein 1
WA1	SARS-CoV-2 2019-nCoV/USA_WA1/2020
WHO	World Health Organization
WRCEVA	World Reference Center for Emerging Viruses and Arboviruses
ΔSGF-WA1	SARS-CoV-2 with 106-108 deletion in nsp6
ΔLSG	Deletion of residues 105-107 found in nsp6
ΔSGF	Deletion residues 106-108 found in nsp6

Chapter 1: Introduction[1]

1.1 Abstract

Severe acute respiratory syndrome coronavirus 2 (SARS-CoV-2) continues to evolve and adapt after its emergence in late 2019. As the causative agent of the coronavirus disease 2019 (COVID-19), the replication and pathogenesis of SARS-CoV-2 have been extensively studied by the research community for vaccine and therapeutics development. Given the importance of viral spike protein in viral infection/transmission and vaccine development, the scientific community has thus far primarily focused on studying the structure, function, and evolution of the spike protein. Other viral proteins are understudied. To fill in this knowledge gap, a few recent studies have identified nonstructural protein 6 (nsp6) as a major contributor to SARS-CoV-2 replication through the formation of replication organelles, antagonism of interferon type I (IFN-I) responses, and NLRP3 inflammasome activation (a major factor of severe disease in COVID-19 patients). Here, we review the most recent progress on the multiple roles of nsp6 in modulating SARS-CoV-2 replication and pathogenesis.

Keywords: SARS-CoV-2, nsp6, interferon, replication, cytokine storm, pathogenesis

[1] This chapter is published: Bills, Cody, Xuping Xie, and Pei-Yong Shi. 2023. "The Multiple Roles of Nsp6 in the Molecular Pathogenesis of SARS-CoV-2." Antiviral Research 213 (May): 105590. https://doi.org/10.1016/J.ANTIVIRAL.2023.105590.

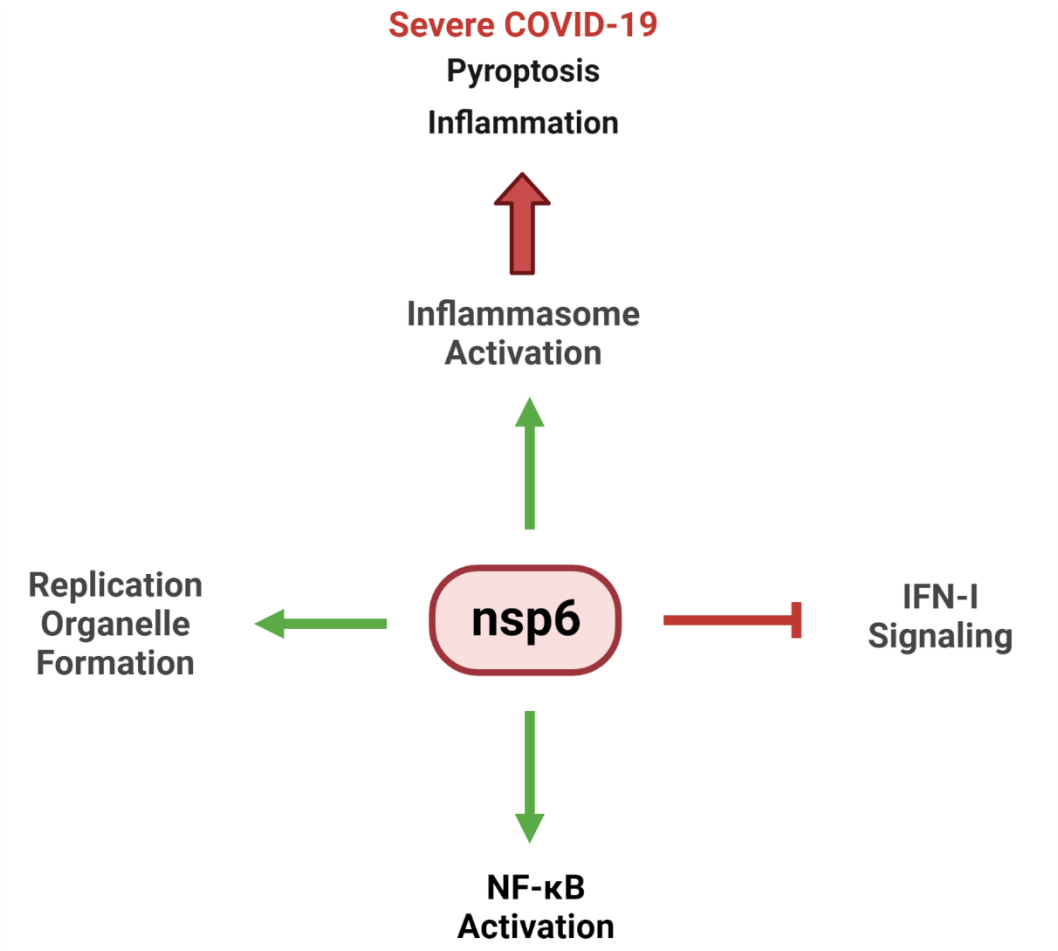

Figure 1: Graphical Abstract

1.2 BACKGROUND

Severe acute respiratory syndrome coronavirus 2 (SARS-CoV-2) emerged in Wuhan, China in late 2019 and quickly spread across the globe to become a major pandemic[1]. SARS-CoV-2 has continuously evolved to generate variants of concern (VoC) with altered viral transmissibility and immune evasion of vaccine- and/or infection-elicited immunity. Different VoCs have led to wave after wave of infections around the world. A large portion of SARS-CoV-2-related research has focused on the spike (S) protein due to its importance in infection and vaccines[2,3]. As a highly immunogenic viral factor, the S protein was an ideal vaccine target for the recently approved vaccines and for the development of effective therapeutic antibodies[2–6]. S protein, however, is just one of many viral factors that contribute to the molecular pathogenesis of SARS-CoV-2.

SARS-CoV-2 is an enveloped betacoronavirus containing a single-stranded positive-sense RNA genome[7]. Once the S protein binds to the host receptor angiotensin-converting enzyme 2 (ACE2), the virus can enter the cell by two methods: (i) via the endocytosis pathway whereupon the viral envelope may fuse with the endosomal membrane to release the viral genome into the cytoplasm, or (ii) via the proteolytic cleavage of the S protein by the host factor TMPRSS2, triggering fusion of the viral envelope with the plasma membrane and release of the viral genome directly into the cell (Fig. 1.1)[8]. The SARS-CoV-2 genome contains a 5' cap and a 3' polyadenylated tail that facilitate protein translation by host machinery without activating cellular immune sensors [9]. Two long open reading frames (ORFs) encoding polyproteins pp1a and pp1ab are co-translationally processed by viral proteases to make 16 individual nonstructural proteins (nsps), which together form the replication complex (Fig. 1.1)[9,10]. Additional ORFs encode 7 accessory

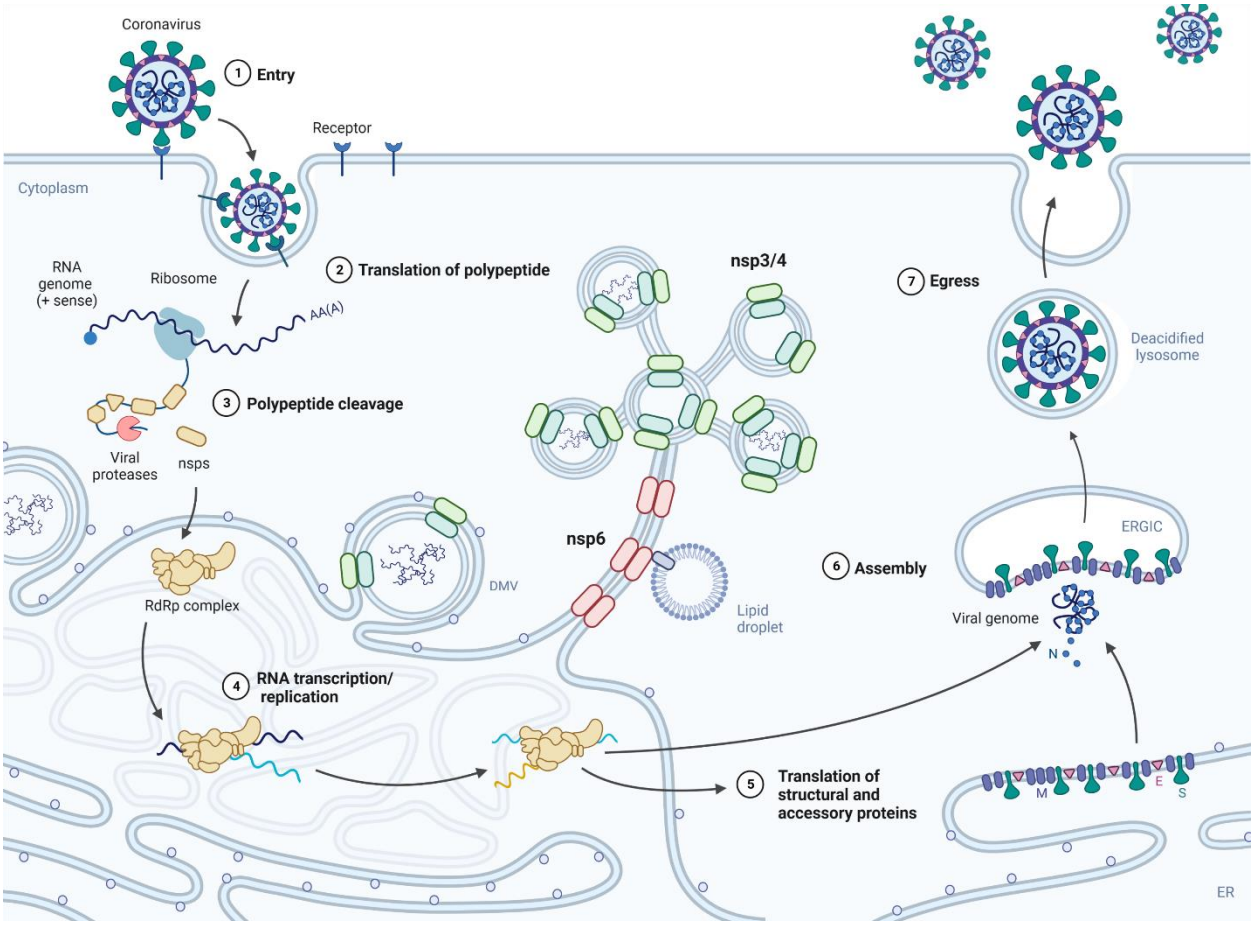

Figure 1.1: SARS-CoV-2 replication cycle

Schematic of the SARS-CoV-2 replication cycle. Upon entry the nonstructural proteins (nsps) are co-translationally cleaved by viral proteases to form the RNA-dependent RNA polymerase (RdRp) complex. Nsp6 proteins embedded in the ER membrane homodimerize to form linear zippered ER structures that connect with nsp3/nsp4 double membrane vesicles (DMVs) that shield nascent viral RNA (vRNA). Nsp6 recruit lipid droplets to replenish DMVs. Newly synthesized genomes are coated with nucleocapsid and are packaged into viral particles with spike (S), envelope (E), and membrane (M) proteins. Adapted from "Life Cycle of Coronavirus", by BioRender.com (2023). Retrieved from https://app.biorender.com/biorender-templates

proteins, thought to antagonize host immune responses[11], and 4 structural proteins that form the virus particle (Fig. 1.2)[10].

Replication of the viral genome occurs in double-membrane vesicles (DMVs) that originate from the endoplasmic reticulum (ER) to form replication organelles that protect nascent viral genomic RNA from pattern recognition receptors (PRRs) that might trigger an interferon response (Fig. 1.1)[12–14]. Translation of structural proteins at the ER begins the process of virion assembly (Fig. 1.1)[15,16]. Newly replicated viral genomes are coated with nucleocapsid (N) proteins that facilitate virion assembly with envelope I and membrane (M) proteins in the ER-to-Golgi intermediate compartment (ERGIC; Fig. 1.1)[17,18]. Finally, rather than egress through the conventional biosynthetic secretory exocytosis pathway like most other RNA viruses, betacoronaviruses including SARS-CoV-2 are released from the infected cell through the lysosomal pathway (Fig. 1.1)[19].

All nonstructural proteins are considered to have crucial roles in replication. While the molecular structure of nsp6 has yet to be solved[20,21], recent studies have suggested that nsp6 contributes to SARS-CoV-2 replication through a variety of mechanisms. Three major functions have been reported for nsp6: (i) It dimerizes to form replication organelles, (ii) it antagonizes host innate immune response by tampering with IFN-I signaling pathways, and (iii) it activates NOD-like receptor (NLR) Family Pyrin Domain Containing 3 (NLRP3) inflammasomes by impeding the acidification of lysosomes[22–25]. Here, we will review these processes and implications for nsp6 in SARS-CoV-2 molecular pathogenesis.

1.3 NSP6 STRUCTURE

Coronavirus nsp6 is a transmembrane protein with an approximate molecular weight of 34 kDa and localizes to the ER membrane and the perinuclear space[22,26–29]. Sequence comparisons show SARS-CoV-2 nsp6 shares 87% identity with SARS-CoV nsp6 (Fig. 1.2A). Alignment with

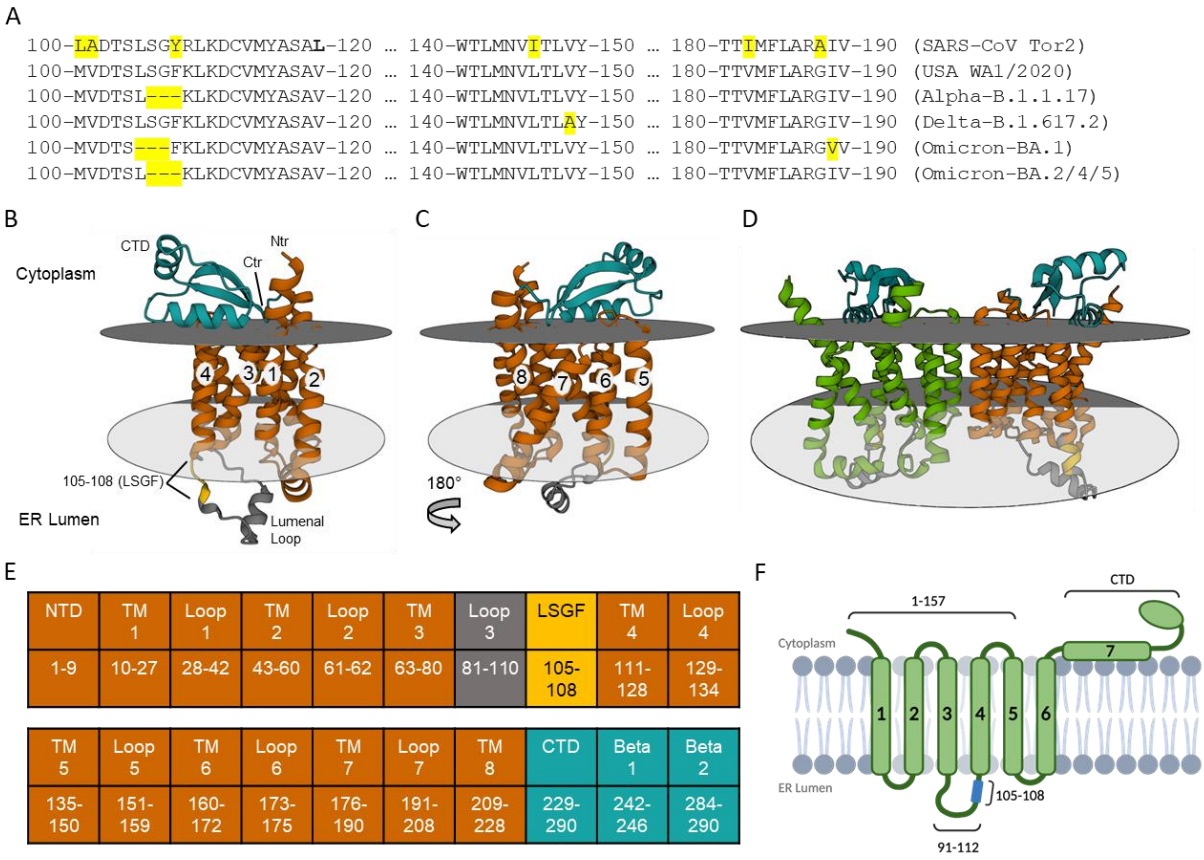

NTD	TM 1	Loop 1	TM 2	Loop 2	TM 3	Loop 3	LSGF	TM 4	Loop 4
1-9	10-27	28-42	43-60	61-62	63-80	81-110	105-108	111-128	129-134

TM 5	Loop 5	TM 6	Loop 6	TM 7	Loop 7	TM 8	CTD	Beta 1	Beta 2
135-150	151-159	160-172	173-175	176-190	191-208	209-228	229-290	242-246	284-290

Figure 1.2: Nsp6 structure and conserved ΔSGF

(A) Alignment of the variants of concern (VOCs) with the USA WA1/2020 strain, isolated from the first COVID-19 case in the USA. Beta, Gamma, Eta, Iota, and Lambda (not shown) are identical to Alpha. (B,C) nsp6 monomers and (D) dimer as predicted by the AI software AlphaFold; The lumenal loop (gray), C-terminal domain (CTD; teal), and the 105-108 region (yellow) are highlighted; gray discs represent membrane layers. (E) Amino acid sequence of nsp6 with secondary structures highlighted according to AlphaFold predictions in (B,C). (F) Schematic of nsp6 structure based on experimental evidence with numbered transmembrane domains and the 105-108 region highlighted (blue). (E-G) 3D structures presented with Mol* 3D. Schematic (F) Created with BioRender.

SARS-CoV-2 variants shows that a three amino-acid deletion (ΔSGF) is common to six previous SARS-CoV-2 variants [Alpha (B.1.1.7), Beta (B.1.351), Gamma (P.1), Eta (B.1.525), Iota (B.1.526), and Lambda (C.37)] (Fig. 1.2A)[30,31]. Phylogenetic analyses using Nextstrain reveal that ΔSGF emerged independently among these variants, suggesting a fitness advantage[22,32]. Separately, the Delta variant nsp6 contains a single unique amino acid change V149A. Interestingly, the initial Omicron BA.1 also contains a three amino-acid deletion (ΔLSG) along with a unique amino acid change (I189V), though the triple deletion is shifted to one amino acid upstream. Subsequent Omicron sublineages (BA.2, BA.4, and BA.5) instead contain the original ΔSGF deletion without additional changes (Fig. 1.2A). Because the shifted ΔLSG from the initial BA.1 was converged to ΔSGF in subsequent Omicron sublineages, it is reasonable to hypothesize that ΔSGF conveys a greater fitness advantage over ΔLSG. Whether V149A and I189V mutations contribute in any way to pathogenesis is unknown. Experiments are needed to test the above hypotheses.

The ΔSGF deletion has been demonstrated to be involved in both the formation of DMVs as well as antagonism of IFN-I signaling pathways and is located in the long lumenal loop (91-112; Fig. 1.2F)[22,23]. Structural simulations of the lumenal loop (91-112) suggest that it is disordered, but experimental evidence under different biological conditions shows that the loop shows partial helicity[33]. The lumenal loop (91-112) and C-terminal domain (CTD; 229-290) consist of clusters of multiple aromatic and charged amino acids that would likely drive protein-protein interactions[22].

Various predictive software have produced contradictory results: DeepTMHMM predicts 8 transmembrane domains and both N- and C-termini end in the cytoplasm, whereas Protter predicts 7 transmembrane domains with the N-terminus in the cytoplasm and the C-terminus in the lumen[34,35]. Both the N-terminal end and the highly conserved C-terminal end should be in the cytoplasm given that they must be proteolytically processed by the cytosolic protease, nsp5[20].

Structural predictions using the artificial intelligence program AlphaFold (DeepMind) yield interesting results[36]. In contrast to predictions by Protter, but in agreement with the DeepTMHMM software, AlphaFold predicts that SARS-CoV-2 nsp6 has 8 transmembrane domains (Fig. 1.2B, C)[34–36]. Accordingly, the N- and C-termini are in the cytoplasm and the structure contains a long lumenal loop (amino acids 91-112) and a structured C-terminal domain. The long lumenal loop, where ΔSGF and ΔLSG occurred in different SARS-CoV-2 variants, shows some degree of helicity and a few non-covalent interactions between the loop and the rest of the protein, suggesting that the loop is flexible to mediate protein-protein interactions. The CTD consists of 2 helices and 2 strands and shows some non-covalent interactions within the CTD and interactions between the CTD and other regions of the protein, suggesting that the CTD maintains a structure to mediate protein-protein interactions. Additionally, the nsp6 structure contains a short lumenal helix between transmembrane domains 1 and 2, and another very short lumenal helix between transmembrane domains 7 and 8 (Fig. 1.2B, C)[36].

AlphaFold also predicts that nsp6 dimerizes through interactions between transmembrane domains 5, 6, and 7 (Fig. 1.2D)[36]. This model, however, does not rule out the possibility of end-to-end homodimerization that would mediate ER zippering, a central function of nsp6 as reported in a recent study, which involves the formation of narrow and exclusive membranous channels through the juxtaposition of adjacent ER membranes[22]. AlphaFold is highly accurate for predicting structures when similar protein structures have been solved [36]. However, caution should be taken with the current nsp6 structure model.

Experimental evidence supports predictions that nsp6 has only seven transmembrane domains, the last of which does not traverse the ER membrane (Fig. 1.2F)[22]. Indeed, immunofluorescence experiments have shown that permeabilization of the plasma membrane allows the detection of N- and C-tagged nsp6[22]. Analysis of another coronavirus, mouse hepatitis virus (MHV), experimentally demonstrated that nsp6 has 7 transmembrane domains[37]. More recent studies of SARS-CoV-2 nsp6 suggest that the 7th transmembrane domain, having an

amphipathic sequence to form a helix, likely associates with the ER membrane rather than traverses the lipid bilayer (Fig. 1.2D)[22]. Indeed, full-length nsp6 forms puncta within the ER, whereas removing the C-terminus or introducing F220Q and T222W mutations in the amphiphilic helix caused nsp6 to diffuse throughout the ER[22]. Compared with the AlphaFold model, this model differs in the structure of the C-terminal region after residue 157, which contains just two transmembrane domains (i.e., transmembrane 6 and the ER-associated helix 7; Fig. 1.2F) rather than 3 transmembrane domains (transmembranes 6-8 and the two C-terminal β-sheets; Fig. 1.2B). An atomic structure of nsp6 is required to validate these models.

1.4 DOUBLE MEMBRANE VESICLE FORMATION

The SARS-COV-2 nsp3, nsp4, and nsp6 proteins have been shown to modify the ER membranes to form DMVs and the same is true for the respective SARS-CoV proteins (Fig. 1.1)[22,27,38,39]. These double membrane structures provide a protective environment where viral RNA replication can occur away from cytoplasmic sensors and defenses[12,13,22]. Ricciardi et al. demonstrated that C-terminally tagged SARS-CoV-2 nsp6 expressed alone disseminates throughout the ER, while N-terminally tagged and untagged nsp6 form round structures and colocalize with the host protein Cb5, an ER marker, demonstrating a role for the C-terminus in DMV formation[22]. Furthermore, they demonstrated that nsp6 homodimerizes to form linear and circular zippered ER structures that encapsulate the surrounding cytoplasm but maintain a clear connection to the ER. Nsp6 is capable of restricting access to these nsp6 compartments, allowing entry only to ER membrane proteins with small lumenal domains such as VAP-A, but not ER lumenal proteins, such as calreticulin (Fig. 1.1)[22]. Interestingly, truncating the C-terminus of nsp6 removed the ability to form zippered ER structures, but the remainder of nsp6 (amino acids 1-157) retained the ability to homodimerize with full-length nsp6[22]. It seems likely that the long lumenal loop (91-112) of nsp6 plays a key role in facilitating homodimerization given its positioning in the ER lumen. Interestingly, the small molecule K22, a known inhibitor of several coronaviruses, reduces ER zippering and results in zippering of the nuclear envelope[22]. The authors suggest that

replication could occur in the DMVs formed from the nuclear envelope; however, given the preference for ER-derived replication organelles, the nuclear envelope is likely an unfavorable location for viral replication[22].

Lipid droplets (LDs) are required for SARS-CoV-2 replication and are thought to replenish lipids in DMV structures[22,40,41]. The C-terminus of nsp6 recruits Double FYVE-containing protein 1 (DFCP1), a host protein known to complex with RAB18 to anchor LDs to lipid membranes[22,42–44]. Nsp6-mediated interactions with LDs promote the growth of DMV structures as the replication organelles form. Additionally, nsp6 zippering controls access to DMVs by blocking entry to any unwelcome ER lumenal proteins or ER membrane proteins with large lumenal domains, while simultaneously maintaining free access to lipids[22].

Previous studies showed that co-expression of nsp3/nsp4 without nsp6 is sufficient to generate DMV structures[41,45]. However, Ricciardi et al. demonstrated that nsp3/nsp4/nsp6 co-expression produces tighter clusters of DMVs that are more numerous, more uniformly shaped, and have a smaller average diameter compared to DMVs produced by nsp3/nsp4 expression without nsp6[22]. The smaller DMVs are tethered to the ER by nsp6 linear zippered ER structures[22]. Importantly, nsp6(ΔSGF) (emerged in SARS-CoV-2 variants) shows higher zippering activity that produces more uniform DMV structures and improved organization of DMVs through a more developed array of zippered ER connections[22]. It was proposed that the enhanced zippering activity of nsp6(ΔSGF) may be a major contributing factor in the immune evasion of variants containing ΔSGF[22,46,47].

Of note, SARS-CoV-2 nsp3/4 induce the production of phosphatidylinositol 3-phosphate (PI3P), a component necessary for DMV formation; class III phosphatidylinositol 3-kinase (PI3K) and the PI3P-binding protein DFCP1 are both essential host factors in this process[41]. TMEM41B and VMP1 are also essential host factors for DMV biogenesis that interact with nsp3/4 complexes and manage phosphatidylserine distribution, an important component for maintaining DMV structures[45]. Other nonstructural proteins, including nsp2/3 and nsp8, also localize in DMVs during

SARS-CoV infection but their role in DMV formation remains unknown[48,49]. Therefore, while the evolution of nsp6 enhances DMV formation and organization, other nonstructural proteins are also essential.

1.5 MODULATION OF AUTOPHAGY

Autophagy is a regular process to manage cellular waste and destroy intracellular infectious material[50]. In the case of viral infection, autophagy is important to control infection and prevent widespread dissemination of the virus throughout the host by targeting viral components for lysis, as well as to process antigens for presentation to major histocompatibility (MHC) molecules[51]. Studies have demonstrated that SARS-CoV-2 nsp6 inhibits the formation of hybrid pre-autophagosomal structures (HyPAS), which are derived from fused *cis* Golgi and endosomal membranes[33]. This results in smaller autophagosomes that likely degrade viral components less efficiently[52,53]. Related coronaviruses, including SARS-CoV, also utilize nsp6 to form smaller ER-derived vesicles with the properties of nascent autophagosomes[26,52]. At late stages of infection, SARS-CoV-2 nsp6 produces smaller autophagosomes to reduce autophagy overall and, in combination with ORF3a, prevents the fusion of compartments containing viral components with lysosomes[54].

1.6 NLRP3 INFLAMMASOME ACTIVATION AND PYROPTOSIS

Rodrigues et al. showed that nsp6 inhibits the lysosome-autophagy system by binding to a lysosomal proton pump component. Nsp6 inhibits lysosomal acidification, resulting in a buildup of non-digestive autophagosomes[55]. In line with these results, Sun et al. demonstrated that nsp6 binds directly to ATP6AP1, a component of the vacuolar ATPase proton pump, to prevent lysosomal acidification in lung epithelial cells (Fig. 1.4)[24,25]. Nsp6 does not, however, block the fusion of autophagosomes with lysosomes; thus, non-digestive lysosomes accumulate and activate the NLRP3 inflammasome, leading to caspase-1-dependent maturation of interleukin-1β (IL-1β)

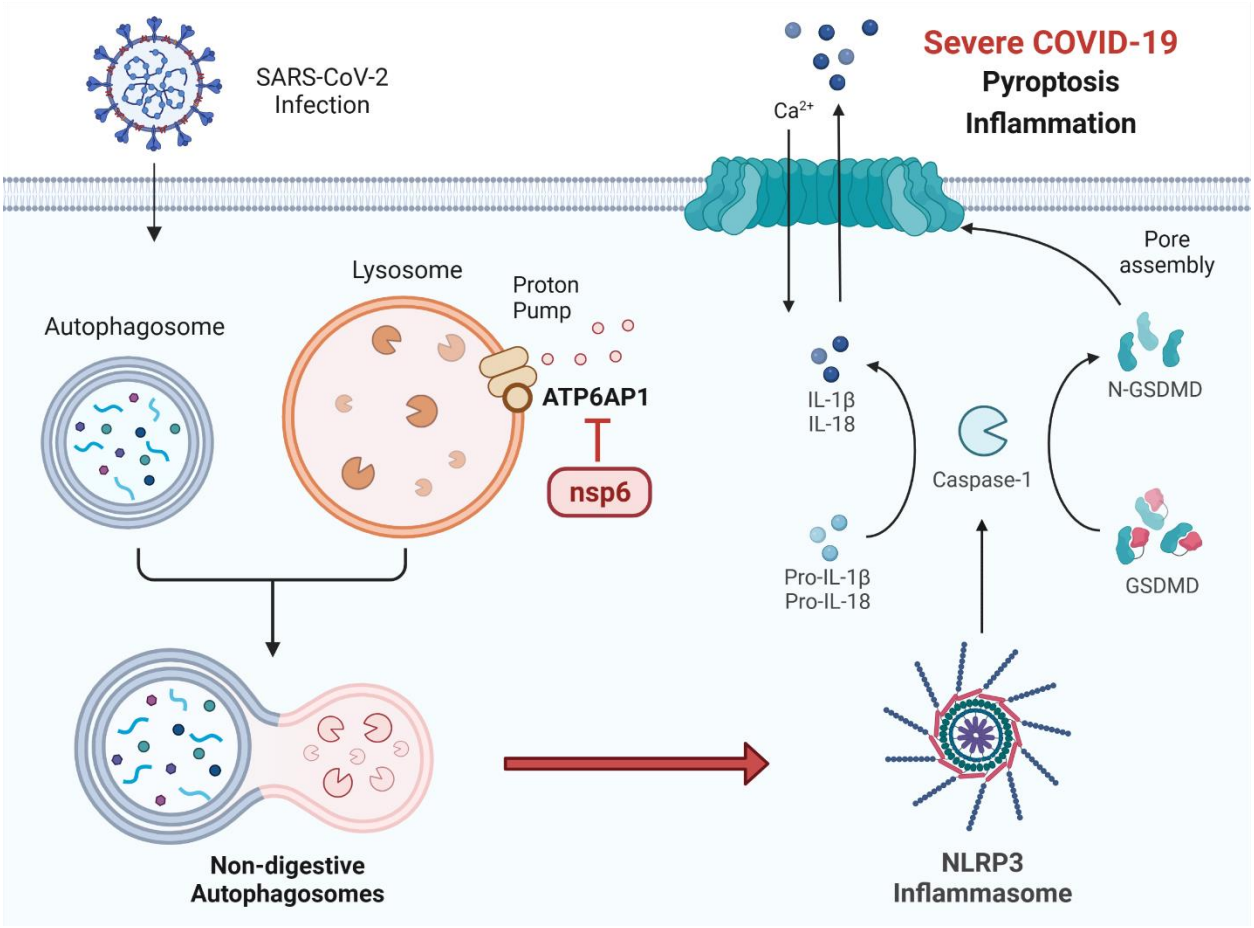

Figure 1.3: Nsp6 suppression of lysosomal acidification activates NLRP3 inflammasome

Nsp6 interacts with ATP6AP1 proton pump component to suppress acidification of lysosomes by blocking cleavage activation of ATP6AP1. This leads to accumulation of non-digestive autophagosomes, which activates the NRLP3 inflammasome instigating pyroptosis, a key feature of severe COVID-19. Created with BioRender. Adapted from Sun et al., 2022.

and IL-18 and triggering pyroptosis, an inflammatory form of apoptosis[24,25,56,57]. In the same study, IL-1β, IL-18, and M65 were identified as markers for severe COVID-19[25,58]. An amino acid substitution of L37F that accumulated in nsp6 of some clinical isolates, which was associated with asymptomatic cases of SARS-CoV-2, reduced nsp6's interactions with ATP6AP1, allowing lysosomal acidification to proceed as normal and consequently failing to stimulate the NLRP3 inflammasome pathway[24,25,59]. Not surprisingly, the L37F variant is not associated with any variants given that it compromises viral fitness in SARS-CoV-2[59].

Recent studies have demonstrated the role of inflammasome-activated pyroptosis in lung-resident macrophages and its contribution to severe disease in COVID-19. About 10% of blood monocytes and 8% of lung macrophages in COVID-19 patients were infected with SARS-CoV-2 through the uptake of antibody-opsonized virus particles by Fcγ receptors on the cell surface [60]. SARS-CoV-2 infection thus activated NLRP3 and AIM2 inflammasomes in nearly a quarter of lung macrophages, leading to pyroptosis, which was shown to be important for preventing persistent replication of the virus within monocytes/macrophages while simultaneously triggering an alarm to mobilize an immune response[60]. As an adverse effect, the release of intracellular contents with an increased concentration of IL-1β and IL-18 could be the cause of a cytokine storm that can damage organs, and cause vascular leakage and respiratory distress in COVID-19 patients[55,60]. A few other studies have similarly shown an increase in IL-1β in the blood and NLRP3 inflammasome activation, which correlate with clinical outcomes in COVID-19 patients[55,61–63]. These data suggest that the nsp6-mediated activation of NLRP3 inflammasomes and subsequent pyroptosis may be a significant contributor to severe disease in SARS-CoV-2 infected individuals.

Of note, a screen using affinity-purification mass spectrometry identified Sigma-1 receptor (SIGMAR1) as well as 3 components of the vacuolar ATPase involved in ion transport, ATP13A3 ATP5MG, and ATP6AP1, as high-confidence nsp6 interactors, corroborating recent studies[64]. A genome-wide CRISPR screen revealed ATP6AP1 as an important host factor for SARS-CoV-2

infection[65]. ATP6AP1 and the SIGMAR1 are both known drug targets[64]. Hydroxychloroquine, an inhibitor of the Sigma-1 receptor, gained much attention at the beginning of the pandemic due to its controversial use despite evidence that the molecule did not offer significant clinical benefits to COVID-19 patients[66]. Haloperidol, however, proved more effective at reducing SARS-CoV-2 infection *in vitro*, possibly by inhibiting SIGMAR1 and nsp6 interactions[66].

1.7 NSP6 ANTAGONISM OF IFN-I PATHWAYS

The IFN pathway, comprising of type I IFNs (IFNα and IFNβ) and type III IFNs (IFNλ), is part of the first line of defense against viral infections[67–69]. A triggered IFN response culminates in the activation of the innate immune response and promotion of adaptive immunity against future infection by the same pathogen. Treatment with IFNα and IFNβ has already been investigated as a possible therapeutic in multiple trials, but the results were variable[70].

We previously reported that several SARS-CoV-2 nonstructural and accessory proteins are responsible for antagonizing the IFN-I induction and signaling pathways in infected host cells (Fig. 1.3)[71]. Nsp6 in particular inhibits IFN-I production by binding to tank-binding kinase 1 (TBK1) to block phosphorylation of interferon regulatory 3 (IRF3), preventing nuclear translocation and subsequent gene activation. To block IFN-I signaling, nsp6 blocks phosphorylation of signal transducer and activator of transcription proteins 1 (STAT1) and STAT2 by receptor-associated Janus kinase 1 (JAK1) and Tyrosine kinase 2 (TYK2), preventing STAT1/2 complexing with interferon regulatory factor 9 (IRF9) and subsequent nuclear translocation to activate interferon-stimulated genes[71]. In support of our findings, another study showed that nsp6 reduced IFN-I induction and IFN-I signaling pathways to a similar degree[72,73]. In contrast, one study similarly reported that nsp6 strongly blocked IFNβ promoter activity as well as suppressed MAVS-induced mRNA expression of IFNβ, IFNλ1, and IFNλ2/3 but had no effect on IFN-I signaling[73], while another study reported that nsp6 enhanced IFN-I signaling but had no effect on IFN-I induction[74]. These differences could be due to distinct experimental methods.

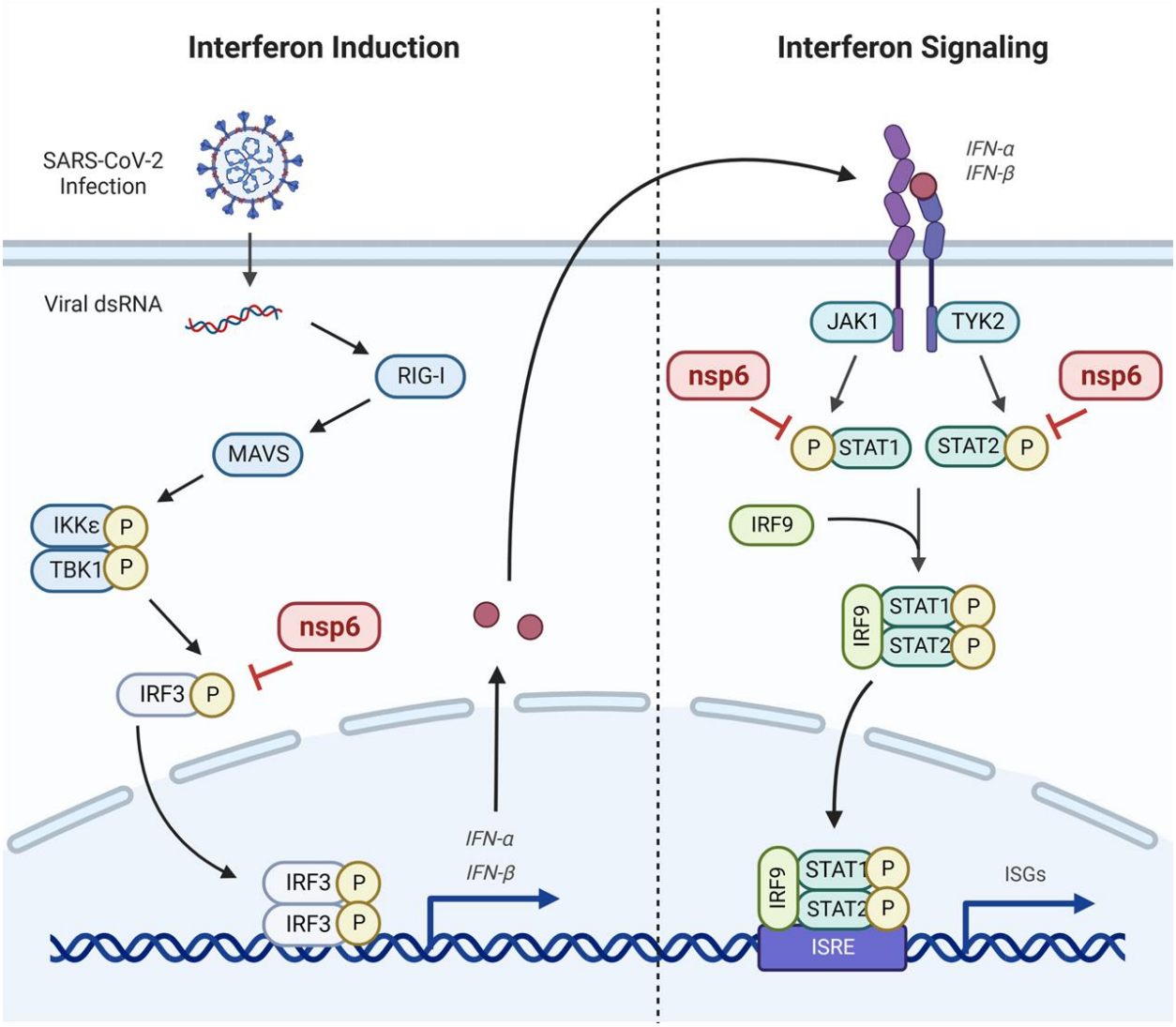

Figure 1.4: Nsp6 antagonizes interferon pathways

Schematic of interferon induction and interferon signaling pathways and the steps antagonized by nsp6. Nsp6 binds to TBK1 to block phosphorylation of IRF3 and prevent IFN-I induction. Nsp6 blocks phosphorylation of STAT1 and STAT2 to suppress IFN-I signaling. Created with BioRender. Adapted from Xia et al., 2020.

The Alpha variant of SARS-CoV-2, one of the first variants that emerged in mid-2020, was shown to be resistant to IFN-I and IFN-III treatment[75]. Recently, we showed that nsp6 contributes to IFN-I resistance in variants[23]. When treated with IFNα, an index SARS-CoV-2 isolate USA-WA1/2020 (WA1) containing the Alpha nsp6(ΔSGF) replicated to a higher level in Vero E6-TMPRSS2 cells than the parental WA1 strain[23]. Furthermore, we showed that expression of variant nsp6(ΔSGF) did not alter IFN-I induction compared to WA1 nsp6; but Alpha, BA.1, and a mutant nsp6(ΔLSG) reduced the activation of interferon-stimulated regulatory element (ISRE) gene promoter while Delta had no effect[23]. These results were corroborated by Western blots showing that Alpha, BA.1, and nsp6(ΔLSG) inhibit the phosphorylation of STAT1/2, but not Delta nsp6[23]. Further substantiating these results, Omicron BA.1 was recently shown to be more resistant to IFNα treatment compared to WA1 and Delta variant (B.1.617.2)[76]. These data suggest that both ΔSGF and ΔLSG mutations in nsp6 variants enhance repression of the host IFN signaling pathway.

The question remains how ΔSGF and ΔLSG impact the overall structure of nsp6. The deletion of three residues shortens the long lumenal loop (91-112), leading to an altered structure of the loop and its interactions with host factors in the IFN signaling pathways. However, the exact mechanism by which nsp6 prevents STAT1/2 phosphorylation is unknown.

On the other hand, enhancement of nsp6 antagonism of IFN-I responses may be due to improved control over DMV formation as discussed above[22]. Since IFN alpha receptors I and 2 (IFNAR1/2) are heavily glycosylated, it's possible that extensive ER remodeling could cause ER stress that would prevent proper maturation of IFNAR1/2 in the ER/Golgi apparatus network[77–80]. Indeed, expression of mCherry-tagged nsp6 alone in HEK293T cells was highly cytotoxic, and nsp6 was similarly cytotoxic in an *in vivo Drosophila* model[29]. Cytotoxicity from nsp6 expression could interfere with IFNAR1/2 trafficking to the plasma membrane, hence, the IFN-I signaling pathway would not be activated. Whether the nsp6-mediated antagonism of IFN-I signaling is due to the direct binding of nsp6 to components of the IFN-I signaling pathway or an indirect effect

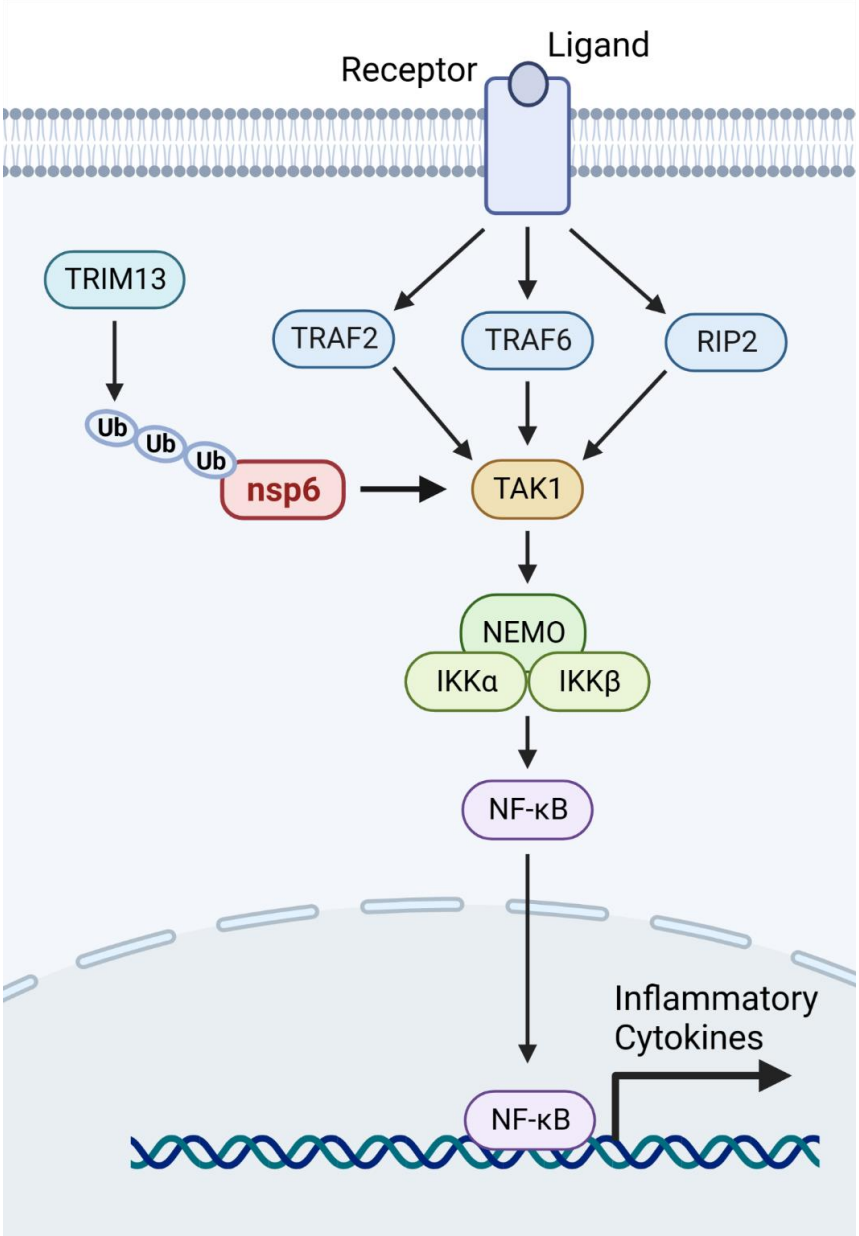

Figure 1.5: Nsp6 ubiquitination activates NF-κB

TRIM13 ubiquitination of nsp6 promotes complexing with TAK1 and NEMO, resulting in activation of NF-κB and upregulation of NF-κB-regulated transcripts of inflammatory cytokines. Created using BioRender. Adapted from Nishitsuji et al, 2020.

resulting from improved DMV organization remains to be seen. Further work is required to elucidate the mechanism by which nsp6 suppresses IFN-I responses.

1.8 Ubiquitination of SARS-CoV-2 nsp6 activates NF-κB expression

As described above in section 6, many studies have demonstrated that nsp6 is involved in antagonism of the IFN-I signaling pathway which would prevent activation of ISG expression and, therefore, limit immune responses and allow propagation of viral replication. Patients who suffer from severe COVID-19, however, tend to have higher levels of proinflammatory cytokines that lead to a cytokine storm, resulting in acute respiratory distress syndrome and organ damage [81–87]. Thus, it's possible that SARS-CoV-2 activates the expression of proinflammatory cytokines via an alternative mechanism during the later stages of infection.

Nishitsuji et al. reported that nsp6 interacts with transforming growth factor β-activated kinase 1 (TAK1), a host factor involved in the activation of the canonical NF-κB pathway (Fig. 1.5)[87]. NF-κB is considered one of the most important transcription factors for the activation of proinflammatory cytokines during SARS-CoV-2 infection[88,89]. Residue K61 of nsp6 is polyubiquitinated by the E3 ubiquitin ligase tripartite motif-containing 13 (TRIM13), which facilitates complexing of nsp6 and TAK1 with NF-κB essential modulator (NEMO) and the subsequent activation of the NF-κB pathway (Fig. 1.5)[87]. Activation of NF-κB signaling leads to increased mRNA expression of IL-8 and IFNγ-induced protein 10 (IP-10), both of which are known to be significantly elevated in serum levels of patients with severe COVID-19[81–87]. It's possible that inhibition of nsp6 or NF-κB signaling may ease the severity of COVID-19 symptoms by suppressing proinflammatory cytokines.

1.9 NSP6 mutations *in vivo*

In addition to showing that nsp6 mutations enhance suppression of IFN-I signaling pathways, we reported that intranasal infection of mice with a mutant WA1 SARS-CoV-2 containing the ΔSGF nsp6deletion (ΔSGF-WA1) produces more viral RNA in lungs than those

inoculated with the parental WA1 virus[23]. Consistently, ΔSGF-WA1-infected mice on average began losing weight a day earlier than WA1-infected mice and the disease-state lasted for seven days, a day longer than WA1-infected mice[23]. ΔSGF-WA1 proved more lethal with a survival rate of 50% compared to 75% for WA1. Surprisingly, analysis of histopathology of infected lung tissues from both groups of mice received similar scores, suggesting ΔSGF-WA1 does not cause greater cytopathic effect in the lungs. Instead, analysis of the host response using the nCounter Analysis System and Ingenuity Pathway Analysis revealed that in both mouse lung tissues and infected primary human airway epithelial cells, cytokine pathways and pathogen-induced cytokine storm pathways were downregulated in the initial stages of infection but by day 4 were significantly upregulated. This suggests that ΔSGF-WA1 efficiently represses early immune responses to allow for viral replication, and the immune system then overcompensates for the overwhelming viral load, causing a cytokine storm that likely results in organ failure and death[23]. This is a common feature of COVID-19 in humans, where IFN-I response is delayed during the early stages of infection (which is consistent with findings from SARS-CoV infection[90,91] followed by a proinflammatory response in the later stages of disease[86,91–94].These results are in agreement with the nsp6-mediated activation of the NLRP3 inflammasome and NF-κB as described above in sections 1.5 and 1.7[25,55,87].

Notably, a recent study showed that parental SARS-CoV-2 containing BA.1 S gene combined with BA.1 nsp6 (ΔLSG+I189V) was drastically attenuated in recombinant ACE2/TMPRSS2/Caco-2 cells and in K18-hACE2 mice, closely resembling the attenuated phenotype of full-length Omicron BA.1[95]. For comparison, only 20% of mice infected with the recombinant BA.1 S virus survived; 71% of mice infected with BA.1 S/nsp6 virus survived; and 100% of full-length BA.1-infected mice survived[95]. This is in line with previous results that mutations in the 5'-UTR-nsp12 region attenuate SARS-CoV-2 replication in K18-hACE2 mice, while BA.1 S mutations increase virulence[96]. This is in contrast to our finding that mice infected with ΔSGF nsp6-WA1 increased mortality in K18-hACE2 mice[23]. The reason for this discrepancy

is unclear given that ΔLSG, ΔLSG+I189V, and ΔSGF nsp6 all showed improved suppression of IFN-I signaling *in vitro*[23]. It was suggested that mutations in BA.1 S alter viral tropism, while nsp6 mutations may function as an adaptation to an altered tissue environment[95]. Whether BA.1 S and nsp6 work in concert is unknown. Given that infection with mutant ΔSGF-WA1 reduces survival while mutant BA.1 S/nsp6 increases survival, the contradictory results may suggest an epistatic interaction between S and nsp6.

1.10 Conclusions

The COVID-19 pandemic has ravaged the world and caused unprecedented social and economic damages in the past century[97–99]. The rapid development and approval of vaccines has changed the course of the pandemic and saved countless lives[100]. However, future variants remain a threat, as are other coronaviruses with pandemic potential[101]. Thus, it is important to continue studying coronaviruses, especially the roles of nonstructural proteins and accessory proteins. Although several functions of SARS-CoV-2 nsp6 protein have been reported, many questions remain. Solving the atomic structure of the nsp6 protein will provide crucial insights into its molecular mechanism, such as how ΔSGF and ΔLSG alter the nsp6 structure to enhance protein-protein interactions or, in the case of L37F, hinder interactions[23,59,102]. The structural information may also improve our understanding of nsp6-mediated DMV formation and designing inhibitors of its function. Additionally, identifying specific interacting partners will be vital to understanding the nsp6 antagonism of IFN-I pathways and other functions.

1.11 Acknowledgements

We thank Dr. Hongjie Xia and other colleagues for helpful discussions during the course of this work. X.X. and P.-Y.S. were supported by awards from the Sealy & Smith Foundation and the Robert J. Kleberg, Jr. and Helen C. Kleberg Foundation.

1.12 REFERENCES:

1. Zhu N, Zhang D, Wang W, et al. A Novel Coronavirus from Patients with Pneumonia in China, 2019. *New England Journal of Medicine*. 2020;382(8):727-733. doi:10.1056/nejmoa2001017
2. Walls AC, Park YJ, Tortorici MA, Wall A, McGuire AT, Veesler D. Structure, Function, and Antigenicity of the SARS-CoV-2 Spike Glycoprotein. *Cell*. 2020;181(2):281-292.e6. doi:10.1016/j.cell.2020.02.058
3. Wang Q, Zhang Y, Wu L, et al. Structural and Functional Basis of SARS-CoV-2 Entry by Using Human ACE2. *Cell*. 2020;181(4):894-904.e9. doi:10.1016/j.cell.2020.03.045
4. Plante JA, Mitchell BM, Plante KS, Debbink K, Weaver SC, Menachery VD. The variant gambit: COVID-19's next move. *Cell Host Microbe*. 2021;29(4):508-515. doi:10.1016/j.chom.2021.02.020
5. Abdolmaleki G, Taheri MA, Paridehpour S, et al. A comparison between SARS-CoV-1 and SARS-CoV2: an update on current COVID-19 vaccines. *DARU, Journal of Pharmaceutical Sciences*. 2022;Sep(2):1-28. doi:10.1007/s40199-022-00446-8
6. Patel R, Kaki M, Potluri VS, Kahar P, Khanna D. A comprehensive review of SARS-CoV-2 vaccines: Pfizer, Moderna & Johnson & Johnson. *Hum Vaccin Immunother*. 2022;18(1). doi:10.1080/21645515.2021.2002083
7. Bar-On YM, Flamholz A, Phillips R, Milo R. SARS-CoV-2 (COVID-19) by the numbers. *Elife*. 2020;9(e57309). doi:10.7326/M20-1190
8. Hoffmann M, Kleine-Weber H, Schroeder S, et al. SARS-CoV-2 Cell Entry Depends on ACE2 and TMPRSS2 and Is Blocked by a Clinically Proven Protease Inhibitor. *Cell*. 2020;181(2):271-280.e8. doi:10.1016/j.cell.2020.02.052
9. Kim D, Lee JY, Yang JS, Kim JW, Kim VN, Chang H. The Architecture of SARS-CoV-2 Transcriptome. *Cell*. 2020;181(4):914-921.e10. doi:10.1016/j.cell.2020.04.011
10. Cui J, Li F, Shi ZL. Origin and evolution of pathogenic coronaviruses. *Nat Rev Microbiol*. 2019;17(3):181-192. doi:10.1038/s41579-018-0118-9
11. Liu Y, Zhang X, Liu J, et al. A live-attenuated SARS-CoV-2 vaccine candidate with accessory protein deletions. *Nature Communications 2022 13:1*. 2022;13(1):1-14. doi:10.1038/s41467-022-31930-z
12. Knoops K, Kikkert M, van den Worm SHE, et al. SARS-coronavirus replication is supported by a reticulovesicular network of modified endoplasmic reticulum. *PLoS Biol*. 2008;6(9):1957-1974. doi:10.1371/journal.pbio.0060226
13. Scutigliani EM, Kikkert M. Cytokine & Growth Factor Reviews Interaction of the innate immune system with positive-strand RNA virus replication organelles. *Cytokine Growth Factor Rev*. 2017;37:17-27. doi:10.1016/j.cytogfr.2017.05.007
14. Yang H, Lyu Y, Hou F. SARS-CoV-2 infection and the antiviral innate immune response. *J Mol Cell Biol*. 2020;12(12):963-967. doi:10.1093/jmcb/mjaa071
15. Fehr AR, Perlman S. Coronaviruses: an overview of their replication and pathogenesis. In: *Coronaviruses: Methods and Protocols*. ; 2015:1-23.
16. Saraste J, Prydz K. Assembly and cellular exit of coronaviruses: Hijacking an unconventional secretory pathway from the pre-golgi intermediate compartment via the golgi ribbon to the extracellular space. *Cells*. 2021;10(3):1-20. doi:10.3390/cells10030503
17. de Haan CAM, Rottier PJM. Molecular Interactions in the Assembly of Coronaviruses. *Adv Virus Res*. 2005;64(January):165-230. doi:10.1016/S0065-3527(05)64006-7

18. V'kovski P, Kratzel A, Steiner S, Stalder H, Thiel V. Coronavirus biology and replication: implications for SARS-CoV-2. *Nat Rev Microbiol*. 2021;19(3):155-170. doi:10.1038/s41579-020-00468-6
19. Ghosh S, Dellibovi-Ragheb TA, Kerviel A, et al. β-Coronaviruses Use Lysosomes for Egress Instead of the Biosynthetic Secretory Pathway. *Cell*. 2020;183(6):1520-1535.e14. doi:10.1016/j.cell.2020.10.039
20. Mariano G, Farthing RJ, Lale-Farjat SLM, Bergeron JRC. Structural Characterization of SARS-CoV-2: Where We Are, and Where We Need to Be. *Front Mol Biosci*. 2020;7(December). doi:10.3389/fmolb.2020.605236
21. Gupta R, Charron J, Stenger CL, et al. SARS-CoV-2 (COVID-19) structural and evolutionary dynamicome: Insights into functional evolution and human genomics. *Journal of Biological Chemistry*. 2020;295(33):11742-11753. doi:10.1074/jbc.ra120.014873
22. Ricciardi S, Guarino AM, Giaquinto L, et al. The role of NSP6 in the biogenesis of the SARS-CoV-2 replication organelle. *Nature*. 2022;606(7915):761-768. doi:10.1038/s41586-022-04835-6
23. Bills CJ, Xia H, Chen JYC, et al. Mutations in SARS-CoV-2 variant nsp6 enhance type-I interferon antagonism. *Submitted 21Feb2023*. Published online 2023.
24. Sun X, Yu J, Wong SH, Chan MTV, Zhang L, Wu WKK. SARS-CoV-2 targets the lysosome to mediate airway inflammatory cell death. *Autophagy*. 2022;18(9):2246-2248. doi:10.1080/15548627.2021.2021496
25. Sun X, Liu Y, Huang Z, et al. SARS-CoV-2 non-structural protein 6 triggers NLRP3-dependent pyroptosis by targeting ATP6AP1. *Cell Death Differ*. 2022;29(6):1240-1254. doi:10.1038/s41418-021-00916-7
26. Cottam EM, Maier HJ, Manifava M, et al. Coronavirus nsp6 proteins generate autophagosomes from the endoplasmic reticulum via an omegasome intermediate. *Autophagy*. 2011;7(11):1335-1347. doi:10.4161/auto.7.11.16642
27. Angelini MM, Akhlaghpour M, Neuman BW, Buchmeier MJ. Severe acute respiratory syndrome coronavirus nonstructural proteins 3, 4, and 6 induce double-membrane vesicles. *mBio*. 2013;4(4). doi:10.1128/mBio.00524-13
28. Snijder EJ, Limpens RWAL, de Wilde AH, et al. A unifying structural and functional model of the coronavirus replication organelle: Tracking down RNA synthesis. *PLoS Biol*. 2020;18(6):1-25. doi:10.1371/journal.pbio.3000715
29. Lee JG, Huang W, Lee H, van de Leemput J, Kane MA, Han Z. Characterization of SARS-CoV-2 proteins reveals Orf6 pathogenicity, subcellular localization, host interactions and attenuation by Selinexor. *Cell Biosci*. 2021;11(1):1-12. doi:10.1186/s13578-021-00568-7
30. Peacock TP, Penrice-Randal R, Hiscox JA, Barclay WS. SARS-CoV- 2 one year on: Evidence for ongoing viral adaptation. *Journal of General Virology*. 2021;102(4):001584. doi:10.1099/jgv.0.001584
31. Romero PE, Dávila-Barclay A, Salvatierra G, et al. The Emergence of Sars-CoV-2 Variant Lambda (C.37) in South America. *Microbiol Spectr*. 2021;9(2):e0078921. doi:10.1128/spectrum.00789-21
32. Hadfield J, Megill C, Bell SM, et al. NextStrain: Real-time tracking of pathogen evolution. *Bioinformatics*. 2018;34(23):4121-4123. doi:10.1093/bioinformatics/bty407
33. Kumar A, Kumar P, Saumya KU, Giri R. Investigating the conformational dynamics of SARS-CoV-2 NSP6 protein with emphasis on non-transmembrane 91–112 & 231–290 regions. *Microb Pathog*. 2021;161(PA):105236. doi:10.1016/j.micpath.2021.105236

34. Hallgren J, Tsirigos KD, Damgaard Pedersen M, et al. DeepTMHMM predicts alpha and beta transmembrane proteins using deep neural networks. *bioRxiv*. Published online 2022:2022.04.08.487609. https://www.biorxiv.org/content/10.1101/2022.04.08.487609v1%0Ahttps://www.biorxiv.org/content/10.1101/2022.04.08.487609v1.abstract
35. Omasits U, Ahrens CH, Müller S, Wollscheid B. Protter: Interactive protein feature visualization and integration with experimental proteomic data. *Bioinformatics*. 2014;30(6):884-886. doi:10.1093/bioinformatics/btt607
36. Jumper J, Evans R, Pritzel A, et al. Highly accurate protein structure prediction with AlphaFold. *Nature*. 2021;596(7873):583-589. doi:10.1038/s41586-021-03819-2
37. Oostra M, Hagemeijer MC, van Gent M, et al. Topology and Membrane Anchoring of the Coronavirus Replication Complex: Not All Hydrophobic Domains of nsp3 and nsp6 Are Membrane Spanning. *J Virol*. 2008;82(24):12392-12405. doi:10.1128/jvi.01219-08
38. Klein S, Cortese M, Winter SL, et al. SARS-CoV-2 structure and replication characterized by in situ cryo-electron tomography. *Nat Commun*. 2020;11(1):1-10. doi:10.1038/s41467-020-19619-7
39. Hagemeijer MC, Monastyrska I, Griffith J, et al. Membrane rearrangements mediated by coronavirus nonstructural proteins 3 and 4. *Virology*. 2014;458-459(1):125-135. doi:10.1016/j.virol.2014.04.027
40. Gomes Dias SS, Cardoso Soares V, Ferreira AC, et al. Lipid droplets fuel SARS-CoV-2 replication and production of inflammatory mediators. *PLoS Pathog*. 2020;16(12):e1009127. doi:10.1371/journal.ppat.1009127
41. Twu WI, Lee JY, Kim H, et al. Contribution of autophagy machinery factors to HCV and SARS-CoV-2 replication organelle formation. *Cell Rep*. 2021;37(8):110049. doi:10.1016/j.celrep.2021.110049
42. Li D, Zhao YG, Li D, et al. The ER-Localized Protein DFCP1 Modulates ER-Lipid Droplet Contact Formation. *Cell Rep*. 2019;27(2):343-358.e5. doi:10.1016/j.celrep.2019.03.025
43. Gao G, Sheng Y, Yang H, Chua BT, Xu L. DFCP1 associates with lipid droplets. *Cell Biol Int*. 2019;43(12):1492-1504. doi:10.1002/cbin.11199
44. Herker E, Vieyres G, Beller M, Krahmer N, Bohnert M. Lipid Droplet Contact Sites in Health and Disease. *Trends Cell Biol*. 2021;31(5):345-358. doi:10.1016/j.tcb.2021.01.004
45. Ji M, Li M, Sun L, et al. VMP1 and TMEM41B are essential for DMV formation during β-coronavirus infection. *Journal of Cell Biology*. 2022;221(6):e202112081. doi:10.1083/jcb.202112081
46. Lee JY, Wing PAC, Gala DS, et al. Absolute quantitation of individual SARS-CoV-2 RNA molecules provides a new paradigm for infection dynamics and variant differences. *Elife*. 2022;11:e74153. doi:10.7554/eLife.74153
47. Thorne LG, Bouhaddou M, Reuschl AK, et al. Evolution of enhanced innate immune evasion by SARS-CoV-2. *Nature*. 2022;602(7897):487-495.
48. Bost AG, Carnahan RH, Lu XT, Denison MR. Four Proteins Processed from the Replicase Gene Polyprotein of Mouse Hepatitis Virus Colocalize in the Cell Periphery and Adjacent to Sites of Virion Assembly. *J Virol*. 2000;74(7):3379-3387. doi:10.1128/jvi.74.7.3379-3387.2000
49. van der Meer Y, Snijder EJ, Dobbe JC, et al. Localization of Mouse Hepatitis Virus Nonstructural Proteins and RNA Synthesis Indicates a Role for Late Endosomes in Viral Replication. *J Virol*. 1999;73(9):7641-7657. doi:10.1128/jvi.73.9.7641-7657.1999

50. Fan Y, Zong WX. The cellular decision between apoptosis and autophagy. *Beyond Apoptosis: Cellular Outcomes of Cancer Therapy*. Published online 2008:127-141. doi:10.3109/9781420020502-9
51. Wu WKK, Yue J. Autophagy in host-microbe interactions. *Semin Cell Dev Biol*. 2020;101(February):1-2. doi:10.1016/j.semcdb.2020.02.001
52. Cottam EM, Whelband MC, Wileman T, Cottam EM, Whelband MC, Wileman T. Coronavirus NSP6 restricts autophagosome expansion. *Autophagy*. 2014;10(8):1426-1441. doi:10.4161/auto.29309
53. Gassen NC, Niemeyer D, Muth D, et al. SKP2 attenuates autophagy through Beclin1-ubiquitination and its inhibition reduces MERS-Coronavirus infection. *Nat Commun*. 2019;10(1):2-4. doi:10.1038/s41467-019-13659-4
54. Miao G, Zhao H, Li Y, et al. ORF3a of the COVID-19 virus SARS-CoV-2 blocks HOPS complex-mediated assembly of the SNARE complex required for autolysosome formation. *Dev Cell*. 2021;56(4):427-442.e5. doi:10.1016/j.devcel.2020.12.010
55. Rodrigues TS, de Sá KSG, Ishimoto AY, et al. Inflammasomes are activated in response to SARS-cov-2 infection and are associated with COVID-19 severity in patients. *Journal of Experimental Medicine*. 2020;218(3). doi:10.1084/JEM.20201707
56. Bergsbaken T, Fink SL, Cookson BT. Pyroptosis: host cell death. *Nat Rev Microbiol*. 2009;7(2):99-109. doi:10.1038/nrmicro2070.Pyroptosis
57. Broz P, Dixit VM. Inflammasomes: Mechanism of assembly, regulation and signaling. *Nat Rev Immunol*. 2016;16(7):407-420. doi:10.1038/nri.2016.58
58. Nagy Á, Pongor S, Győrffy B. Different mutations in SARS-CoV-2 associate with severe and mild outcome. *Int J Antimicrob Agents*. 2021;57(2):106272. doi:10.1016/j.ijantimicag.2020.106272
59. Wang R, Chen J, Hozumi Y, Yin C, Wei GW. Decoding Asymptomatic COVID-19 Infection and Transmission. *Journal of Physical Chemistry Letters*. 2020;11(23):10007-10015. doi:10.1021/acs.jpclett.0c02765
60. Junqueira C, Crespo Â, Ranjbar S, et al. FcγR-mediated SARS-CoV-2 infection of monocytes activates inflammation. *Nature*. Published online 2022. doi:10.1038/s41586-022-04702-4
61. Hadjadj J, Yatim N, Barnabei L, et al. Impaired type I interferon activity and inflammatory responses in severe COVID-19 patients. *Science (1979)*. 2020;369(6504):718-724. doi:10.1126/science.abc6027
62. Zheng J, Wang Y, Li K, Meyerholz DK, Allamargot C, Perlman S. Severe Acute Respiratory Syndrome Coronavirus 2-Induced Immune Activation and Death of Monocyte-Derived Human Macrophages and Dendritic Cells. *Journal of Infectious Diseases*. 2021;223(5):785-795. doi:10.1093/infdis/jiaa753
63. Hui KPY, Cheung MC, Perera RAPM, et al. Tropism, replication competence, and innate immune responses of the coronavirus SARS-CoV-2 in human respiratory tract and conjunctiva: an analysis in ex-vivo and in-vitro cultures. *Lancet Respir Med*. 2020;8(7):687-695. doi:10.1016/S2213-2600(20)30193-4
64. Gordon DE, Jang GM, Bouhaddou M, et al. A SARS-CoV-2 protein interaction map reveals targets for drug repurposing. *Nature*. 2020;583(7816):459-468. doi:10.1038/s41586-020-2286-9
65. Hou J, Wei Y, Zou J, et al. Integrated multi-omics analyses identify key anti-viral host factors and pathways controlling SARS-CoV-2 infection. Published online August 15, 2022. doi:10.21203/RS.3.RS-1910932/V1

66. WHO Solidarity Trial Consortium. Repurposed Antiviral Drugs for Covid-19 — Interim WHO Solidarity Trial Results. *New England Journal of Medicine*. 2021;384(6):497-511. doi:10.1056/nejmoa2023184
67. Hoffmann HH, Schneider WM, Rice CM. Interferons and viruses: An evolutionary arms race of molecular interactions. *Trends Immunol*. 2015;36(3):124-138. doi:10.1016/j.it.2015.01.004
68. Kotenko S v., Durbin JE. Contribution of type III interferons to antiviral immunity: Location, location, location. *Journal of Biological Chemistry*. 2017;292(18):7295-7303. doi:10.1074/jbc.R117.777102
69. Levy DE, Marié IJ, Durbin JE. Induction and function of type i and III interferon in response to viral infection. *Curr Opin Virol*. 2011;1(6):476-486. doi:10.1016/j.coviro.2011.11.001
70. Jhuti D, Rawat A, Guo CM, Wilson LA, Mills EJ, Forrest JI. Interferon Treatments for SARS-CoV-2: Challenges and Opportunities. *Infect Dis Ther*. 2022;11(3):953-972. doi:10.1007/s40121-022-00633-9
71. Xia H, Cao Z, Xie X, et al. Evasion of Type I Interferon by SARS-CoV-2. *Cell Rep*. 2020;33(1):108234. doi:10.1016/j.celrep.2020.108234
72. Yuen CK, Lam JY, Wong WM, et al. SARS-CoV-2 nsp13, nsp14, nsp15 and orf6 function as potent interferon antagonists. *Emerg Microbes Infect*. 2020;9(1):1418-1428. doi:10.1080/22221751.2020.1780953
73. Shemesh M, Aktepe TE, Deerain JM, et al. *SARS-CoV-2 Suppresses IFNβ Production Mediated by NSP1, 5, 6, 15, ORF6 and ORF7b but Does Not Suppress the Effects of Added Interferon*. Vol 17.; 2021. doi:10.1371/journal.ppat.1009800
74. Lei X, Dong X, Ma R, et al. Activation and evasion of type I interferon responses by SARS-CoV-2. *Nat Commun*. 2020;11(1):1-12. doi:10.1038/s41467-020-17665-9
75. Guo K, Barrett BS, Morrison JH, et al. Interferon resistance of emerging SARS-CoV-2 variants. *Proc Natl Acad Sci U S A*. 2022;119(32):e2203760119. doi:10.1073/pnas.2203760119
76. Shalamova L, Felgenhauer U, Wilhelm J, et al. Omicron variant of SARS-CoV-2 exhibits an increased resilience to the antiviral type I interferon response. *PNAS Nexus*. 2022;1(2):1-4. doi:10.1093/pnasnexus/pgac067
77. Ling LE, Zafari M, Reardon D, Brickelmeier M, Goelz SE, Benjamin CD. Human Type I Interferon Receptor, IFNAR, Is a Heavily Glycosylated 120-130 kD Membrane Protein. *Journal of Interferon and Cytokine Research*. 1995;15(1):55-61. doi:10.1089/jir.1995.15.55
78. Sommereyns C, Michiels T. N-glycosylation of murine IFN-β in a putative receptor-binding region. *Journal of Interferon and Cytokine Research*. 2006;26(6):406-413. doi:10.1089/jir.2006.26.406
79. Smirle J, Au CE, Jain M, Dejgaard K, Nilsson T, Bergeron J. Cell Biology of the Endoplasmic Reticulum and the Golgi Apparatus through Proteomics. *Cold Spring Harb Perspect Biol*. 2013;5(1):a015073. doi:10.1101/CSHPERSPECT.A015073
80. Sprooten J, Garg AD. Type I interferons and endoplasmic reticulum stress in health and disease. *Int Rev Cell Mol Biol*. 2020;350(January):63-118. doi:10.1016/bs.ircmb.2019.10.004
81. del Valle DM, Kim-Schulze S, Huang HH, et al. An inflammatory cytokine signature predicts COVID-19 severity and survival. *Nat Med*. 2020;26(10):1636-1643. doi:10.1038/s41591-020-1051-9
82. Karki R, Sharma BR, Tuladhar S, et al. Synergism of TNF-α and IFN-γ Triggers Inflammatory Cell Death, Tissue Damage, and Mortality in SARS-CoV-2 Infection and Cytokine Shock Syndromes. *Cell*. 2021;184(1):149-168.e17. doi:10.1016/j.cell.2020.11.025

83. Kesmez Can F, Özkurt Z, Öztürk N, Sezen S. Effect of IL-6, IL-8/CXCL8, IP-10/CXCL 10 levels on the severity in COVID 19 infection. *Int J Clin Pract*. 2021;75(12):e14970. doi:10.1111/ijcp.14970
84. Huang C, Wang Y, Li X, et al. Clinical features of patients infected with 2019 novel coronavirus in Wuhan, China. *The Lancet*. 2020;395(10223):497-506. doi:10.1016/S0140-6736(20)30183-5
85. Zhou Y, Fu B, Zheng X, et al. Pathogenic T-cells and inflammatory monocytes incite inflammatory storms in severe COVID-19 patients. *Natl Sci Rev*. 2020;7(6):998-1002. doi:10.1093/nsr/nwaa041
86. Blanco-Melo D, Nilsson-Payant BE, Liu WC, et al. Imbalanced Host Response to SARS-CoV-2 Drives Development of COVID-19. *Cell*. 2020;181(5):1036-1045.e9. doi:10.1016/j.cell.2020.04.026
87. Nishitsuji H, Iwahori S, Ohmori M, Shimotohno K, Murata T. Ubiquitination of SARS-CoV-2 NSP6 and ORF7a Facilitates NF-κB Activation. *mBio*. 2022;13(4):1-18. doi:10.1128/mbio.00971-22
88. Neufeldt CJ, Cerikan B, Cortese M, et al. SARS-CoV-2 infection induces a pro-inflammatory cytokine response through cGAS-STING and NF-κB. *Commun Biol*. 2022;5(1). doi:10.1038/s42003-021-02983-5
89. Nilsson-Payant BE, Uhl S, Grimont A, et al. The NF-κB Transcriptional Footprint Is Essential for SARS-CoV-2 Replication. *J Virol*. 2021;95(23). doi:10.1128/jvi.01257-21
90. Channappanavar R, Fehr AR, Vijay R, et al. Dysregulated Type I Interferon and Inflammatory Monocyte-Macrophage Responses Cause Lethal Pneumonia in SARS-CoV-Infected Mice. *Cell Host Microbe*. 2016;19(2):181-193. doi:10.1016/j.chom.2016.01.007
91. Arunachalam PS, Wimmers F, Mok CKP, et al. Systems biological assessment of immunity to mild versus severe COVID-19 infection in humans. *Science (1979)*. 2020;369(6508):1210-1220. doi:10.1126/SCIENCE.ABC6261
92. Vabret N, Britton GJ, Gruber C, et al. Immunology of COVID-19: Current State of the Science. *Immunity*. 2020;52(6):910-941. doi:10.1016/j.immuni.2020.05.002
93. Lucas C, Wong P, Klein J, et al. Longitudinal analyses reveal immunological misfiring in severe COVID-19. *Nature*. 2020;584(7821):463-469. doi:10.1038/s41586-020-2588-y
94. Ramos-Casals M, Brito-Zerón P, Mariette X. Systemic and organ-specific immune-related manifestations of COVID-19. *Nat Rev Rheumatol*. 2021;17(6):315-332. doi:10.1038/s41584-021-00608-z
95. Chen D yuan, Chin CV, Kenney D, et al. Spike and nsp6 are key determinants of SARS-CoV-2 Omicron BA.1 attenuation. *Nature*. Published online 2023. doi:10.1038/s41586-023-05697-2
96. Liu S, Selvaraj P, Sangare K, Luan B, Wang TT. Spike protein-independent attenuation of SARS- CoV-2 Omicron variant in laboratory mice. *CellReports*. 2022;40(11):111359. doi:10.1016/j.celrep.2022.111359
97. Collaborators C 19 EM. Estimating excess mortality due to the COVID-19 pandemic: a systematic analysis of COVID-19-related mortality, 2020-21. *Lancet*. 2022;399(10334):1513-1536. doi:10.1016/S0140-6736(21)02796-3
98. Lopez-Leon S, Wegman-Ostrosky T, Perelman C, et al. More than 50 long-term effects of COVID-19: a systematic review and meta-analysis. *Sci Rep*. 2021;11(1):1-14. doi:10.1038/s41598-021-95565-8
99. Rose A. COVID-19 economic impacts in perspective: A comparison to recent U.S. disasters. *International Journal of Disaster Risk Reduction*. 2021;60(December 2020):102317. doi:10.1016/j.ijdrr.2021.102317

100. Watson OJ, Barnsley G, Toor J, Hogan AB, Winskill P, Ghani AC. Global impact of the first year of COVID-19 vaccination: a mathematical modelling study. *Lancet Infect Dis*. 2022;22(9):1293-1302. doi:10.1016/S1473-3099(22)00320-6
101. Gralinski LE, Menachery VD. Return of the Coronavirus: 2019-nCoV. *Viruses*. 2020;12(135).
102. Aiewsakun P, Nilplub P, Wongtrakoongate P, Hongeng S, Thitithanyanont A. SARS-CoV-2 genetic variations associated with COVID-19 pathogenicity. *Microb Genom*. 2021;7(12). doi:10.1099/mgen.0.000734

Chapter 2: Methods and Materials

2.1 Cell culture

African green monkey kidney epithelial cells expressing TMPRSS2 (Vero E6-TMPRSS2) for enhanced infectivity and human epithelial kidney cells (HEK293T) cells were cultured in growth medium containing high-glucose Dulbecco's modified Eagle's medium (DMEM) (Gibco) supplemented with 10% fetal bovine serum (FBS; Hyclone Laboratories, Logan, UT) and 1% penicillin/streptomycin (P/S; Invitrogen) and maintained at 37°C with 5% CO2. Antibiotics and culture media were purchased from ThermoFisher Scientific (Waltham, MA). All cell lines tested negative for mycoplasma contamination.

2.2 Constructing SARS-COV-2 infectious clones

The stock of SARS-CoV-2 strain 2019-nCoV/USA_WA1/2020 was isolated from the first COVID-19 patient diagnosed in the US and provided to the World Reference Center for Emerging Viruses and Arboviruses (WRCEVA) at the University of Texas Medical Branch at Galveston (UTMB). SARS-CoV-2 infectious clones were constructed as previously described[1,2]. Altogether, six mutant viruses were generated containing individual gene mutations from Alpha nsp6(ΔSGF), ORF3a, M, and N or a combination of mutations from Alpha ORF3a, M, and N. Separately, an infectious clone was constructed containing BA.1 nsp6 mutations (ΔLSG+I189V). Briefly, cDNA fragments encoding the viral genome were cloned into a single copy vector pCC1BAC, and variant-specific mutations were introduced using overlapping PCR. Purified amplicons were then assembled with the vector using the NEBuilder kit (New England Biolabs (NEB), Ipswich, MA). The assembled plasmids were propagated in TransforMax™ EPI300™ E. coli cells (Biosearch Technologies) and isolated using MaxiPrep kits (Qiagen), then digested and ligated using T4 DNA ligase (NEB) to create linear full-length DNA. RNA was transcribed in vitro from the full-length DNA using mMESSAGE mMACHINE T7 Transcription Kit (ThermoFisher Scientific) and then electroporated into Vero E6-TMPRSS2 cells along with in vitro transcribed N gene transcript to

enhance infectivity of the synthetic viral RNA. Cells were incubated overnight at 37°C with 5% CO2 then culture medium was replaced with 2% FBS DMEM. When cytopathic effect (CPE) reached approximately 50%, the supernatants from infected cell cultures were collected and frozen at -80°C, or used to infect a new T-175 flask containing fresh Vero E6-TMPRSS2 cells to generate passage 1 virus, whereupon the flask was incubated for 2 days, then supernatants were collected and stored at -80°C. One volume supernatant was added to 4 volumes TRIzol LS Reagent (Thermo Fisher Scientific) and purified using Direct-zol RNA Miniprep Plus Kits (Zymo, Irvine, CA). cDNA was synthesized SuperScript™ IV One-Step RT-PCR system (ThermoFisher Scientific) and sequenced to verify the presence of introduced mutations. Mock electroporated cells were used as controls. Experiments were performed with passage 1 virus. All work following electroporation was performed in a biosafety level 3 laboratory.

2.3 IFN-I TREATMENT OF SARS-COV-2

Vero E6-TMPRSS2 cells were seeded in 24-well plates (2 x 10^5 cells/well) and incubated at least 5 hours. Cells were pretreated for 16-18 hours with IFN-α subtype 2 (Millipore, Darmstadt, Germany) serially diluted 2-fold in growth medium or added following infection. Cells were washed with DPBS then infected at MOI 0.02 with 0.2 mL virus inoculum diluted in maintenance medium (DMEM 2% FBS + 1% P/S) and incubated for 1 hour at 37°C with 5% CO2. The inoculum was then removed and the cells washed with DPBS, then fresh IFN-α diluted in maintenance medium was added. After 48 hours incubation, supernatants were harvested for plaque assays and RT-qPCR.

2.4 REVERSE TRANSCRIPTION QUANTITATIVE PCR

To quantify viral RNA in vitro, 0.2 mL infected culture supernatants were harvested 48 hours post infection and added to 4 volumes of Trizol LS Reagent (Thermo Fisher Scientific). RNA was purified using Direct-zol RNA Miniprep Plus Kits (Zymo) according to manufacturer's instructions, eluted in 50 µL nuclease-free water, then quantified using iTaq™ Universal SYBR®

Green One-Step Kit (Bio-Rad) and primers 2019nCoV-N2-Fwd/Rev (TTACAAACATTGGCCGCAAA/GCGCGACATTCCGAAGAA) targeting 67 conserved nucleotides (891-957) of the N gene. Viral RNA was amplified using The QuantStudio™ 7 Flex system (Applied Biosystems, Waltham, MA) and RNA copies were quantitated using a 6-point standard curve (2 x 104 to 2 x 1010 SARS-CoV-2 N2 copies per µL).

2.5 PLAQUE ASSAYS

Vero E6-TMPRSS2 cells were seeded in 6-well plates at a density of $1.2x10^6$ cells per well. The next day, cells were infected with 10-fold serial dilutions of infected sample or virus stock in maintenance medium with 0.2 mL per well and incubated for 1 h at 37°C with 5% CO2, rocking every 10 minutes to prevent the cells drying out. The inoculum was then removed, and the cells were washed with 1xDPBS. An overlay consisting of DMEM mixed with 2% FBS, 1% P/S, and 1% sea plaque agar was added to each well and the plates were incubated for two days at 37°C with 5% CO2. A similar overlay containing 2% Neutral Red (Sigma) stain was added to each well and plates were then incubated for another 24 hours whereupon plaques were counted, and titers calculated.

2.6 NEUTRALIZATION GROWTH KINETICS

Approximately $3x10^5$ Vero E6 cells were seeded per well in a 12 well plate in growth medium and incubated overnight at 37°C with 5% CO2. Next day, cells were washed twice with 1x DPBS then infected with virus diluted in maintenance medium 0.2 mL per well at an MOI of 0.02 in triplicate. Cells were incubated with virus for 1 h at 37°C with 5% CO2, rocking every 10 minutes to keep cells wet. The inoculum was then removed, and the cells washed twice more with 1x DPBS. Bispecific neutralizing anti-Spike antibody[3] diluted in maintenance medium to a concentration of 10 µg/mL was then added to the cells. Extracellular RNA was collected by transferring 200 µL to 800 µL TRIzol LS reagent in 2 mL screw cap O-ring tubes. Intracellular

RNA was collected by removing the remaining maintenance medium, washing twice with 1x DPBS, then adding 500 µL TRIzol. After 3-5 minutes, the TRIzol lysate was collected in 2 mL screw cap O-ring tubes. RNA was purified using the Direct-zol-96 MagBead RNA kit (Zymo) with a KingFisher Apex System (ThermoFisher Scientific). RT-qPCR was performed as described above with 20 ng RNA per reaction.

2.7 Reverse Transcription PCR and detection of Xbp1

To detect ER stress markers such as Xbp1, Chop, and Bip, HEK293T cells were seeded in 6 well plates at a density of $2x10^6$ and incubated overnight at 37°C with 5% CO2. Cells were then transfected by mixing 2 µg pXJ-nsp6 plasmids with 2 µL X-TremeGENE™ 360 transfection reagent in OptiMEM, incubated for 20-30 minutes at room temperature, then added dropwise to the cells without removing the growth medium. After 24 h post transfection, cells were collected by removing the growth medium, washing with 1x DPBS, then adding 300 µL TRIzol reagent (ThermoFisher Scientific), collecting the TRIzol in a 1.5 mL tube, then adding an additional 300 µL TRIzol to collect any remaining RNA. RNA was purified using the Direct-zol RNA Miniprep Plus Kits (Zymo) with a DNase I treatment, according to manufacturer's instructions. RNA was diluted in 50 µL nuclease-free water and stored at -80°C until ready for use. Reverse transcription PCR was performed using SuperScript™ IV One-Step RT-PCR system (ThermoFisher Scientific). Reactions were performed with technical duplicates according to manufacturer's instructions with 20 ng RNA per reaction. To amplify Xbp1 spicing variants, primers XBP1 fwd and XBP1 rev were used (Table 2.1)[4]. RT-qPCR was performed to quantify the ER stress markers Chop and Bip as described above using the primers BIP fwd BIP rev, CHOP fwd, and CHOP rev (Table 2.1). RPL19 was used as a housekeeping gene and amplified for both RT-PCR and RT-qPCR using the primers RPL19 fwd and RPL19 rev (Table 2.1).

2.8 SDS-PAGE and Western blots

HEK293T cells (1 x 10^6 cells/well) were seeded in a 6-well plate and incubated overnight. The next day, cells were transfected with 1 μg plasmid DNA using X-tremeGENE™ 360 Transfection Reagent (Sigma-Aldrich, St. Louis, MO) according to the manufacturer's instructions. The next day, cells were washed gently with DPBS and then lysed with immunoprecipitation (IP) lysis buffer [20 mM Tris, pH 7.5, 100 mM NaCl, 0.05% n-Dodecyl β-D-maltoside (Anatrace, Maumee, OH), and EDTA-free protease inhibitor cocktail (Roche)] for 5 minutes at room temperature then collected for SDS-PAGE.

Proteins were resolved by SDS polyacrylamide gel electrophoresis using a 4-15% Mini-PROTEAN® TGX Precast Protein Gel at 130 volts for 40 minutes. Proteins were transferred to a polyvinylidene difluoride (PVDF) membrane using a Trans-Blot Turbo Transfer System (Bio-Rad, Hercules, CA), washed with 1X TBS, then blocked for 1 hour with 5% skim milk in TBS then probed for FLAG tag (DYKDDDDK) using Mouse anti-FLAG (8146S; Cell Signaling Technology (CST), Danvers, MA; 1:2000), washed three times for ten minutes, then probed with secondary Goat anti-Mouse IgG-Peroxidase antibody (A4416; Sigma-Aldrich, 1:4000) and washed three times for ten minutes. Proteins were visualized with SuperSignal Femto Maximum Sensitivity Substrate (ThermoFisher Scientific) and imaged using ChemiDoc Imaging Systems (Bio-Rad). STAT1 and STAT2 proteins were detected with anti-STAT1 (14994S; CST) and anti-STAT2 (72604S; CST), and phosphorylated STAT1 and STAT2 proteins were detected with anti-pSTAT1 (7649S; CST) and anti-pSTAT2 (88410S; CST). GAPDH was detected using Rabbit anti-GAPDH (G9545; Sigma).

Table 2.1: Primers

Name	**Sequence (5’-3’)**
RPL19 fwd	ATGTATCACAGCCTGTACCTG
RPL19 rev	TTCTTGGTCTCTTCCTCCTTG
BIP fwd	CGGGCAAAGATGTCAGGAAAG
BIP rev	TTCTGGACGGGCTTCATAGTAGAC
CHOP fwd	ACCAAGGGAGAACCAGGAAACG
CHOP rev	TCACCATTCGGTCAATCAGAGC
XBP1 fwd	TTACGAGAGAAAACTCATGGC
XBP1 rev	GGGTCCAAGTTGTCCAGAATGC

Chapter 3: Mutations in SARS-CoV-2 Alpha Variant Impact IFN-I Sensitivity

3.1 Introduction

2019-nCoV/USA-WA1/2020 (WA1) was isolated from the first patient diagnosed with COVID-19 in the United States with a direct connection to Wuhan, China, and has become the prototypical strain used for SARS-CoV-2 experiments. WA1 was used as a wild-type control for the following experiments. Guo et al. demonstrated that the Alpha variant is less sensitive to IFN-I treatment *in vitro* and members of the Shi lab previous sly showed that various viral proteins antagonize both the IFN induction and IFN signaling pathways to prevent activation of innate immune responses and promote viral replication[5,6]. It is likely that specific mutations found in the Alpha variant contribute to reduced sensitivity to IFN-I; thus, Alpha mutations found in individual nsp6(ΔSGF), ORF3a(T223I), M(V70L), or N(D3L+R203K+G204R+S235F) genes were introduced individually into the WA1 backbone using a reverse genetics system described previously (Fig. 3.1; Table 3.1)[1,2]. The Alpha-Spike, which contains 3 amino acid deletions and 7 substitutions, and the full-length Alpha infectious clones were generated previously by members of the lab. Genes were selected based on previous results demonstrating a role in suppressing IFN-I production and/or IFN-I signaling pathways as well as the presence of mutations in the Alpha variant[6]. We suspected that a combination of viral proteins might work in concert to inhibit IFN-I pathways; thus, an infectious clone containing a combination of mutations found in ORF3a, M, and N (Alpha-3a.M.N) was developed. Another combination of Alpha-3a.M was unsuccessfully produced. Given the number of viruses that were successfully developed, the Alpha-3a.M was suspended to maintain a manageable workload for each experiment.

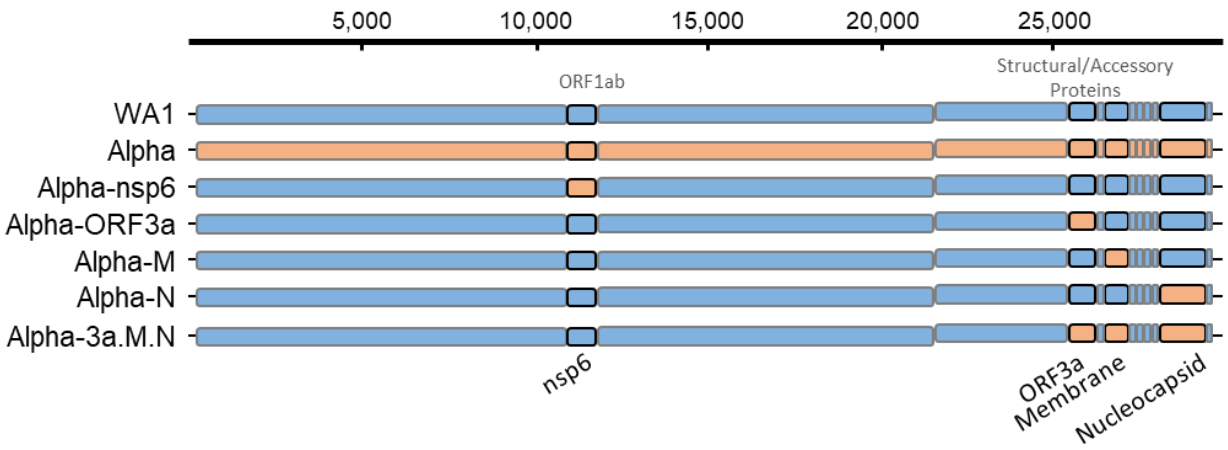

Figure 3.1: Schematic of mutant viruses containing Alpha mutations

Mutations from Alpha variant were introduced into the WA1 strain to generate multiple infectious clones to investigate which mutations might contribute to reduced IFN-I sensitivity seen in the Alpha variant. Vero E6-TMPRSS2 cells were electroporated with in vitro transcribed RNA. After about 20% cytopathic effect (CPE) was visible, supernatant was collected and stored at -80C or transferred to a new flask of cells to develop passage one virus for experiments.

Table 3.1: Selected Alpha mutations

Infectious clone	Mutation
Alpha-nsp6	Nsp6: delS106, delG107, delF108 (ΔSGF)
Alpha-ORF3a	ORF3a:T223I
Alpha-M	M: V70L
Alpha-N	N: D3L, R203K, G204R, S235F
Alpha-3a.M.N	ORF3a:T223I; M: V70L; N: D3L, R203K, G204R, S235F

3.2 RESULTS

3.2.1 Replication kinetics of Alpha mutants

Vero E6 cells stably expressing human TMPRSS2 (Vero E6-TMPRSS2) were selected for the following experiments due to susceptibility and permissiveness; TMPRSS2 is an important cofactor for viral infection and allows more rapid replication of virus stocks. After titrating the virus stocks, growth kinetics experiments were performed to compare replication of the mutant viruses to WA1 and Alpha. WA1 grew more rapidly than Alpha and peaked at 24 hours post-infection (hpi) with a peak titer of $6.7x10^6$ PFU/mL while Alpha did not peak until 36 hpi, but with a similar peak titer of $7x10^6$ PFU/mL (Fig. 3.2A). Similar to WA1, Alpha-ORF3a, Alpha-M, and Alpha-N all grew quickly by 12 h then peaked by 24 hpi, except Alpha-M peaked at 36 hpi (Fig. 3.2A). Alpha-3a.M.N grew quickly but peaked at 24 hpi with a peak titer of about $7x10^5$, 10-fold lower than WA, suggesting that this particular combination of mutations attenuates SARS-CoV-2 replication (Fig. 3.2A). Interestingly, similar to Alpha, mutant Alpha-nsp6 grew slower at 12 hours and peaked at 36 hpi. The peak titer was slightly lower than Alpha at $2.2x10^6$ PFU/mL (Fig. 3.2A).

Plaque morphologies of the mutant viruses corroborate differences in replication kinetics. On average, WA1 produces larger plaques (2.6 mm) in Vero E6-TMPRSS2 cells while Alpha produces smaller plaques (2.0 mm; Fig. 3.2B,C). Alpha-ORF3a (1.6 mm) and Alpha-M (1.8 mm) produced significantly smaller plaques than WA1 (Fig. 3.2B,C). Plaques produced by the combination mutant Alpha-3a.M.N were particularly small (1.3 mm) at about a full millimeter smaller than WA1 plaques (Fig. 3.2B,C). Alpha-nsp6 (2.4 mm) and Alpha-N (2.3 mm) plaques were on average slightly smaller than WA1 but the differences were not statistically significant (Fig. 3.2B,C). Together with the replication kinetics, these data suggest that the majority of Alpha mutations attenuate SARS-CoV-2 replication.

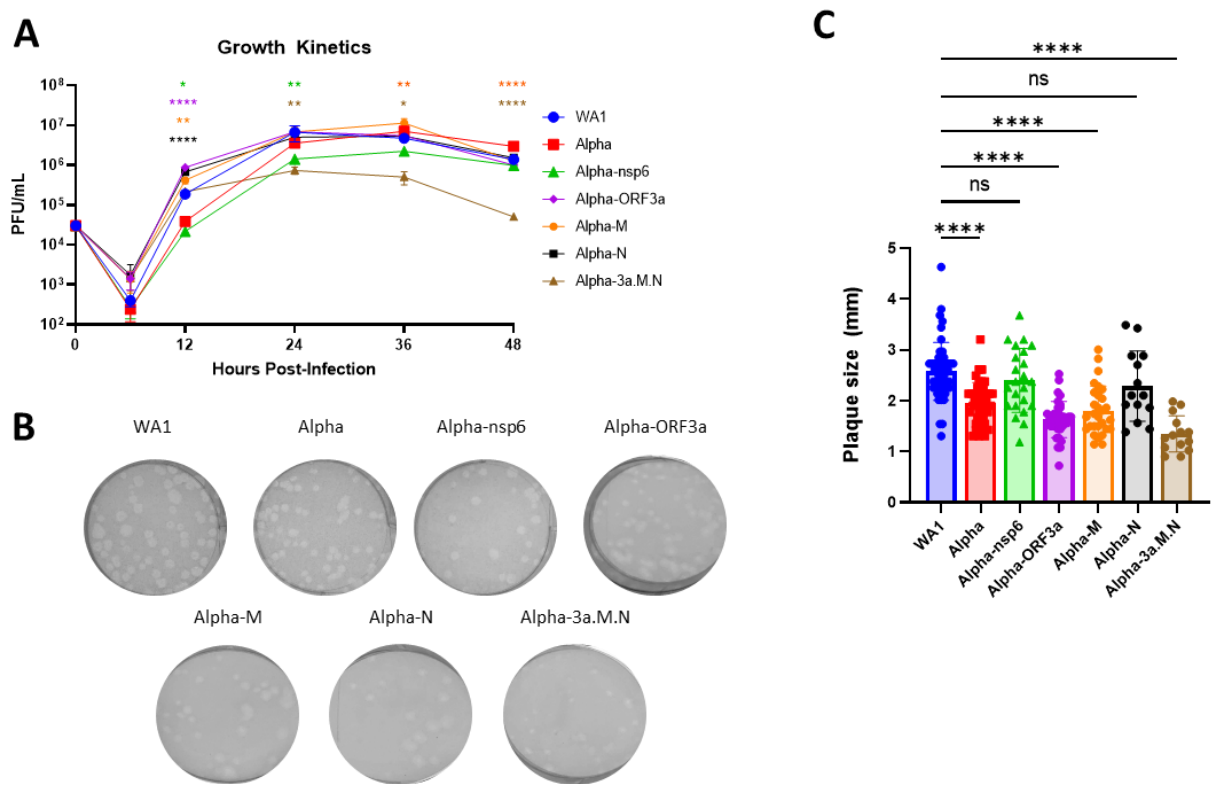

Figure 3.2: Comparing replication kinetics of viruses with Alpha mutations

(A) Growth kinetics experiment to analyze virus production over 48 hours. Vero E6-TMPRSS2 cells were infected at an MOI of 0.02 and supernatants collected for plaque assays. (B) Representative images of plaque sizes on Vero E6-TMPRSS2 cells and (C) measurements of plaques formed by the indicated SARS-CoV-2 viruses where each datapoint represents a single plaque from the same well. Significance for growth kinetics was determined using One-Way ANOVA at each timepoint, and significance for plaque measurements was determined using One-Way ANOVA. $p \leq 0.05$ (*), $p \leq 0.01$ (**), $p \leq 0.001$ (***), $p < 0.0001$ (****).

3.2.2 IFN-I sensitivity of Alpha mutants

To test IFN-I sensitivity of the infectious clones, Vero E6-TMPRSS2 cells were pre-treated for 16-18h with two-fold serial dilutions of IFN-α then infected for 1 h at 37°C with the mutant viruses at a low multiplicity of infection (MOI) of 0.02. Inoculum was then removed, the cells washed wash 1x DPBS, then maintenance medium with fresh IFN-α dilutions was replaced. Cells were pre-treated with IFN-α to see a more potent effect on viral replication and thereby see greater differences between the parental and mutant viruses. After 48 hours, the supernatant was harvested to evaluate levels infectious virus and viral RNA, using plaque assays and RT-qPCR, respectively. IFN-α treatment of SARS-CoV-2 WA1, Alpha, and Alpha mutants reduced virus titers in a dose-dependent manner. Comparison of raw virus titers demonstrates that Alpha and Alpha-nsp6 were significantly less susceptible to IFN-α treatment at 1000 U/mL (p-value: 0.0005 & 0.0199, respectively; Fig. 3.3A); however, after normalizing to the untreated controls (0 IFN-α U/mL), the difference between WA1 and Alpha-nsp6 was not statistically significant (Fig. 3.3B). None of the other Alpha mutants were significantly affected by IFN-α treatment, though Alpha-ORF3a does appear to be more sensitive to IFN-α, but this result was not significant either (Fig. 3.3A,B).

Comparison of viral RNA in the extracellular space corroborates the virus titer results. Replication of both WA1, Alpha, and mutant SARS-CoV-2 viral RNA was inhibited by IFN-α in a dose-dependent manner. Viral RNA from the Alpha variant appeared higher than WA1 but due to variability between replicates, the difference was not statistically significant (Fig.3.2)[7]. Mutant Alpha-M and Alpha-N mutations were also slightly higher than WA1, but the difference was not statistically significant (Fig.4B). Importantly, levels of viral RNA from Alpha-nsp6 were significantly higher than WA1 and matched the levels of Alpha SARS-CoV-2 at every dose of IFN-α, suggesting that Alpha nsp6 mutations reduce SARS-CoV-2 susceptibility to IFN-α treatment.

In this chapter, I demonstrate that Alpha and Alpha-nsp6 both grow more slowly than WA1 but plaques produced by Alpha-nsp6 on Vero-E6-TMPRSS2 cells are more similar to WA1. This

indicates that nsp6 plays a role in replication of the virus and the nsp6 mutation ΔSGF is responsible for the replication phenotype seen in Alpha. However, the larger Alpha-nsp6 plaques are likely due to the presence of the WA1 Spike protein which plays a larger role in infection of cells but not replication per se. I also validate previous studies showing that Alpha is less sensitive to IFN-α7. I showed that parental WA1 SARS-CoV-2 containing the nsp6 mutation ΔSGF as seen in Alpha contributes to reduced IFN-I sensitivity. Vero E6-TMPRSS2 cells were ideal for this experiment due to a deficiency in IFN-I production, however, repeating this experiment with additional cell lines such as A549-hACE2, Huh7, or CALU-3 would provide additional insight. Guo et al. originally performed the same experiment and showed that IFN-α subtype 2, as used in this study, reduced WA1 N1 RNA copies by about 300-fold and reduced Alpha N1 RNA copies by only about 10-fold, representing a 30-fold difference7. Here, a concentration of 500 U/mL reduced WA1 N2 RNA copies by 2.44x107 while Alpha and Alpha-nsp6 were reduced by 2.16x104 and 2.85x103, respectively. Therefore, Alpha and Alpha-nsp6 N2 RNA copies were reduced 1130- and 8,580-fold less than WA1. Furthermore, IFN-α subtype 2 was not the most potent of the tested subtypes, instead, IFN-β was consistently the most potent. However, IFN-α subtype 2 was used for these experiments because it utilizes the same signaling pathway as IFN-β, it showed a similar reduction in antiviral activity between WA1 and Alpha (~70-fold difference versus ~80-fold for IFN-β), and it was readily available in the lab.

From this point forward in the writing, Alpha-nsp6 will be referred to as ΔSGF-WA1.

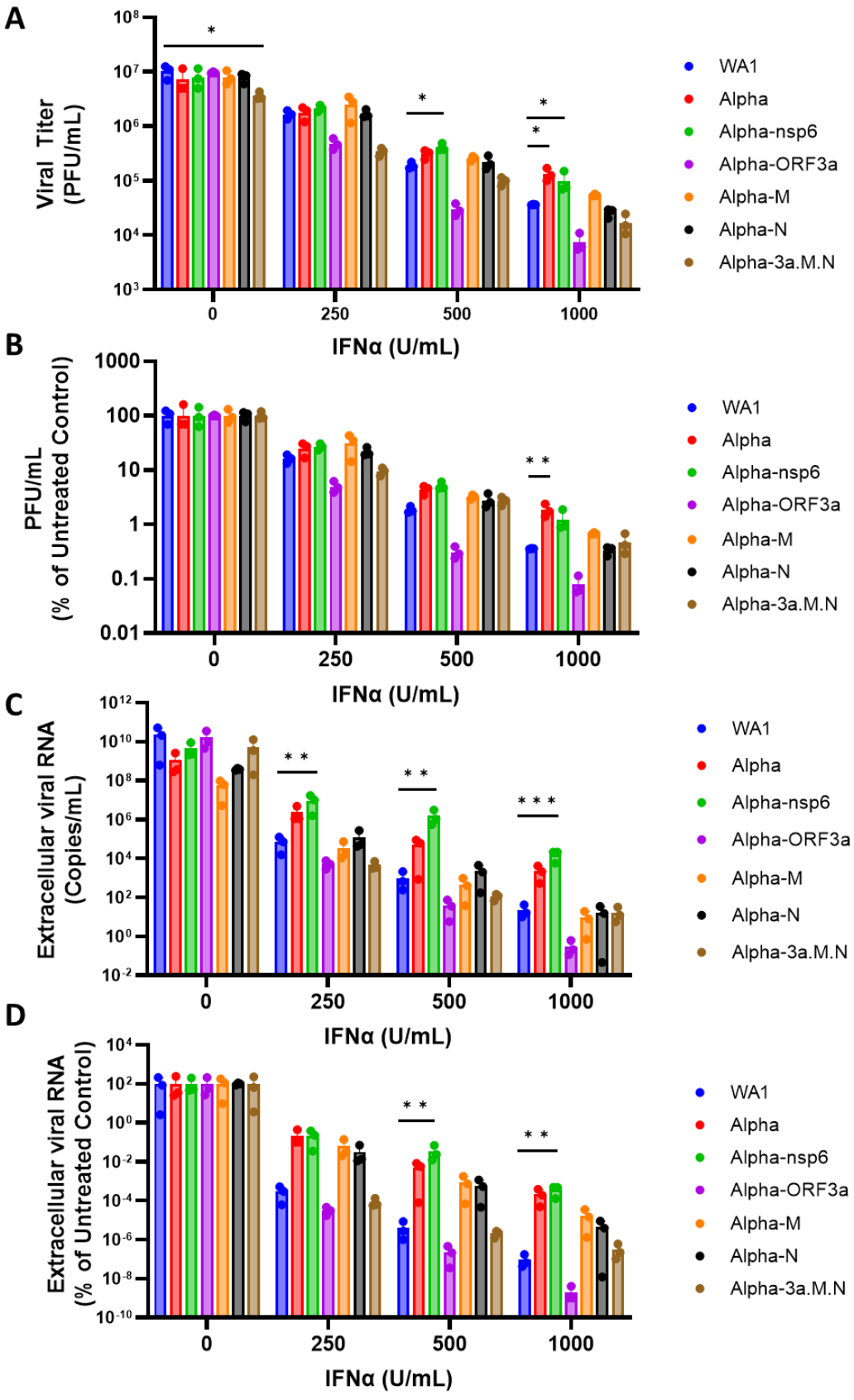
A
Viral Titer (PFU/mL)
IFNα (U/mL)
B
PFU/mL (% of Untreated Control)
IFNα (U/mL)
C
Extracellular viral RNA (Copies/mL)
IFNα (U/mL)
D
Extracellular viral RNA (% of Untreated Control)
IFNα (U/mL)
WA1
Alpha
Alpha-nsp6
Alpha-ORF3a
Alpha-M
Alpha-N
Alpha-3a.M.N

Figure 3.3: Various Alpha mutations influence IFN-I sensitivity of SARS-CoV-2

(A) Levels of extracellular viral RNA quantified by RT-qPCR using a standard curve and (B) normalized to the untreated controls (0 IFN-α U/mL). (C) Levels of infectious virus quantified by plaque assays and (D) normalized to the untreated controls. Vero E6-TMPRSS2 cells were pre-treated with 2-fold serial dilutions of IFN-α for 16-18 h then infected with SARS-CoV-2 mutants at MOI 0.02 for 1 h, whereupon the inoculum was removed and replaced with fresh dilutions of IFN-α. Significance for each concentration of IFN-α was determined using One-Way ANOVA with $p \leq 0.05$ (*), $p \leq 0.01$ (**), and $p \leq 0.001$ (***)

Chapter 4: Mutations in SARS-CoV-2 Variant nsp6 Enhance Type-I Interferon Antagonism[b]

4.1 Abstract

Severe acute respiratory syndrome coronavirus 2 (SARS-CoV-2) continues to evolve after its emergence. Given its importance in viral infection and vaccine development, mutations in the viral Spike gene have been studied extensively; however, the impact of mutations outside the Spike gene are poorly understood. Here, we report that a triple deletion (ΔSGF or ΔLSG) in nonstructural protein 6 (nsp6) independently acquired in Alpha and Omicron sublineages of SARS-CoV-2 augments nsp6-mediated antagonism of type-I interferon (IFN-I) signaling. Specifically, these triple deletions enhance the ability of mutant nsp6 to suppress phosphorylation of STAT1 and STAT2. A parental SARS-CoV-2 USA-WA1/2020 strain containing the nsp6 ΔSGF deletion (ΔSGF-WA1) shows reduced susceptibility to IFN-I treatment in vitro, outcompetes the parental strain in human primary airway cultures, and increases virulence in mice; however, the ΔSGF-WA1 virus is less virulent than the Alpha variant (which has the nsp6 ΔSGF deletion and additional mutations in other genes). Analyses of host responses from ΔSGF-WA1-infected mice and primary airway cultures reveal activation of pathways indicative of a cytokine storm. These results provide evidence that mutations outside the Spike protein affect virus-host interactions and may alter pathogenesis of SARS-CoV-2 variants in humans.

Keywords: SARS-CoV-2, variants, nsp6, interferon, cytokine storm

[b] This chapter: Bills CJ, Xia H, Chen JY-C, et al. Mutations in SARS-CoV-2 variant nsp6 enhance type-I interferon antagonism. *Emerging Microbes and Infections* Accepted 26Apr2023.

4.2 BACKGROUND

Severe acute respiratory syndrome coronavirus 2 (SARS-CoV-2) variants continue to emerge three years after SARS-CoV-2 was initially identified.[1–4] Due to the importance of the viral Spike protein in transmission and immunogenicity, COVID-19 vaccines utilize the Spike protein as the primary antigen.[5–9] Less attention has been devoted to studying the impact of variant mutations in nonstructural proteins (nsps) and accessory proteins and their roles in viral replication and pathogenesis.[9] Recent studies have reported the importance of non-spike mutations in promoting viral replication and antagonizing innate immune responses; for example, mutations in ORF8 were associated with increased virulence and antagonism of type-I interferon (IFN-I) pathways, exemplifying the need to understand the impact of non-spike mutations.[10–18]

Two-thirds of the SARS-CoV-2 genome encodes two polypeptides (pp1a and pp1ab) that are cleaved into 16 nsps to form the replication complex.[19,20] The remaining third of the genome encodes 7 accessory and 4 structural proteins.[19] Many SARS-CoV-2 nsps and accessory proteins antagonize the interferon type I (IFN-I) response.[21–25] Nsp6 specifically inhibits both IFN-I induction and signaling pathways *in vitro*.[21] The Alpha variant of SARS-CoV-2, which was first identified in late 2020 in the United Kingdom and circulated globally, was reported to be less susceptible to treatment with IFN-I and IFN-III compared to the ancestral strain.[26] Based on these findings, we hypothesized that mutations in Alpha nsp6 would contribute to increased IFN-I resistance in the Alpha variant and other emerging variants of SARS-CoV-2. Here, we demonstrate that a convergent deletion in the nsp6 genes of Alpha and Omicron variants of SARS-CoV-2 confers a fitness advantage through enhanced antagonism of IFN-I signaling.

4.3 METHODS

4.3.1 Ethics statement

Mouse studies were performed in accordance with the Care and Use of Laboratory Animals of the University of Texas Medical Branch (UTMB). The protocol (IACUC#: 2103023) received

approval from the Institutional Animal Care and Use Committee (IACUC) at UTMB. Animals were anesthetized using isoflurane prior to operations to minimize animal suffering. Infections were performed in ABSL-3 facilities at UTMB by trained personnel.

4.3.2 Cell Culture and Animal Care

African green monkey kidney epithelial cells expressing TMPRSS2 (Vero E6-TMPRSS2; purchased from SEKISUI XenoTech, LLC, Kansas City, KS) and human epithelial kidney cells (HEK293T; purchased from ATCC, Bethesda, MD) cells were cultured in high-glucose Dulbecco's modified Eagle's medium (DMEM; Gibco/Thermo Fisher, Waltham, MA, USA) supplemented with 10% fetal bovine serum (FBS; Hyclone Laboratories, South Logan, UT) and 1% penicillin/streptomycin (P/S; Gibco). All culture media and antibiotics were purchased from ThermoFisher Scientific (Waltham, MA). Primary human airway epithelial (HAE) cells and culture medium for HAE cells were purchased from MatTek Life Science (Ashland, MA, USA). All cell lines were maintained at 37°C with 5% CO_2 and tested negative for mycoplasma contamination. Female K18-hACE2 c57BL/6J (strain: 2B6.Cg-Tg(K18-ACE2)Primn/J) mice aged 8-10 weeks were purchased from Jackson Laboratory (Bar Harbor, ME) and housed in ABSL-3 facilities at UTMB. Animals were randomized and housed in groups of <5 mice per cage and fed standard chow. The ABSL-3 rooms were maintained between 68-74°F with 30%-60% humidity. Lights maintained day/night cycles of 12h intervals. Animals were allowed 3-4 days to acclimate before virus challenge.

4.3.3 Constructing SARS-CoV-2 WA1-ΔSGF

The stock of SARS-CoV-2 strain 2019-nCoV/USA_WA1/2020 was isolated from the first COVID-19 patient diagnosed in the U.S. and provided to the World Reference Center for Emerging Viruses and Arboviruses (WRCEVA) at the University of Texas, Medical Branch (UTMB, Galveston, TX, USA). An infectious clone of the Alpha variant (GISAID: EPI_ISL_999340) was previously constructed[27]. SARS-CoV-2 infectious clones were constructed

as previously described from a cDNA clone of USA-WA1/2020 and generated in Vero E6-TMPRSS2 cells.[28,29] All work following electroporation was performed in a biosafety level 3 (BSL3) laboratory.

4.3.4 IFN-I treatment of SARS-CoV-2

Vero E6-TMPRSS2 cells were seeded in 24-well plates (2 x 105 cells/well) and incubated for at least 5 h. Cells were pre-treated for 16-18 h with IFN-α (Millipore, Darmstadt, Germany) diluted in 10% FBS DMEM. Cells were washed with DPBS and then infected at MOI 0.02 with 0.2 mL WA1 or ΔSGF-WA1 diluted in 2% FBS DMEM medium and incubated for 1 h at 37°C with 5% CO2. Inoculum was removed and cells were washed with DPBS then fresh IFN-α diluted in 2% FBS DMEM medium was added. After 48 h incubation, supernatants were harvested for plaque assays and RT-qPCR.

4.3.5 Plaque Assays and Reverse transcription quantitative PCR

Infectious virus from experiments was quantified using plaque assays performed as previously described using Vero E6-TMPRSS2 cells.[30]

To quantify viral RNA *in vitro*, 0.2 mL infected culture supernatants were harvested 48 h post-infection and added to 4 volumes of Trizol LS Reagent (Thermo Fisher Scientific). RNA was purified using Direct-zol RNA Miniprep Plus Kits (Zymo, Irvine, CA) according to the manufacturer's instructions, eluted in 50 μL nuclease-free water, then amplified using iTaq™ Universal SYBR® Green One-Step Kit (Bio-Rad) with QuantStudio™ 7 Flex system (ThermoFisher Scientific). The Ct values of the N gene were normalized to the Ct values of the M-GAPDH for mouse lung tissues or HuGAPDH for HAE cells. Table S1 summarizes the sequences for primer sets.

4.3.6 Mouse challenge

To compare variants *in vivo*, 8-week-old female K18-hACE2 mice were anesthetized with isoflurane and then challenged intranasally with 50 μL (25 μL per nostril) inoculum of WA1 or ΔSGF-WA1 virus normalized to 10^3 PFU/dose. For day 2, ten mice were in each infection group; for days 4 and 6, 14 mice were included in each group; four mice were mock infected, totalling 80 mice (Fig. 2D-F). For survival experiments, ten mice were included in each group, totalling 40 mice (Fig. 2G,2H). After inoculation, the K18-hACE2 mice were weighed daily and evaluated and scored based on visible indicators until the termination of the experiment. At the end of the experiment, mice were anesthetized and tissue samples were collected in 2 mL tubes containing PBS for plaque assays or TRIzol Reagent for RNA purification and stored at -80°C until use. Tissues were weighed and then processed by homogenizing with glass beads for 60 seconds at 6000 rpm using a MagNA Lyser (Roche Diagnostics) and centrifuged for 5 minutes at 10,000 rpm. Supernatants were transferred to fresh tubes for downstream analysis and then stored at -80°C. RNA was purified using the Direct-zol-96 MagBead RNA kit (Zymo) with a KingFisher Apex System (ThermoFisher Scientific).

4.3.7 Histology

Left lungs from mice were harvested on days 4 and 6 and fixed in 10% buffered formalin solution for 7 days. The lung tissues were embedded in paraffin and cut into sections 5 μm thin to mount on slides, then stained with hematoxylin and eosin (H&E) on a SAUKRA VIP6 processor at the UTMB Histology Laboratory. Histology slides were scored by an independent histopathologist.

4.3.8 Competition Assays

HAE cells were infected with a mix of the WA1 or mutant virus with an equal MOI of 0.4 and samples were collected as previously described.[30] For analysis, RNA was purified from each sample and cDNA fragments corresponding to codon positions 72-147 of nsp6 were generated

using the SuperScript™ IV One-Step RT–PCR System. See Supplementary Information for primer sets.

4.3.9 IFN-I induction and signaling luciferase assays

Luciferase assays were performed as previously described,[21,31] except plasmids were transfected into $1x10^5$ HEK293T cells using X-treme-GENE™ 360 (Roche, Mannheim, Germany) with a ratio of 1:1.

4.3.10 SDS-PAGE and Western blots

Exogenous expression of viral proteins and endogenous proteins were detected using Western blots as previously described.[21]

4.3.11 Analysis of nCounter Analysis System (NanoString) Data

RNA was purified from mouse lung tissues as described above and concentrations were normalized to 20 ng/μL. The RNA was prepared and analyzed using the nCounter Pro Analysis System and the nSolver Analysis Software. All plots in Figure 3 were made using R version 4.1.2. The NanoString nCounter platform was used to profile gene expression in virus infected samples. The normalized quantities of transcripts were measured using the CodeSets nCounter Mouse Host Response Panel (NS_Mm_HostResponse_v1.0) and nCounter Human Host Response Panel (NS_Hs_HostResponse_v1.). These panels include genes related to host susceptibility, interferon response, innate immune cell activation, adaptive immune response, and homeostasis. An un-adjusted p-value cutoff of 0.05 was used to determine differentially expressed genes (DEGs).Using a Benjamini-Hochberg adjusted p value threshold of 0.05, few genes in nsp6 mutant vs wild-type comparisons were deemed significant due to the available sample size and magnitude of phenotypic difference between the two viruses. In order to identify biological processes that may be involved but with a greater likelihood of false positive signals, we continued pathway analysis using an unadjusted p value threshold of 0.05.

An additional log2 fold change cutoff of + or – 0.6 was used to label up- and down-regulated genes in volcano plots for each condition. The Venn diagram for differentially expressed genes across conditions was made using the 'ggvenn' package version 0.1.9. The 'biomaRt' package version 2.50.3 was used to convert between human and mouse gene names to detect overlapping DEGs. Ingenuity pathway analysis (version 84978992) core analysis was performed on each condition based on gene p values with an unadjusted threshold of 0.05. The User Dataset (corresponding to the nCounter Analysis target geneset) was used as the reference set. Canonical pathway and upstream regulator data was derived from a comparison analysis including mouse day 2 & 4, and human airway epithelial day 2 groups. -log(p-values) and z-scores were used to generate the bubble plot, using ascending p-value or descending -log(p-value) for ordering. Analysis of upstream regulators did not yield significant results.

4.3.12 Statistical Analysis

Data are presented as means ± standard deviations. Statistical significance was performed using Student's T-test, One-Way ANOVA, or a Log-rank Mantel-Cox test calculated with the software Prism 9 (GraphPad) version 9.5.0.

4.3.13 Data Availability

The data supporting these findings are available upon request from the corresponding authors.

4.4 RESULTS

4.4.1 Deletions in the nsp6 105-108 region arose independently in SARS-CoV-2 variants

SARS-CoV-2 WA1 strain was isolated from the first imported COVID-19 patient in the United States, and is the standard strain used for SARS-CoV-2 experiments.[1,2] Alignment of nsp6 sequences reveals a convergent deletion of amino acids 106-108 (ΔSGF) in Alpha and Omicron sublineages (BA.2, BA.4, BA.5; Fig. 1A). Notably, Omicron BA.1 also contains a deletion that is shifted to 105-107 (ΔLSG) as well as a unique I189V mutation. Delta nsp6 contains only a unique V149A change, suggesting that ΔSGF and ΔLSG emerged independently in the Alpha and Omicron sublineages and such deletions may have biological functions and consequences. Sequence analysis showed that ΔSGF and ΔLSG were present in 42% and 19% of the ~15 million GISAID sequences, respectively. ΔSGF was prevalent in at least 95% of contemporary sequences, including XBB.1.5, CH.1.1, and BQ.1.1, whereas ΔLSG accounted for <0.5% (Table S2).[32]

The nsp6 structure is predicted to form 7 transmembrane domains[12]. The last domain is amphipathic and may associate with, but does not traverse, the membrane. Thus, both the N- and C-termini lie in the cytoplasm (Fig. 1B).[12,33] The 105-108 region, where ΔSGF and ΔLSG deletions occur, lies in an unstructured lumenal loop between transmembrane domains 3 and 4 (Fig. 1B), a region thought to play a role in nsp6-mediated ER zippering.[12,33]

4.4.2 ΔSGF-WA1 SARS-CoV-2 replicates like the Alpha variant

To investigate the biological function of nsp6 mutations, we introduced ΔSGF into WA1 SARS-CoV-2 (ΔSGF-WA1) using a reverse genetics system described previously (Fig. 1C).[28,29] We first sought to compare the replication of ΔSGF-WA1 to WA1 and Alpha in IFN-I production-deficient Vero E6-TMPRSS2 cells. Mutant ΔSGF-WA1 produced plaques similar to WA1, but slightly larger than Alpha (Fig. 1D, 1E). In a replication kinetics experiment, WA1 titers peaked at 24 h, while Alpha and ΔSGF-WA1 peaked at 36 h and maintained peak titers for slightly

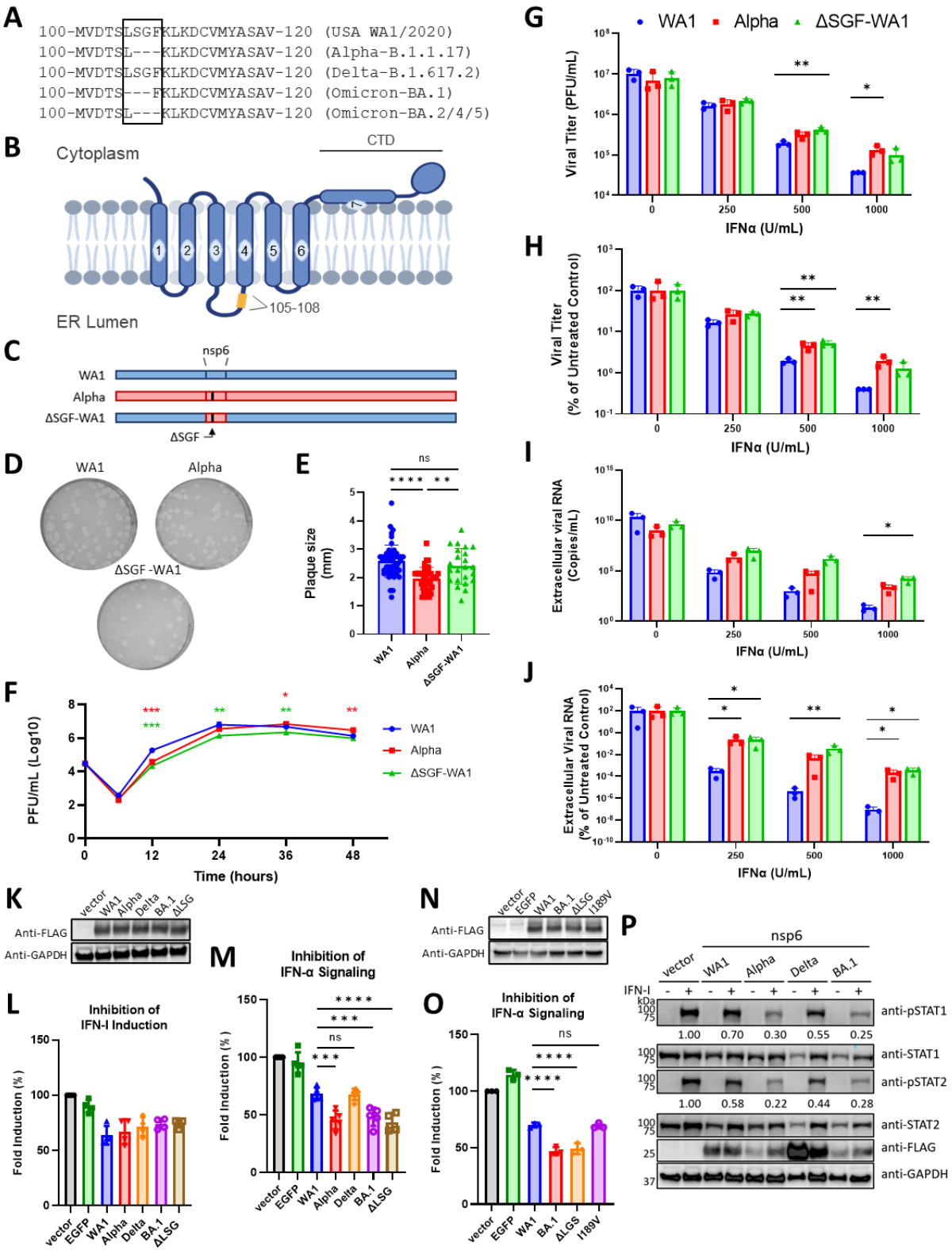
A
100-MVDTSLSGFKLKDCVMYASAV-120 (USA WA1/2020)
100-MVDTSL---KLKDCVMYASAV-120 (Alpha-B.1.1.17)
100-MVDTSLSGFKLKDCVMYASAV-120 (Delta-B.1.617.2)
100-MVDTS---FKLKDCVMYASAV-120 (Omicron-BA.1)
100-MVDTSL---KLKDCVMYASAV-120 (Omicron-BA.2/4/5)
B
Cytoplasm
CTD
ER Lumen
105-108
C
nsp6
WA1
Alpha
ΔSGF-WA1
ΔSGF
D
WA1
Alpha
ΔSGF -WA1
E
Plaque size (mm)
F
PFU/mL (Log10)
Time (hours)
WA1
Alpha
ΔSGF-WA1
G
WA1
Alpha
ΔSGF-WA1
Viral Titer (PFU/mL)
IFNα (U/mL)
H
Viral Titer (% of Untreated Control)
IFNα (U/mL)
I
Extracellular viral RNA (Copies/mL)
IFNα (U/mL)
J
Extracellular Viral RNA (% of Untreated Control)
IFNα (U/mL)
K
vector
WA1
Alpha
Delta
BA.1
ΔLSG
Anti-FLAG
Anti-GAPDH
L
Inhibition of IFN-I Induction
Fold Induction (%)
M
Inhibition of IFN-α Signaling
Fold Induction (%)
N
vector
EGFP
WA1
BA.1
ΔLGS
I189V
Anti-FLAG
Anti-GAPDH
O
Inhibition of IFN-α Signaling
Fold Induction (%)
P
nsp6
vector
WA1
Alpha
Delta
BA.1
IFN-I
anti-pSTAT1
1.00 0.70 0.30 0.55 0.25
anti-STAT1
anti-pSTAT2
1.00 0.58 0.22 0.44 0.28
anti-STAT2
anti-FLAG
anti-GAPDH

Figure 4.1: ΔSGF and ΔLSG enhance nsp6 suppression of IFN-I signaling

(A) Alignment of parental and variant nsp6 amino acid sequences of the region containing the independently acquired triple deletions. Delta nsp6 contains a unique V149A mutation and BA.1 nsp6 contains I189V in addition to ΔLSG. (B) Diagram of the predicted structure of nsp6 with enumerated transmembrane domains and the 105-108 region, where ΔSGF and ΔLSG occur, highlighted in yellow. (C) Schematic of the parental WA1, Alpha variant, and mutant ΔSGF-WA1 infectious clone generated by reverse genetics. (D) Representative images of plaque morphologies and (E) comparison of average plaque sizes. (F) Viral titers from a growth kinetics experiment where Vero E6-TMPRSS2 cells were infected at MOI 0.02 and supernatants were collected for plaque assays. (G) Raw viral titers from supernatants of Vero E6-TMPRSS2 cells infected with SARS-CoV-2 viruses at MOI 0.02 and treated with 2-fold serial dilutions of IFN-α. (H) Viral titers from (G) presented as a percent of untreated controls (0 IFN-α U/mL). (I) Extracellular viral RNA from supernatants of IFN-α treated quantified by RT-qPCR using a standard curve. (J) Extracellular viral RNA from (I) normalized to untreated controls (0 IFN-α U/mL). (G-J) Data are representative of three replicate experiments. (K) Western blot validating protein expression of nsp6 variant genes from pXJ plasmids in HEK293T cells. (L) IFN-α induction assay and (M) IFN-α signaling assay in HEK293T cells; values represent measured Firefly luciferase signals normalized to Renilla luciferase signals then cells transfected with normalized to the vector control; data are combined from at least three replicate experiments; no statistical differences were detected for (L). (N) Western blot demonstrating expression of nsp6 variant genes from pXJ plasmids in HEK293T. (O) IFN-α signaling assay in HEK293T cells presented as in (M). (P) Representative Western blot from three replicate experiments measuring levels of phosphorylated STAT1 or STAT2 (pSTAT1 or pSTAT2) in cells transfected with respective variant nsp6 genes and treated with IFN-α; values represent fold change of pSTAT1 or pSTAT2 for each variant nsp6 gene relative to vector control and normalized to GAPDH. Significance was determined using One-Way ANOVA with ns (not significant), $p \leq 0.05$ (*), $p \leq 0.01$ (**), and $p \leq 0.001$ (***). Diagram (B) was created using BioRender. Additional figures created using GraphPad Prism 9.

longer than WA1 (Fig. 1F). Thus, ΔSGF-WA1 replication appears to resemble Alpha SARS-CoV-2 more than WA1.

4.4.3 ΔSGF-WA1 mutant is less susceptible to IFN-I treatment

We next examined whether ΔSGF-WA1 showed reduced susceptibility to IFN-α treatment as observed with the Alpha variant in previous studies.[26] Vero E6-TMPRSS2 cells were pre-treated with IFN-α and subsequently infected with WA1, Alpha, or ΔSGF-WA1 SARS-CoV-2. Both ΔSGF-WA1 and Alpha produced significantly higher titers than WA1 when treated with 500 or 1000 U/mL of IFN-α (p-values: 0.0044, 0.0218; Fig. 1G). After normalizing virus titers to the untreated controls, ΔSGF-WA1 replicated to significantly higher levels than WA1 at 500 U/mL of IFN-α (Fig. 1H). Raw extracellular viral RNA levels were higher for ΔSGF-WA1 compared to WA1 when treated with 1000 U/mL of IFN-α (p-value: 0.0176; Fig. 1I), and normalized extracellular ΔSGF-WA1 RNA was consistently higher than WA1 at every IFN-α concentration (Fig. 1J). The overall data suggest that ΔSGF reduced IFN-α sensitivity of the Alpha variant.

4.4.4 Deletions in the 105-108 region of nsp6 augment antagonism of IFN-I signaling

To understand how variant nsp6 mutations contribute to IFN-α resistance, we performed an IFN-I induction assay as previously described.[21,31] Briefly, we cloned nsp6 genes from WA1, Alpha (ΔSGF), Delta (V149A), and Omicron BA.1 (ΔLSG+I189V) variants into a pXJ expression plasmid with a C-terminal FLAG tag (Fig. 1K). To determine whether BA.1 ΔLSG has the same effect as Alpha ΔSGF, we also cloned a ΔLSG nsp6 plasmid. To evaluate IFN-I production, the nsp6 gene plasmids were co-transfected into HEK293T cells with (i) a plasmid encoding a firefly luciferase gene controlled by the IFN-β promoter, (ii) a plasmid containing the RIG-I gene with a CARD domain, which renders the expressed RIG-I constitutively active, and (iii) a plasmid expressing Renilla luciferase to normalize transfection efficiencies. An empty pXJ plasmid and pXJ-EGFP were transfected as controls. At 24 h post-transfection, luciferase signals were measured to quantify the effect of nsp6 protein on IFN-β promoter activity. As expected, WA1

nsp6 reduced luciferase signals by about 36% (Fig. 1L). The luciferase signals from the Alpha (ΔSGF), Delta (V149A), and BA.1 (ΔLSG+I189V or ΔLSG) nsp6-expressing cells were not significantly different from the WA1 nsp6-expressing cells (Fig. 1L). The results suggest that nsp6 mutations do not affect nsp6's antagonism of IFN-I induction.

Next, we tested whether the nsp6 mutations modulate IFN-I signaling. Using a similar luciferase assay, we co-transfected HEK293T cells with three plasmids: (i) an nsp6-expressing plasmid, (ii) a firefly luciferase plasmid regulated by the ISRE promoter, and (iii) a control Renilla luciferase plasmid. The transfected cells were treated with 250 U/mL of IFN-α to determine whether variant nsp6 proteins repress ISRE promoter activity, as measured by the luciferase signal. As expected,[21] the WA1 nsp6 reduced luciferase signals by 32%; Alpha (ΔSGF), BA.1 (ΔLSG+I189V), and BA.1 (ΔLSG) nep6 reduced luciferase signals by 55%, 52%, and 56%, respectively (Fig. 1M). Repression of IFN-α signaling by Delta (V149A) nsp6 was not different from WA1 (Fig. 1M). These results suggest that both ΔSGF and ΔLSG mutations enhance nsp6 antagonism of IFN-α signaling, which may drive IFN-α resistance in the Alpha variant and likely Omicron sublineages.

To validate whether the ΔLSG mutation found in BA.1 nsp6 indeed contributes to enhanced antagonism of IFN-α signaling, we constructed an additional plasmid expressing BA.1 (I189V) nsp6 without the ΔLSG mutation (Fig. 1N) and repeated the IFN-α signaling assay as above (Fig. 1M). As expected, inhibition of IFN-α signaling by BA.1 (I189V) nsp6 was comparable to WA1 nsp6 while IFN-α signaling was reduced significantly more by BA.1 (ΔLSG) nsp6 (Fig. 1O). These data confirm the results above and demonstrate that a triple deletion in the 105-108 region of nsp6 enhances inhibition of IFN-α signaling.

4.4.5 ΔSGF and ΔLSG augment the suppression of STAT1 and STAT2 phosphorylation

We previously showed that nsp6 represses the IFN-I signaling pathway by blocking phosphorylation of STAT1 and STAT2.[21] So, we hypothesized that Alpha and Omicron nsp6

would more potently block STAT1 and STAT2 phosphorylation. To test this hypothesis, we transfected HEK293T cells with variant nsp6 plasmids or a vector control, treated the cells with IFN-α, and analyzed phosphorylation of STAT1 and STAT2 using Western blotting. WA1 nsp6 reduced STAT1 and STAT2 phosphorylation by 30% and 42%, respectively (Fig. 1P). Alpha (ΔSGF), Delta (V149A), and BA.1 (ΔLSG+I189V) nsp6 further reduced phosphorylation of both STAT1 by 70%, 45%, and 75%, respectively; and STAT2 by 78%, 56%, and 72% (Fig. 1P). These results demonstrate that Alpha and Omicron nsp6 more efficiently reduce phosphorylation of STAT1 and STAT2 compared to controls; Delta, which lacks the 105-108 deletion, reduced STAT1 and STAT2 phosphorylation slightly more than WA1, but not to the same degree as Alpha or Omicron (Fig. 1P). This might suggest that the unique V149A mutation in Delta nsp6 still enhances the blockage of STAT1 and STAT2 phosphorylation, but not as well as ΔSGF and ΔLSG. Altogether, these data demonstrate that ΔSGF and ΔLSG in the 105-108 region of nsp6 enhance its antagonism of IFN-α signaling by more efficiently suppressing phosphorylation of STAT1 and STAT2.

4.4.6 ΔSGF-WA1 outcompetes WA1 in primary human airway epithelial cells

To evaluate ΔSGF-WA1 replication in a more relevant cell line, we infected primary human airway epithelial (HAE) cells. After 96 h, ΔSGF-WA1 infectious titers and extracellular viral RNA were comparable to WA1 at each timepoint (Fig. 2A, 2B). However, intracellular ΔSGF-WA1 viral RNA was significantly higher than WA1 after 48 and 72 hpi (Fig. 2C). The higher levels of intracellular ΔSGF-WA1 RNA could result from improved antagonism of IFN-I responses; however, it's unclear why ΔSGF-WA1 does not produce higher levels of extracellular viruses. Previous reports indicate that ΔSGF improves nsp6-mediated formation of replication organelles, providing better protection of replicating RNA from immune sensors and thus leading to higher levels of intracellular viral RNA;[12,34–39] however, the enhanced replication organelles may reduce the efficiency of virion assembly and/or release. Future experiments are needed to test these hypotheses.

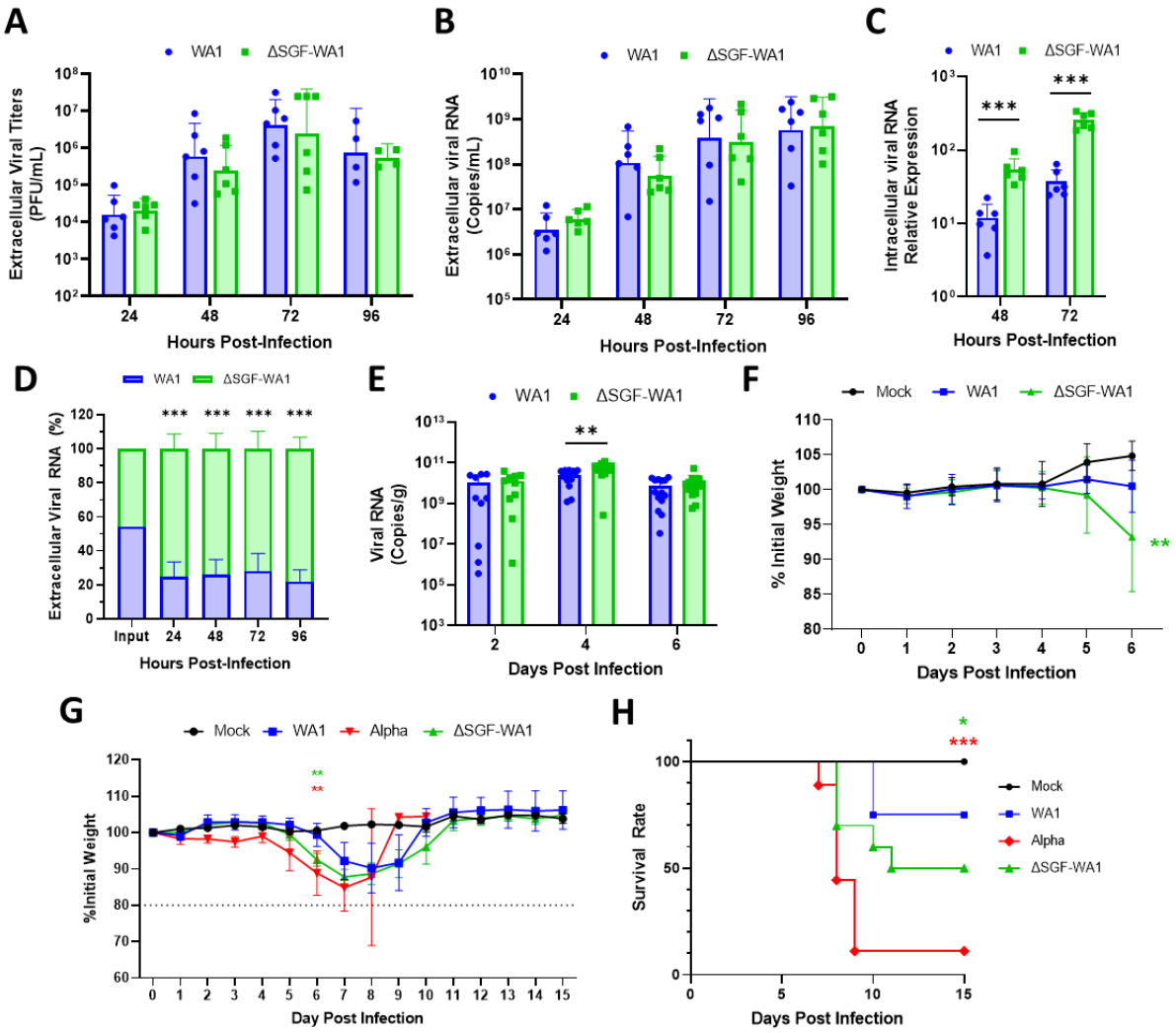
A
WA1
ΔSGF-WA1
Extracellular Viral Titers (PFU/mL)
Hours Post-Infection
B
Extracellular viral RNA (Copies/mL)
C
Intracellular viral RNA Relative Expression
D
Extracellular Viral RNA (%)
Input
E
Viral RNA (Copies/g)
Days Post Infection
F
Mock
% Initial Weight
G
Alpha
%Initial Weight
Day Post Infection
H
Survival Rate

Figure 4.2: ΔSGF-WA1 outcompetes WA1 in HAE cells and augments disease severity in mice

(A) Extracellular viral titers and (B) levels of viral RNA over 96 hours from supernatants of infected HAE cells at MOI 0.4 using (A) plaque assays and (B) RT-qPCR with a standard curve. (C) Levels of intracellular viral RNA from infected HAE cell lysates normalized to GAPDH. (D) Competition assay from the supernatants of HAE cells infected with equal MOI of WA1 and ΔSGF-WA1. Copy numbers of each virus were quantified using next-generation sequencing and are presented as percentages of the total number of viral copies. (E) Viral titers from infected mouse lung tissues normalized to tissue weights measured by plaque assays. (F) Viral RNA from mouse lung tissues normalized to tissue weights measured by RT-qCPR. (G) Average weights of mice infected with WA1 SARS-CoV-2 or ΔSGF-WA1 measured daily up to day 6. Significance is based on a comparison of ΔSGF-WA1 to WA1. (H) Average weights of infected mice and (I) survival curves over 15 days. Mice were humanely euthanized if the weight dropped below 80% of the initial weight (dashed line). Significance was determined using Student's T-test for each timepoint to compare mutants to WA1 or using a Log-rank Mantel-Cox test for survival curves with $p \leq 0.05$ (*), $p \leq 0.01$ (**), and $p \leq 0.001$ (***). Figures created using Prism.

To improve the sensitivity of viral fitness experiments, we performed a competition assay by infecting HAE cells with both WA1 and ΔSGF-WA1 with an equal MOI of 0.4. Next-generation sequencing was used to quantify the proportion of two viral RNA species. In contrast to the non-competition experimental results (Fig. 2A, 2B), the competition assay showed that ΔSGF-WA1 outcompeted WA1 by 24 hpi (Fig. 2D); the discrepancy is most likely caused by the difference in experimental sensitivity. The competition assay has been proven more sensitive to compare viral fitness due to the elimination of host-to-host variation.[40–43]

4.4.7 ΔSGF-WA1 SARS-CoV-2 is more virulent than WA1, but less than Alpha variant, in K18-hACE2 mice

To examine whether ΔSGF affects the *in vivo* virulence of SARS-CoV-2, we infected K18-hACE2 mice with 10^3 PFU WA1 or ΔSGF-WA1, and quantified the lung viral loads at different days post-infection (dpi). ΔSGF-WA1 generated significantly more lung viral RNA than WA1 at 4 dpi ($p = 0.0031$) and a similar trend was observed at 2 and 6 dpi, but the differences were not statistically significant ($p = 0.6455$ and $p = 0.3746$, respectively; Fig. 2E). Interestingly, mice infected with ΔSGF-WA1 lost significantly more weight by 6 dpi than WA1-infected mice ($p = 0.0040$; Fig. 2F). However, histopathology analysis of the infected lungs revealed similar histopathology scores at 4 and 6 dpi (Fig. S1), suggesting that infections with WA1 or ΔSGF-WA1 develops similar severity of lung pathology.

To further analyze disease severity in ΔSGF-WA1-infected mice, we performed a 15-day experiment to compare weight loss and survival rates of mice intranasally inoculated with WA1, ΔSGF-WA1, or full-length Alpha variant. Both Alpha- ($p = 0.0039$) and ΔSGF-WA1-infected mice ($p = 0.0084$) began losing weight on day 5 and, by day 6, had already lost significantly more weight than WA1-infected mice (Fig. 2G). Mice infected with ΔSGF-WA1 did not fully recover until approximately day 11, while WA1-infected mice recovered by day 10, representing a disease period of 6 and 4 days for ΔSGF-WA1- and WA1-infected mice, respectively (Fig. 2G). Alpha-infected mice experienced a greater average weight loss (15.2%) than ΔSGF-WA1- (12.2%) and

WA1-infected mice (7.8%; Fig. 2G). An accurate estimate of the disease period for the Alpha variant cannot be determined because, by day 9, the survival rate for Alpha-infected mice was only 10% (Fig. 2H). Mice infected with WA1 or ΔSGF-WA1 had a 75% or 50% survival rate, respectively (Fig. 2H). Together, these results indicate that ΔSGF-WA1 is more virulent in mice than WA1, but less virulent than Alpha.

4.4.7 Upregulation of cytokine storm in ΔSGF-WA1-infected mice and HAE cells

To understand how nsp6 ΔSGF affects host responses to SARS-CoV-2 infection, we compared mRNA expression of 785 host genes from lung tissues of WA1- and ΔSGF-WA1-infected mice, as well as infected HAE cells, using the probe-based nCounter Analysis System. These analyses revealed a total of 43, 57, and 12 differentially expressed genes in ΔSGF-WA1-infected mouse lung tissues on 2, 4, and 6 dpi, respectively, and 85 differentially expressed genes in ΔSGF-WA1-infected HAE cells at 2 dpi, compared to WA1 infections (Fig. 3A). Of these, 26 total genes were shared between different pairwise groups (Fig. 3B). Ingenuity Pathway Analysis (IPA) identified “Pathogen Induced Cytokine Storm Signaling Pathway” as a significantly altered host pathway for three datasets that was initially downregulated 2 dpi in mouse tissues, then significantly upregulated 4 dpi in ΔSGF-WA1-infected mouse tissues and 2 dpi in HAE cells (Fig. 3C). Additional pathways identified by IPA support this finding, namely, IL-17 and NOD1/2 signaling pathways, which also contribute to cytokine storms, were significantly upregulated in ΔSGF-WA1-infected mice and HAE cells (Fig. 3C). It should be noted that pathways from day-2 mouse tissues reveal a distinct pattern from the other data sets, suggesting a dynamic and complex *in vivo* virus-host interaction network.

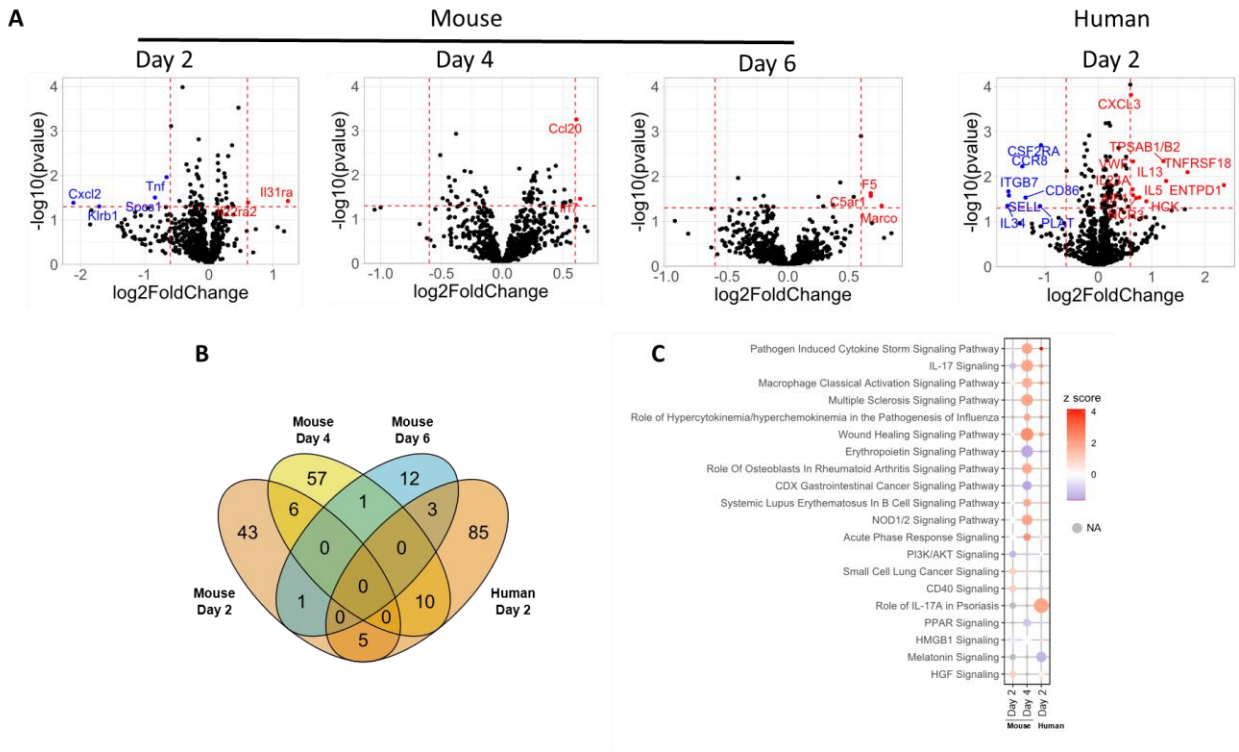
A
Mouse
Human
Day 2
Day 4
Day 6
Day 2
-log10(pvalue)
log2FoldChange
Cxcl2
Tnf
Spon1
Klrb1
Il22ra2
Il31ra
Ccl20
F5
C5ar1
Marco
CXCL3
TPSAB1/B2
CSF2RA
CCR8
VWF
IL13
TNFRSF18
ITGB7
CD86
IL5
ENTPD1
SELL
HCK
IL34
PLAT
B
Mouse Day 4
Mouse Day 6
Mouse Day 2
Human Day 2
57
12
43
85
6
1
3
0
0
0
1
10
0
0
5
C
Pathogen Induced Cytokine Storm Signaling Pathway
IL-17 Signaling
Macrophage Classical Activation Signaling Pathway
Multiple Sclerosis Signaling Pathway
Role of Hypercytokinemia/hyperchemokinemia in the Pathogenesis of Influenza
Wound Healing Signaling Pathway
Erythropoietin Signaling Pathway
Role Of Osteoblasts In Rheumatoid Arthritis Signaling Pathway
CDX Gastrointestinal Cancer Signaling Pathway
Systemic Lupus Erythematosus In B Cell Signaling Pathway
NOD1/2 Signaling Pathway
Acute Phase Response Signaling
PI3K/AKT Signaling
Small Cell Lung Cancer Signaling
CD40 Signaling
Role of IL-17A in Psoriasis
PPAR Signaling
HMGB1 Signaling
Melatonin Signaling
HGF Signaling
z score
NA
Day 2
Day 4
Day 2
Mouse
Human

Figure 4.3: ΔSGF alters host responses causing extensive cytokine expression

(A) Volcano plots from NanoString data for mouse whole lung specimens and human airway epithelial cultures (HAE) at specified days post infection. All comparisons are between nsp6 mutant and WT. Horizontal dotted line corresponds to a p-value cutoff of 0.05 and vertical lines correspond to -0.6 and 0.6 log2(fold change). (B) Venn diagram of differentially expressed genes between four conditions (Day 2 mouse, Day 4 mouse, Day 6 mouse, and Day 2 HAE). (C) Bubble plot of the top 20 canonical pathways by ascending Benjamini-Hochberg adjusted p-value from comparison analysis in Ingenuity Pathway Analysis. Dot size corresponds to –log(B-H p-value). Color corresponds to activation z-score communicating the directionality (activation or inhibition) for that pathway. Gray indicates z-score values which could not be calculated. Pathway analysis for the comparison between nsp6 mutant and wild-type virus for Day 6 infected mice whole lung samples was non-informative.

We suspect that the suppression of IFN-I signaling by ΔSGF-WA1 may delay initial host responses, allowing for the accumulation of viral RNA, eventually triggering an overpowering immune response to in an attempt to suppress the higher viral load. These data suggest that ΔSGF-WA1 may dysregulate inflammatory responses, possibly causing a deadly cytokine storm in mice and HAE cells.

4.5 DISCUSSION

Our results showed that variant mutations in nsp6 alter the virulence of SARS-CoV-2 through enhanced antagonism of STAT1 and STAT2 phosphorylation and dysregulation of inflammatory cytokines. The mechanism by which nsp6 antagonizes IFN-α pathways is currently unclear. Based on the predicted topology of SARS-CoV-2 nsp6, the 105-108 region resides in the ER lumen. It is currently unclear how ΔSGF and ΔLSG affects protein-protein interactions with components of the IFN-α signaling pathway. Shortening the lumenal loop might impact the overall structure of nsp6, leading to altered protein-protein interactions on the cytoplasmic side. Proteomics studies have identified some host interactors, but none that are related to the IFN-α signaling pathway.[44] Thus, it is important to study nsp6's interactions with specific components of the IFN-α pathway. Alternatively, viral infections can induce ER stress responses to protect cells from apoptosis and allow continued viral replication;[44,45] activated ER stress may prevent maturation and presentation of the IFN-α receptor 1 (IFNAR1).

Coronavirus nsp6 localizes almost exclusively to the ER where, in collaboration with nsp3 and nsp4, nsp6 promotes the formation of double membrane vesicles (DMVs) that protect replicative viral RNA from host sensors.[12,34–39] ΔSGF was reported to enhance nsp6-mediated ER zippering (bringing the ER membranes close together with barely visible lumen) for more efficient formation and organization of replication organelles.[12] In line with this theory, we show that mutant ΔSGF-WA1 produces higher levels of intracellular viral RNA and outcompetes the parental strain in HAE cells (Fig. 2C, 2D); however, ΔSGF-WA1 produced similar levels of secreted virus particles and viral RNA as WA1 in HAE cells (Fig. 2A, 2B). The discrepancy

between the intracellular and extracellular viral RNA levels may be caused by a negative effect of nsp6 (ΔSGF) on virus assembly and/or release.

Mice infected with ΔSGF-WA1 experienced more severe disease that resulted in earlier weight loss, a longer recovery period, and lower survival rates compared to WA1-infected mice (Fig. 2G, 2H). IPA analysis of data from the nCounter Analysis System provides evidence that more severe disease and higher mortality in ΔSGF-WA1-infected mice may be due to pathogen induced cytokine storm. Many of the pathways and upstream regulators are unaffected or even downregulated at 2 dpi but are then upregulated by 4 dpi. This may be because ΔSGF-WA1 more efficiently suppresses initial host responses thereby allowing for increased replication of viral RNA, resulting in an overwhelming upregulation of cytokine responses later. Therefore, reduced survivability in mice may be due to an imbalanced immune response.[46] Indeed, nsp6 is known to activate the NLRP3 inflammasome by suppressing acidification of lysosomes leading to pyroptosis; whether ΔSGF affects this pathway is unclear.[47,48] Furthermore, ubiquitinated nsp6 binds to transforming growth factor β-activated kinase 1 (TAK1) to activate the NF-κB signaling cascade, a major component of cytokine storms.[49] In contrast to our results, a prototype SARS-CoV-2 (with a Spike D614G mutation) bearing both BA.1 spike and nsp6 genes was attenuated.[50] Combined with our results, the collective data suggest that mutant nsp6 alone augments virulence (this study), whereas an epistatic Spike/nsp6 interaction may drive attenuation of the Omicron variant.[50]

Since the beginning of the COVID-19 pandemic, SARS-CoV-2 has continued to evolve and adapt to the human host. This study demonstrates the enhanced functions of SARS-CoV-2 nsp6 by a triple deletion ΔSGF: (i) ΔSGF reduces SARS-CoV-2 susceptibility to IFN-α treatment by improving suppression of phosphorylation of STAT1 and STAT2 in the IFN-α signaling pathway; (ii) ΔSGF improves viral fitness in primary human airway cultures, as well as increases virulence in mice, likely through increased cytokine expression, leading to cytokine storm. Our study provides another example that mutations outside of structural proteins contribute to viral

fitness and pathogenesis, underscoring a need to investigate the impact of novel mutations in emerging variants.

4.6 ACKNOWLEDGMENTS

We thank Vineet Menachery and other colleagues at the University of Texas Medical Branch (UTMB) for helpful discussions This research was supported by an award from the Sealy & Smith Foundation.

4.7 DECLARATION OF INTEREST STATEMENT

X.X. and P.-Y.S. have filed a patent on the reverse genetic system. Other authors declare no competing interests.

4.8 REFERENCES

1 Zhou P, Yang X Lou, Wang XG *et al.* A pneumonia outbreak associated with a new coronavirus of probable bat origin. *Nature* 2020; **579**: 270–273.

2 Rambaut A, Holmes EC, O'Toole Á *et al.* A dynamic nomenclature proposal for SARS-CoV-2 lineages to assist genomic epidemiology. *Nat Microbiol* 2020; **5**: 1403–1407.

3 Faria NR, Mellan TA, Whittaker C *et al.* Genomics and epidemiology of the P.1 SARS-CoV-2 lineage in Manaus, Brazil. *Science (80-)* 2021; **821**: 815–821.

4 Parums D V. Editorial: World Health Organization (WHO) Variants of Concern Lineages Under Monitoring (VOC-LUM) in Response to the Global Spread of Lineages and Sublineages of Omicron, or B.1.1.529, SARS-CoV-2. Med. Sci. Monit. 2022; **28**: e937676.

5 Walls AC, Park YJ, Tortorici MA, Wall A, McGuire AT, Veesler D. Structure, Function, and Antigenicity of the SARS-CoV-2 Spike Glycoprotein. *Cell* 2020; **181**: 281-292.e6.

6 Wang Q, Zhang Y, Wu L *et al.* Structural and Functional Basis of SARS-CoV-2 Entry by Using Human ACE2. *Cell* 2020; **181**: 894-904.e9.

7 Patel R, Kaki M, Potluri VS, Kahar P, Khanna D. A comprehensive review of SARS-CoV-2 vaccines: Pfizer, Moderna & Johnson & Johnson. Hum. Vaccines Immunother. 2022; **18**. doi:10.1080/21645515.2021.2002083.

8 Abdolmaleki G, Taheri MA, Paridehpour S *et al.* A comparison between SARS-CoV-1 and SARS-CoV2: an update on current COVID-19 vaccines. DARU, J. Pharm. Sci. 2022; **Sep**: 1–28.

9 Plante JA, Liu Y, Liu J *et al.* Spike mutation D614G alters SARS-CoV-2 fitness. *Nature* 2021; **592**: 116–121.

10 Rashid F, Dzakah EE, Wang H, Tang S. The ORF8 protein of SARS-CoV-2 induced endoplasmic reticulum stress and mediated immune evasion by antagonizing production of interferon beta. *Virus Res* 2021; **296**: 198350.

11 Colson P, Gautret P, Delerce J *et al.* The emergence spread and vanishing of a French SARS-CoV-2 variant.pdf. *J Med Virol* 2023; **95**: e28102.

12 Ricciardi S, Guarino AM, Giaquinto L *et al.* The role of NSP6 in the biogenesis of the SARS-CoV-2 replication organelle. *Nature* 2022; **606**: 761–768.

13 Lin J wen, Tang C, Wei H cheng *et al.* Genomic monitoring of SARS-CoV-2 uncovers an Nsp1 deletion variant that modulates type I interferon response. *Cell Host Microbe* 2021; **29**: 489-502.e8.

14 Laha S, Chakraborty J, Das S, Manna SK, Biswas S, Chatterjee R. Characterizations of SARS-CoV-2 mutational profile, spike protein stability and viral transmission. *Infect Genet Evol* 2020; **85**: 104445.

15 Nagy Á, Pongor S, Győrffy B. Different mutations in SARS-CoV-2 associate with severe and mild outcome. *Int J Antimicrob Agents* 2021; **57**: 106272.

16 Wang R, Chen J, Gao K, Hozumi Y, Yin C, Wei GW. Analysis of SARS-CoV-2 mutations in the United States suggests presence of four substrains and novel variants. *Commun Biol 2021 41* 2021; **4**: 1–14.

17 Ramesh S, Govindarajulu M, Parise RS *et al.* Emerging SARS-CoV-2 Variants: A Review of Its Mutations, Its Implications and Vaccine Efficacy. *Vaccines 2021, Vol 9, Page 1195* 2021; **9**: 1195.

18 Bills CJ, Xia X, Shi P-Y. The multiple roles of nsp6 in the molecular pathogenesis of SARS-CoV-2. *Press* 2023.

19 Cui J, Li F, Shi ZL. Origin and evolution of pathogenic coronaviruses. *Nat Rev Microbiol* 2019; **17**: 181–192.

20 Kim D, Lee JY, Yang JS, Kim JW, Kim VN, Chang H. The Architecture of SARS-CoV-2 Transcriptome. *Cell* 2020; **181**: 914-921.e10.

21 Xia H, Cao Z, Xie X *et al.* Evasion of Type I Interferon by SARS-CoV-2. *Cell Rep* 2020; **33**: 108234.

22 Miorin L, Kehrer T, Sanchez-Aparicio MT *et al.* SARS-CoV-2 Orf6 hijacks Nup98 to block STAT nuclear import and antagonize interferon signaling. *Proc Natl Acad Sci U S A* 2020; **117**: 28344–28354.

23 Yuen CK, Lam JY, Wong WM *et al.* SARS-CoV-2 nsp13, nsp14, nsp15 and orf6 function as potent interferon antagonists. *Emerg Microbes Infect* 2020; **9**: 1418–1428.

24 Lei X, Dong X, Ma R *et al.* Activation and evasion of type I interferon responses by SARS-CoV-2. *Nat Commun* 2020; **11**: 1–12.

25 Shemesh M, Aktepe TE, Deerain JM *et al. SARS-CoV-2 suppresses IFNβ production mediated by NSP1, 5, 6, 15, ORF6 and ORF7b but does not suppress the effects of added interferon*. 2021 doi:10.1371/journal.ppat.1009800.

26 Guo K, Barrett BS, Morrison JH *et al.* Interferon resistance of emerging SARS-CoV-2 variants. *Proc Natl Acad Sci U S A* 2022; **119**: e2203760119.

27 Liu Y, Liu J, Johnson BA *et al.* Delta spike P681R mutation enhances SARS-CoV-2 fitness over Alpha variant. *Cell Rep* 2022; **39**: 110829.

28 Xie X, Lokugamage KG, Zhang X *et al.* Engineering SARS-CoV-2 using a reverse genetic system. *Nat Protoc* 2021; **16**: 1761–1784.

29 Xie X, Muruato A, Lokugamage KG *et al.* An Infectious cDNA Clone of SARS-CoV-2. *Cell Host Microbe* 2020; **27**: 841-848.e3.

30 Xia H, Yeung J, Kalveram B *et al.* Cross-neutralization and viral fitness of SARS-CoV-2 Omicron sublineages. *Emerg Microbes Infect* 2023; **12**. doi:10.1080/22221751.2022.2161422.

31 Xia H, Luo H, Shan C *et al.* An evolutionary NS1 mutation enhances Zika virus evasion of host interferon induction. *Nat Commun* 2018; **9**. doi:10.1038/s41467-017-02816-2.

32 Gangavarapu K, Latif AA, Mullen JL *et al.* Outbreak.info genomic reports: scalable and dynamic surveillance of SARS-CoV-2 variants and mutations. *Nat Methods 2023* 2023; : 1–11.

33 Omasits U, Ahrens CH, Müller S, Wollscheid B. Protter: Interactive protein feature visualization and integration with experimental proteomic data. *Bioinformatics* 2014; **30**: 884–886.

34 Klein S, Cortese M, Winter SL *et al.* SARS-CoV-2 structure and replication characterized by in situ cryo-electron tomography. *Nat Commun* 2020; **11**: 1–10.

35 Angelini MM, Akhlaghpour M, Neuman BW, Buchmeier MJ. Severe acute respiratory syndrome coronavirus nonstructural proteins 3, 4, and 6 induce double-membrane vesicles. *MBio* 2013; **4**. doi:10.1128/mBio.00524-13.

36 Hagemeijer MC, Monastyrska I, Griffith J *et al.* Membrane rearrangements mediated by coronavirus nonstructural proteins 3 and 4. *Virology* 2014; **458**–**459**: 125–135.

37 Scutigliani EM, Kikkert M. Cytokine & Growth Factor Reviews Interaction of the innate immune system with positive-strand RNA virus replication organelles. *Cytokine Growth Factor Rev* 2017; **37**: 17–27.

38 Knoops K, Kikkert M, Van Den Worm SHE *et al.* SARS-coronavirus replication is supported by a reticulovesicular network of modified endoplasmic reticulum. *PLoS Biol* 2008; **6**: 1957–1974.

39 Cortese M, Lee J, Cerikan B, Chatel-chaix L, Schwab Y, Bartenschlager R. Integrative Imaging Reveals SARS-CoV-2-Induced Reshaping of Subcellular Morphologies. *Cell Host Microbe* 2020; **28**: 853–866.

40 Liu J, Liu Y, Shan C *et al.* Role of mutational reversions and fitness restoration in Zika virus spread to the Americas. *Nat Commun* 2021; **12**: 595.

41 Liu Y, Liu J, Plante KS *et al.* The N501Y spike substitution enhances SARS-CoV-2 infection and transmission. *Nature* 2022; **602**: 249–299.

42 Plante JA, Mitchell BM, Plante KS, Debbink K, Weaver SC, Menachery VD. The variant gambit: COVID-19's next move. Cell Host Microbe. 2021; **29**: 508–515.

43 Shan C, Xia H, Haller SL *et al.* A Zika virus envelope mutation preceding the 2015 epidemic enhances virulence and fitness for transmission. *Proc Natl Acad Sci U S A* 2020. doi:10.1073/pnas.2005722117.

44 Gordon DE, Jang GM, Bouhaddou M *et al.* A SARS-CoV-2 protein interaction map reveals targets for drug repurposing. *Nature* 2020; **583**: 459–468.

45 Echavarría-Consuegra L, Cook GM, Busnadiego I *et al. Manipulation of the unfolded protein response: A pharmacological strategy against coronavirus infection*. 2021 doi:10.1371/journal.ppat.1009644.

46 Brodin P. Immune determinants of COVID-19 disease presentation and severity. *Nat Med* 2021; **27**: 28–33.

47 Sun X, Liu Y, Huang Z *et al.* SARS-CoV-2 non-structural protein 6 triggers NLRP3-dependent pyroptosis by targeting ATP6AP1. *Cell Death Differ* 2022; **29**: 1240–1254.

48 Sun X, Yu J, Wong SH, Chan MTV, Zhang L, Wu WKK. SARS-CoV-2 targets the lysosome to mediate airway inflammatory cell death. *Autophagy* 2022; **18**: 2246–2248.

49 Nishitsuji H, Iwahori S, Ohmori M, Shimotohno K, Murata T. Ubiquitination of SARS-CoV-2 NSP6 and ORF7a Facilitates NF-κB Activation. *MBio* 2022; **13**: 1–18.

50 Chen D, Chin CV, Kenney D *et al.* Spike and nsp6 are key determinants of SARS-CoV-2 Omicron BA.1 attenuation. *Nature* 2023. doi:10.1038/s41586-023-05697-2.

4.9 SUPPLEMENTARY MATERIALS

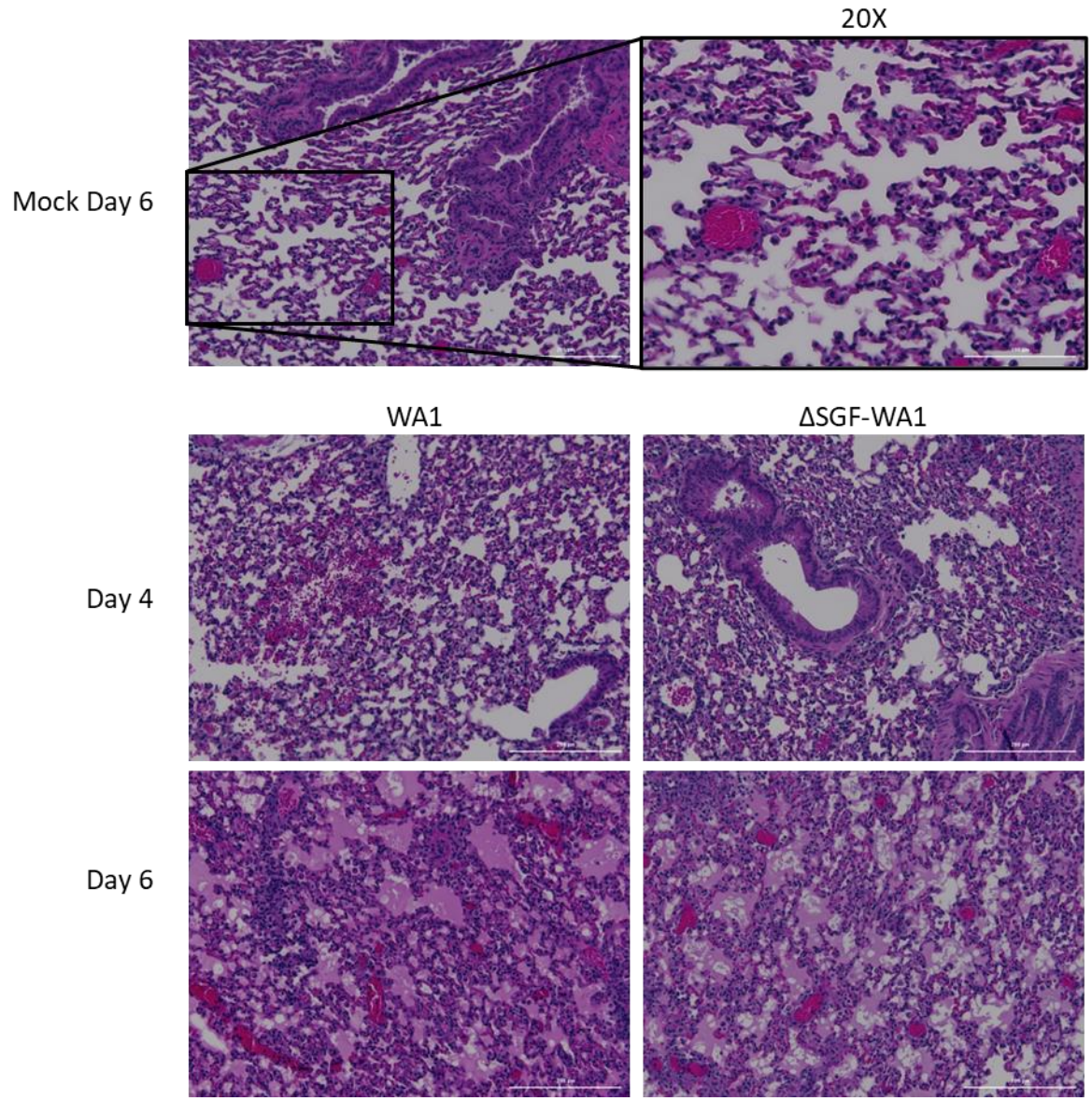

Supplementary Figure 4.1: ΔSGF-WA1 does not cause more severe pathology in mouse lung tissues

Mouse lung tissue samples stained with H&E for analysis from mock, WA1-, or ΔSGF-WA1-infected mice at 4 and 6 dpi. Slight hemorrhaging in mock samples is attributable to the method of euthanasia. By 4 dpi, both WA1 and ΔSGF-WA1 caused interstitial pneumonia, perivasculitis, peribronchiolitis, and arterial mononuclear margination. By 6 dpi, alveolar edema was common.

Supplementary Table 4.1: Primers

2019-nCoV_N2-F	(5’-TTACAAACATTGGCCGCAAA-3’)
2019-nCoV_N2-R	(5’-GCGCGACATTCCGAAGAA-3’)
HuGAPDH-F	(5’-TGTTGCCATCAATGACCCCTT-3’)
HuGAPDH-R	(5’-CTCCACGACGTACTCAGCG-3’)
Mu_GAPDH-F	(5’-AGGTCGGTGTGAACGGATTTG-3’)
Mu_GAPDH-R	(5’TGTAGACCATGTAGTTGAGGTCA-3’)
nsp6-F	(5’-ACCTTCTCTTGCCACTG-3’)
nsp6-R	(5’- AAACGAGTGTCAAGACATTCATAA -3’)

Table 4.1 – Target genes in nCounter Analysis System[c]

ABCF1	CCL26	CXCL9	HMOX1	IL27	MAP3K5	PLCG2	TANK
ACE	CCL27	CXCR1	HPGD	IL27RA	MAP3K7	PLEK	TAP1
ACKR2	CCL28	CXCR2	HPRT1	IL2RA	MAP3K8	PLEKHA1	TAP2
ACKR3	CCL3/L1/L3	CXCR3	HSD11B1	IL2RB	MAPK1	PLG	TBK1
ACKR4	CCL4/L1/L2	CXCR4	HSP90AA1	IL2RG	MAPK13	PLIN4	TBP
ACOX1	CCL5	CXCR5	HSP90AB1	IL3	MAPK14	PNOC	TBX21
ACSL1	CCL7	CXCR6	HSP90B1	IL31	MAPK8	PPIA	TBXAS1
ACSL3	CCL8	CYP2E1	ICAM3	IL31RA	MAPK9	PRCP	TCF7
ACSL4	CCNC	CYSTM1	ICOS	IL32	MAPKAPK2	PRDM1	TCIRG1
ACVR1	CCR1	DDAH2	ICOSLG	IL33	MARCKS	PRF1	TCL1A
ADAR	CCR10	DDIT3	IDO1	IL34	MARCO	PRKCA	TCN2
ADGRE5	CCR2	DDOST	IFI16	IL36A	MAVS	PRKCD	TGFB1
ADGRG3	CCR3	DDX5	IFI27	IL36B	MCL1	PRKCQ	TGFB2
ADORA2A	CCR4	DDX58	IFI35	IL36G	MDFIC	PRKCSH	TGFB3
AGT	CCR5	DEFA4	IFI44	IL36RN	MEFV	PSAP	TGFBR2
AHR	CCR6	DEFB103A/B	IFI6	IL37	MGAM	PSEN1	THBS1
AIF1	CCR7	DERL1	IFIH1	IL3RA	MIF	PSMB10	THOP1
AIM2	CCR8	DHX58	IFIT1	IL4	MKNK1	PSMB8	TIFA
AKT1	CCR9	DIABLO	IFIT2	IL4R	MLKL	PSMB9	TIGIT
AKT2	CCRL2	DNAJA2	IFIT3	IL5	MME	PSTPIP1	TIMP2
AKT3	CD14	DNAJC10	IFITM1	IL5RA	MRC1	PTGER2	TLN1
ALAS1	CD163	DTX3L	IFITM2	IL6	MRPS7	PTGER4	TLR1
ALOX12	CD19	DYSF	IFITM3	IL6R	MS4A1	PTGS2	TLR2
ALOX15	CD1E	EBI3	IFNA1/13	IL6ST	MS4A2	PTK2B	TLR3
ALOX5	CD2	EGLN1	IFNA14/16	IL7	MS4A4A	PTPN4	TLR4
ALOX5AP	CD209	EIF2AK2	IFNA2	IL7R	MS4A7	PTPN6	TLR5
ALPK1	CD22	EIF2AK3	IFNA4/7/10/17/21	IL9	MSRA	PTPRC	TLR6
ALPL	CD244	EIF3F	IFNA5	IL9R	MT2A	PXN	TLR7
ANPEP	CD247	ELANE	IFNA6	IRAK1	MTOR	PYCARD	TLR8
AP1G1	CD27	ENTPD1	IFNA8	IRAK3	MVP	RAB31	TLR9
AP1M1	CD274	EOMES	IFNAR1	IRAK4	MX1	RAB5C	TMEM140
AP1S2	CD276	EPHX2	IFNAR2	IRF1	MYC	RAB7A	TMPRSS2
APBB1IP	CD28	ERN1	IFNB1	IRF3	MYD88	RAC2	TNF
APEX1	CD36	ETS1	IFNG	IRF4	NAE1	RACK1	TNFRSF10B
APOBEC3G	CD38	EVL	IFNGR2	IRF7	NAMPT	RAF1	TNFRSF17
APOL6	CD3D	F5	IFNK	IRF9	NCF1	RASGRP1	TNFRSF18
APP	CD3E	FAM30A	IFNL1	ISG15	NCF2	RASGRP4	TNFRSF1A

[c] This table was not published with the rest of chapter 4.

ARRB2	CD3G	FAS	IFNL2/3	ITGAE	NCF4	RB1CC1	TNFRSF25
ATF2	CD4	FASLG	IFNL4	ITGAL	NCR1	RBCK1	TNFRSF4
ATF4	CD40	FBXO6	IFNLR1	ITGAM	NCR3	RBPJ	TNFRSF9
ATF6	CD40LG	FCAR	IFNW1	ITGAX	NDUFS8	REL	TNFSF10
ATG10	CD44	FCGR1A/B	IGFBP7	ITGB2	NEO1	RELA	TNFSF13B
ATG12	CD45R0	FCGR2A	IKBKB	ITGB7	NEU1	RELB	TNFSF18
ATG13	CD45RA	FCGR3A/B	IKBKE	ITK	NFAT5	RGMA	TNFSF4
ATG3	CD45RB	FCGRT	IKBKG	ITLN1	NFATC1	RHOG	TNFSF9
ATG4A	CD59	FCRL2	IL10	ITPR3	NFATC2	RIPK1	TOLLIP
ATG7	CD6	FCRL4	IL10RA	JAK1	NFATC3	RIPK2	TPP1
ATM	CD68	FGR	IL10RB	JAK2	NFATC4	RIPK3	TPSAB1/B2
ATP6AP2	CD69	FOS	IL11	JAK3	NFE2L2	RNASEL	TRAF2
ATP6V0D1	CD70	FOXO1	IL11RA	JAML	NFKB1	RNF114	TRAF3
ATP6V1B2	CD79A	FOXP3	IL12A	JUN	NFKB2	RNF135	TRAF6
BATF	CD79B	FPR1	IL12B	JUNB	NGLY1	RNF31	TRAM1
BCL2	CD80	FPR2	IL12RB1	KDM6B	NKG7	RPS6KA1	TRAT1
BCL2L1	CD81	FURIN	IL12RB2	KIR2DL1	NLRC4	RPS6KA3	TRIM21
BCL3	CD84	FYN	IL13	KIR2DL3	NLRC5	RPS6KB1	TRIM22
BCL6	CD86	GAB2	IL13RA1	KIR3DL1/2	NLRP1	RSAD2	TRIM25
BCR	CD8A	GADD45B	IL13RA2	KLRB1	NLRP3	RUNX3	TRIM33
BDKRB1	CD8B	GATA3	IL15	KLRC1	NMT1	S100A12	TRIM5
BDKRB2	CDH1	GBA	IL15RA	KLRD1	NOD2	SAMHD1	TRIM56
BECN1	CDK4	GBP1	IL16	KLRK1	NOS2	SCARB2	TRIM6
BLK	CEACAM3	GBP2	IL17A	KPNB1	NOTCH1	SDHA	TXK
BNIP3	CEBPB	GBP4	IL17B	KRAS	NOX1	SELE	TXN
BPI	CFLAR	GBP5	IL17C	LAG3	NPC2	SELENOS	TXNIP
BST2	CGAS	GCA	IL17D	LAMP1	NRAS	SELL	TYK2
C1QBP	CHUK	GK	IL17F	LAMP2	NRDE2	SEM1	TYROBP
C2	CPA3	GLA	IL17RA	LAMP3	NT5E	SERPINA1	UBA52
C3	CR1	GLB1	IL17RB	LANCL1	NTNG2	SH2D1A	UBE2L6
C3AR1	CREBBP	GNLY	IL17RC	LAT	OAS1	SIGIRR	UBE2N
C5	CRK	GNS	IL17RD	LAT2	OAS2	SIGLEC5	ULK1
C5AR1	CRP	GPX7	IL17RE	LCK	OAS3	SIRPA	ULK2
CALM1	CSF1	GSK3B	IL18	LCN2	OASL	SLC11A1	VAMP3
CAP1	CSF1R	GSTM4	IL18BP	LCP1	OAZ1	SLC2A3	VCAM1
CARD11	CSF2	GUCY1A1	IL18R1	LCP2	OS9	SMAD3	VEGFA
CARD16	CSF2RA	GUCY1B1	IL18RAP	LDHB	OSM	SMAD4	VRK3
CARD17	CSF2RB	GUSB	IL19	LEF1	P2RX7	SMAD5	VSIR
CASP1	CSF3	GZMA	IL1A	LGALS3	PAK1	SOCS1	VWF
CASP10	CSF3R	GZMB	IL1B	LIF	PANX1	SOCS3	WAS
CASP3	CTLA4	GZMH	IL1F10	LILRA3	PARP1	SOD1	WIPI1

CASP4	CTSA	HAMP	IL1R1	LILRA5	PARP9	SOD2	XAF1
CASP5	CTSG	HAVCR2	IL1R2	LILRA6	PDCD1	SORT1	XBP1
CASP8	CTSL	HCK	IL1RAP	LILRB2	PDCD1LG2	SP1	XCL1/2
CBFB	CTSS	HCST	IL1RAPL1	LIMK2	PDHB	SP100	XCR1
CBL	CTSW	HDC	IL1RAPL2	LITAF	PECAM1	SPI1	YWHAQ
CBLB	CTSZ	HERC5	IL1RL1	LRG1	PELI1	SPIB	ZAP70
CCL1	CUL1	HK3	IL1RL2	LRRK2	PELI2	SSR1	ZBP1
CCL11	CX3CL1	HLA-A	IL1RN	LTA4H	PFKFB3	STAT1	
CCL13	CX3CR1	HLA-B	IL2	LTB	PGK1	STAT2	
CCL14	CXCL1	HLA-C	IL20	LTBR	PIK3C3	STAT3	
CCL15	CXCL10	HLA-DMA	IL20RA	LTC4S	PIK3CA	STAT4	
CCL16	CXCL11	HLA-DMB	IL20RB	LTF	PIK3CB	STAT5A	
CCL17	CXCL12	HLA-DOB	IL21	LYN	PIK3CD	STAT5B	
CCL18	CXCL13	HLA-DPA1	IL21R	MAF	PIK3CG	STAT6	
CCL19	CXCL14	HLA-DPB1	IL22	MAFB	PIK3R3	STING1	
CCL20	CXCL16	HLA-DQA	IL22RA1	MAP1LC3A	PIK3R4	STK11IP	
CCL2	CXCL17	HLA-DQB1	IL22RA2	MAP2K2	PIK3R5	STRAP	
CCL21	CXCL2	HLA-DRA	IL23A	MAP2K3	PIK3R6	STT3B	
CCL22	CXCL3	HLA-DRB	IL23R	MAP2K4	PLAT	SUGT1	
CCL23	CXCL5	HLA-E	IL24	MAP2K7	PLAU	SYK	
CCL24	CXCL6	HLX	IL25	MAP3K1	PLAUR	TAB1	
CCL25	CXCL8	HMGB1	IL26	MAP3K3	PLCG1	TAB2	

Chapter 5: Investigating mechanisms of nsp6(ΔSGF)

5.1 Introduction

The results from the previous chapter leaves a number of unanswered questions. Some theories were presented in chapter 1 and in chapter 4. In this chapter, I provide further results that provide direction in regard to how nsp6(ΔSGF) affects IFN-I resistance in SARS-CoV-2. Nsp6(ΔSGF) shows enhanced antagonism of IFN-I signaling pathway by more efficiently blocking phosphorylation of STAT1 and STAT2 (Fig. 4.1)[8]. It is possible that suppression of IFN-I signaling is an indirect effect due to ER stress resulting from manipulation of the ER membrane by nsp6, as seen with SARS-CoV ORF3a[9]. Viral infection draws significant resources away from the host to promote replication. Enhanced formation of replication organelles via nsp6(ΔSGF) enhances replication of SARS-CoV-2 (Fig. 4.2); thus, it is likely that ΔSGF results in a greater allocation of host resources to viral replication, leaving numerous host proteins improperly modified or mis-folded, resulting in activation of the unfolded protein response (UPR)[4].

5.2 ΔSGF does not enhance replication of SARS-CoV-2

ΔSGF-WA1 virus appears to produce more viral RNA in Vero E6-TMPRSS2 cells and in HAE cells, in addition to augmented antagonism of IFN-I responses. As a result, nsp6(ΔSGF) might increase replication of viral RNA due to augmented formation of replication organelles in the ER[10]. To investigate this, Vero E6 cells were infected with WA1 or ΔSGF-WA1 and then treated with a bispecific anti-Spike antibody to neutralize newly produced viruses[3]. Vero E6 cells were used instead of Vero E6-TMPRSS2 cells to further discourage entry of new virus particles. Samples of cell lysates were harvested at multiple timepoints to analyze replication kinetics without new infections. Interestingly, in Vero E6-TMPRSS2 cells, ΔSGF-WA1 produced significantly less intracellular and secreted extracellular viral RNA than WA1 by 6 hours, and WA1 maintained higher levels of viral RNA throughout the experiment (Fig. 5.1A). ΔSGF-WA1

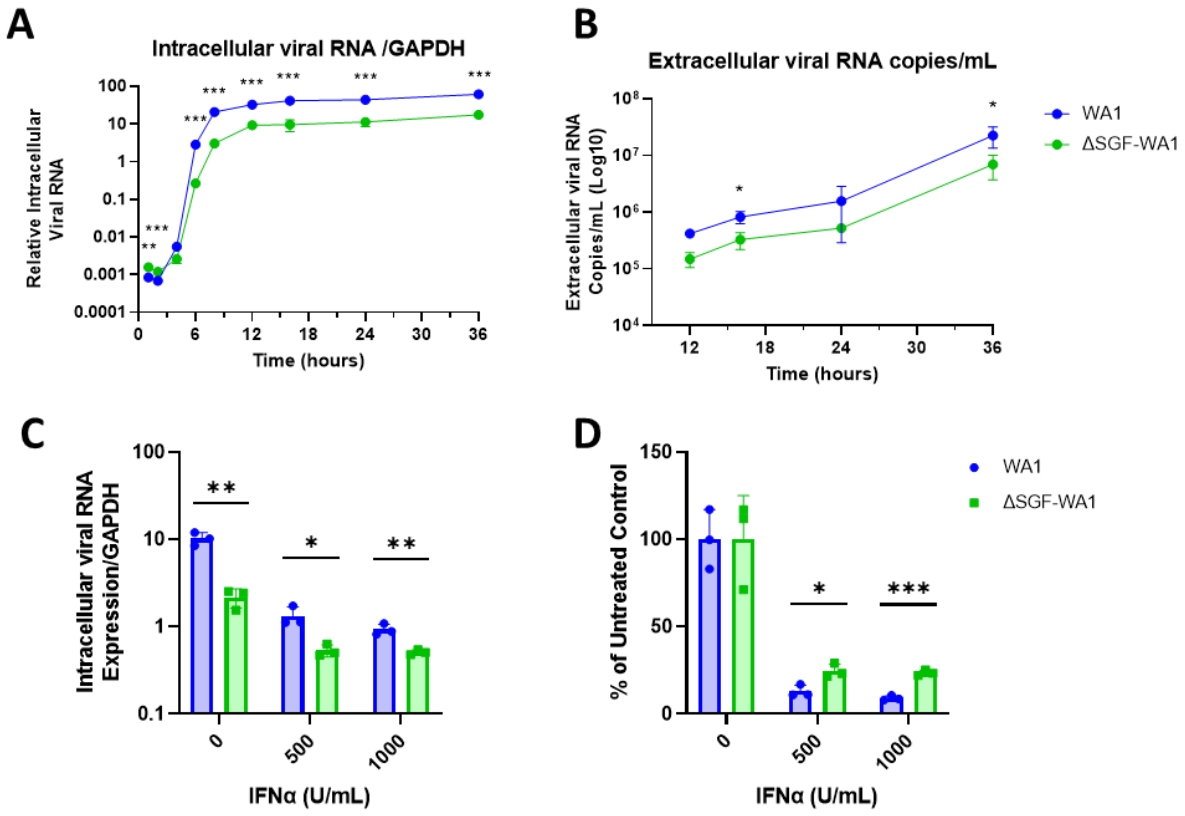

Figure 5.1 ΔSGF does not promote more effective viral RNA replication

(A) Levels of intracellular and (B) extracellular viral RNA normalized to GAPDH from Vero E6-TMPRSS2 cells infected with WA1 or ΔSGF-WA1 and treated with anti-Spike neutralizing antibodies. (C) Ratio of (A) extracellular and (B) intracellular RNA. (D) Levels of intracellular viral RNA normalized to GAPDH levels then (E) normalized to the untreated controls (0 IFN-α U/mL). Vero E6-TMPRSS2 cells were pre-treated with 2-fold dilutions of IFN-α then infected at MOI 0.02.;samples were harvested at 8 hpi. Significance for each timepoint or concentration of IFN-α was determined using Student's T-test with $p \leq 0.05$ (*), $p \leq 0.01$ (**), and $p \leq 0.001$ (***).

RNA levels could not grow to the same levels as WA1 (Fig.5.1A). These data suggest that nsp6(ΔSGF) does not improve viral replication.

We suspected that increased replication of viral RNA seen in previous experiments must be due to improved antagonism of IFN-I responses, rather than augmented formation of replication organelles[10,11]. To test this, a similar experiment was performed as in Fig. 3.4A,B, except Vero E6-TMPRSS2 cells were pretreated with IFN-α prior to infection, then treated with a cocktail of anti-Spike neutralizing antibody and IFN-α. A single timepoint was collected at 8 hpi given that the previous experiment showed that a difference between replication of WA1 and ΔSGF-WA1 was evident by 8 hpi (Fig. 5.1A,B). Cells were treated with 500 or 1000 IFN-α U/mL and normalized to untreated cells. Comparison of WA1 and ΔSGF-WA1 viral RNA normalized to GAPDH expression reveals that WA1 grew faster than ΔSGF-WA1 (Fig. 5.1C), however, after normalizing to infections without IFN-α demonstrates that ΔSGF-WA1 is indeed less susceptible to IFN-α treatment (Fig. 5.1D). Together, these data suggest that ΔSGF-WA1 replication is attenuated but remains less susceptible to IFN-α treatment.

5.3 BA.1-NSP6 IS LESS SUSCEPTIBLE TO IFN-A TREATMENT

BA.1 nsp6(ΔLSG+I189V) contains unique mutations that were demonstrated to enhance antagonism of IFN-I signaling *in vitro* (Fig. 4.1M,N). In chapter 3 and chapter 4, experiments with the infectious clone ΔSGF-WA1 demonstrate that IFN-I antagonism translated to improved viral fitness. To investigate whether the effects of BA.1 nsp6(ΔLSG+I189V) also impact viral replication, another infectious clone was constructed containing BA.1 nsp6 mutations (BA.1-nsp6). Interferon treatment experiments were then performed as in Fig. 3.3 and Fig. 4.1G-J. As expected, full-length BA.1 RNA replication was significantly suppressed by IFN-α treatment in a dose-dependent manner (Fig. 5.4A,B). BA.1-nsp6 viral RNA replication, however, was less sensitive to IFN-α treatment than WA1 (Fig. 5.4A,B). BA.1 produced significantly less virus compared to WA1, specifically, 63-fold less when treated with just 250 IFN-α U/mL (Fig.

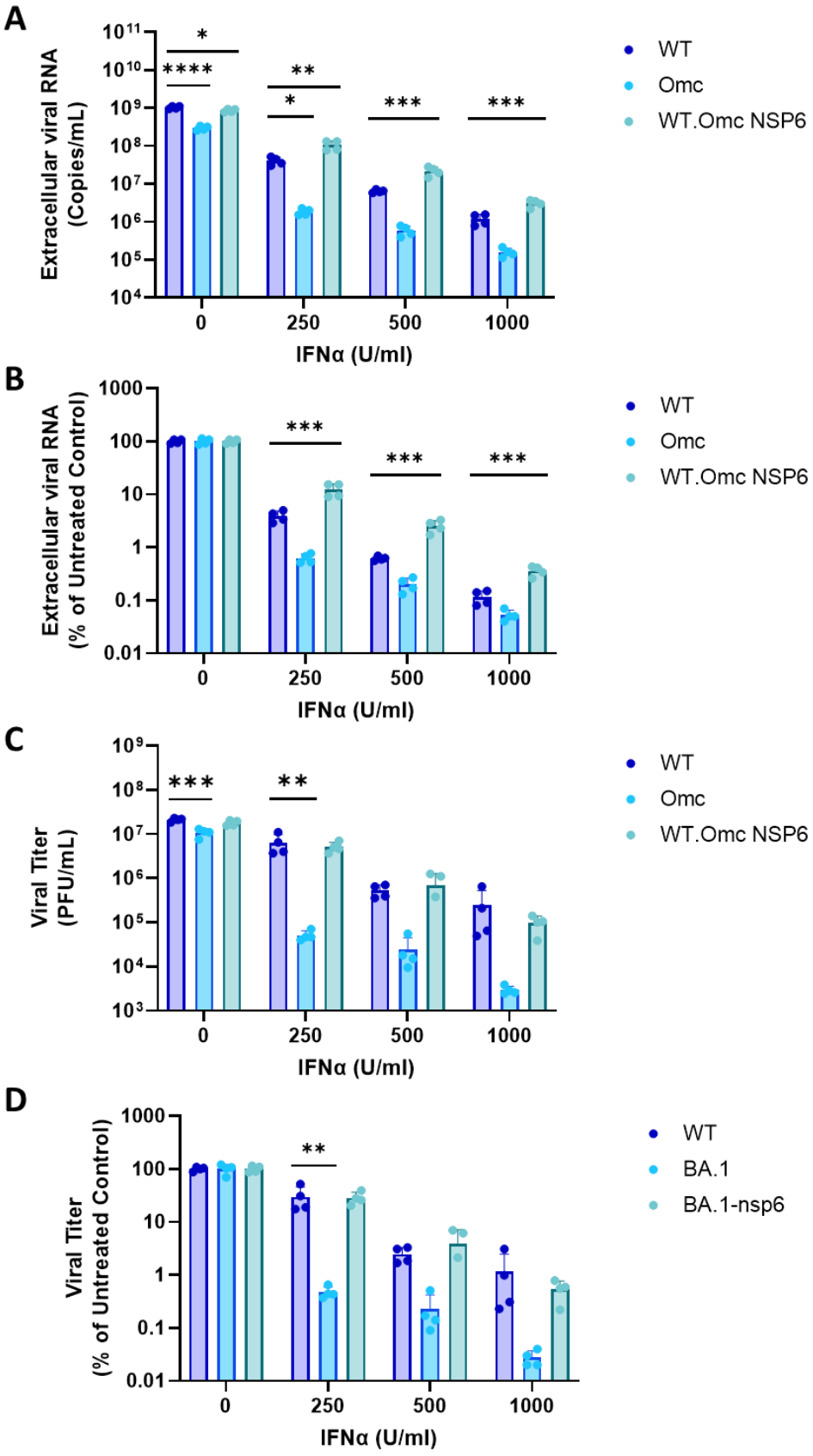
A
Extracellular viral RNA (Copies/mL)
IFNα (U/ml)
WT
Omc
WT.Omc NSP6
B
Extracellular viral RNA (% of Untreated Control)
IFNα (U/ml)
WT
Omc
WT.Omc NSP6
C
Viral Titer (PFU/mL)
IFNα (U/ml)
WT
Omc
WT.Omc NSP6
D
Viral Titer (% of Untreated Control)
IFNα (U/ml)
WT
BA.1
BA.1-nsp6

Figure 5.4 nsp6 (ΔLSG+I189V) affects SARS-CoV-2 IFN-I sensitivity

(A) Levels of extracellular viral RNA quantified by RT-qPCR using a standard curve and (B) normalized to the untreated controls (0 IFN-α U/mL). (C) Levels of infectious virus quantified by plaque assays and (D) normalized to the untreated controls. Vero E6-TMPRSS2 cells were pre-treated with 2-fold serial dilutions of IFN-α for 16-18 h then infected with SARS-CoV-2 mutants at MOI 0.02 for 1 h, whereupon the inoculum was removed and replaced with fresh dilutions of IFN-α. Significance for each concentration of IFN-α was determined using One-Way ANOVA with $p \leq 0.05$ (*), $p \leq 0.01$ (**), and $p \leq 0.001$ (***).

5.4C,D). Levels of BA.1-nsp6 infectious virus were not significantly different than WA1 (Fig. 5.4C,D). These data suggest that BA.1 nsp6(ΔLSG+I189V), similar to nsp6(ΔSGF), reduces sensitivity to IFN-α treatment to produce higher levels of viral RNA, but similar levels of infectious virus. Due to concerns over gain-of-function with the BA.1 mutations, experiments with the BA.1-nsp6 mutant virus were discontinued.

5.4 NSP6 EXPRESSION CAUSES ER STRESS BUT IS NOT ENHANCED BY MUTATIONS

Nsp6 antagonizes IFN-I signaling pathways by blocking phosphorylation of STAT1 and STAT2[6]. The ΔSGF deletion enhances nsp6-mediated antagonism of IFN-I signaling, however, the exact mechanism is unclear[8]. As discussed in chapter 1[11], it's possible that improved formation of replication organelles by nsp6(ΔSGF) results in significant ER stress and, consequently, activation of the UPR. Inositol-requiringenzyme-1α (IRE1α) acts as a sensor for ER stress. Activation of IRE1α leads to cytoplasmic splicing of (*Xbp1-u*, specifically, removal of a 26 nucleotide (nt) intron that causes a frameshift[12,13]. Spliced *Xbp1* (*Xbp1-s*) expresses a longer protein (XBP1-s) that acts as a potent transcription factor that promotes expression of the ER-associated degradation (ERAD) pathway[4]. Published experiments from chapter 4 involved C-terminal FLAG tagged nsp6 proteins, however, the addition of a FLAG tag to the C-terminus of nsp6 was shown to block formation of ER-based structures. Therefore, N-terminal FLAG tagged nsp6 plasmids were developed to test ER stress. To begin testing this hypothesis, HEK293T cells were transfected with plasmids expressing nsp6 variant proteins with either C-terminal (nsp6-FLAG) or N-terminal (FLAG-nsp6) FLAG tags. SARS-CoV-2 ORF8 accessory protein, which was shown to activate ER stress markers, was included as a positive control. After 24 h, RNA was collected and extracted for analysis of ER stress markers. Splicing of the *Xbp1* transcript was apparent in ORF8 and nsp6 transfected cells, but variant nsp6 proteins did not reveal a detectable increase in *Xbp1-s* (Fig. 5.2A,B). BIP and CHOP are activators of two additional branches of the UPR. Interestingly, expression of nsp6-FLAG resulted in little to no upregulation of *Bip* or *Chop*, however, higher levels of *Bip* and *Chop* transcripts were evident in FLAG-nsp6 transfected cells

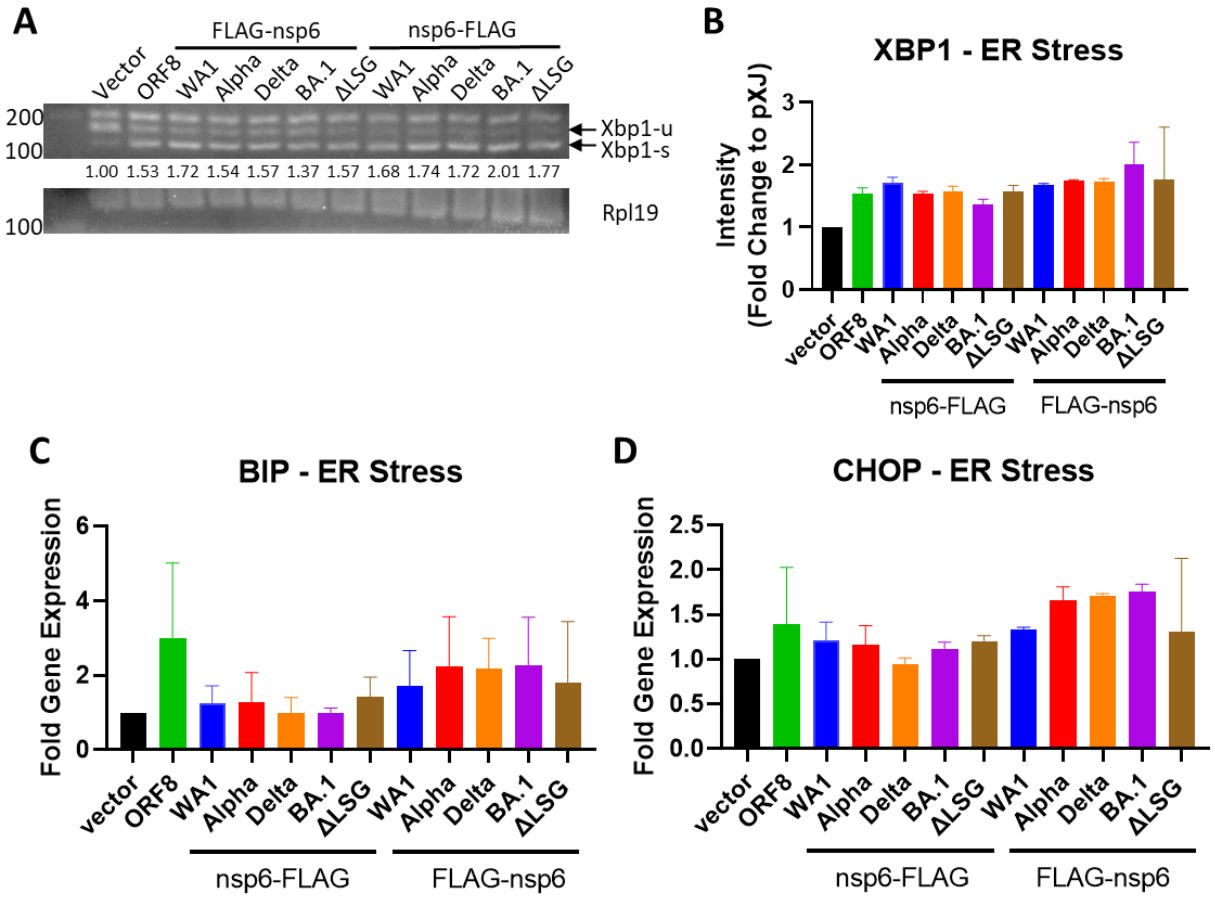

Figure 5.2 Transient expression of nsp6 leads to mild ER stress

2 ug plasmid was transfected into HEK293T and samples harvested after 24 h. (A) RT-PCR analysis showing the spliced (Xbp1-s) and unspliced (Xbp1-u) RNA and (B) quantification of band intensities presented as a ratio of Xbp1-s to the sum of Xbp1-s and Xbp1-u band intensities. The top band is thought to be a "hybrid" dimer of Xbp1-s and Xbp1-u. Molecular size markers are shown at left. (C-D) RT-qPCR analysis of (C) Bip and (D) Chop for 2 biological replicates normalized to the housekeeping gene Rpl19 then normalized to the pXJ empty vector control. Band intensities were quantified using Image Lab software.

(Fig. 5.2C,D). For each ER stress marker, there were no major differences between variant nsp6 proteins (Fig. 5.2C,D). These data suggest that nsp6 does cause ER stress and is dependent on availability of the nsp6 C-terminus, but nsp6 mutations such as ΔSGF do not cause more significant ER stress. This agrees with previous studies showing that the C-terminus is important for manipulation of ER membranes[10].

ORF3a was shown to reduce expression of IFN alpha receptor (IFNAR) by activation ER stress responses. To test whether nsp6 has a similar effect, HEK293T cells were transfected with nsp6-FLAG or FLAG-nsp6. Protein lysates were collected after 24 h for Western blot analysis. Only one biological replicate of this experiment is available for analysis at this time. All nsp6 variants reduced IFNAR levels by at least 30% (Fig. 5.3A,B). WA1 nsp6 had the least effect (30% reduction) while , surprisingly, Delta nsp6 (V149A) had the strongest effect on IFNAR levels and reduced IFNAR expression by as much as 65% (Fig. 5.3A,B). Placement of the FLAG tag did not appear to impact nsp6-mediated reduction of IFNAR. These data indicate that nsp6 does reduce IFNAR expression, but additional replicates must be performed in the future to determine statistical significance. Importantly, a luciferase assay to test inhibition of IFN-I signaling, as used in Chapter 1 (Fig. 4.2L,M), shows that the position of the FLAG tag does not affect the nsp6-mediated antagonism of IFN-I signaling (Fig. 5.4). Ultimately, this suggests that enhanced antagonism of IFN-I signaling by nsp6(ΔSGF) and nsp6(ΔLSG) is unrelated to ER stress caused by enhanced ER zippering.

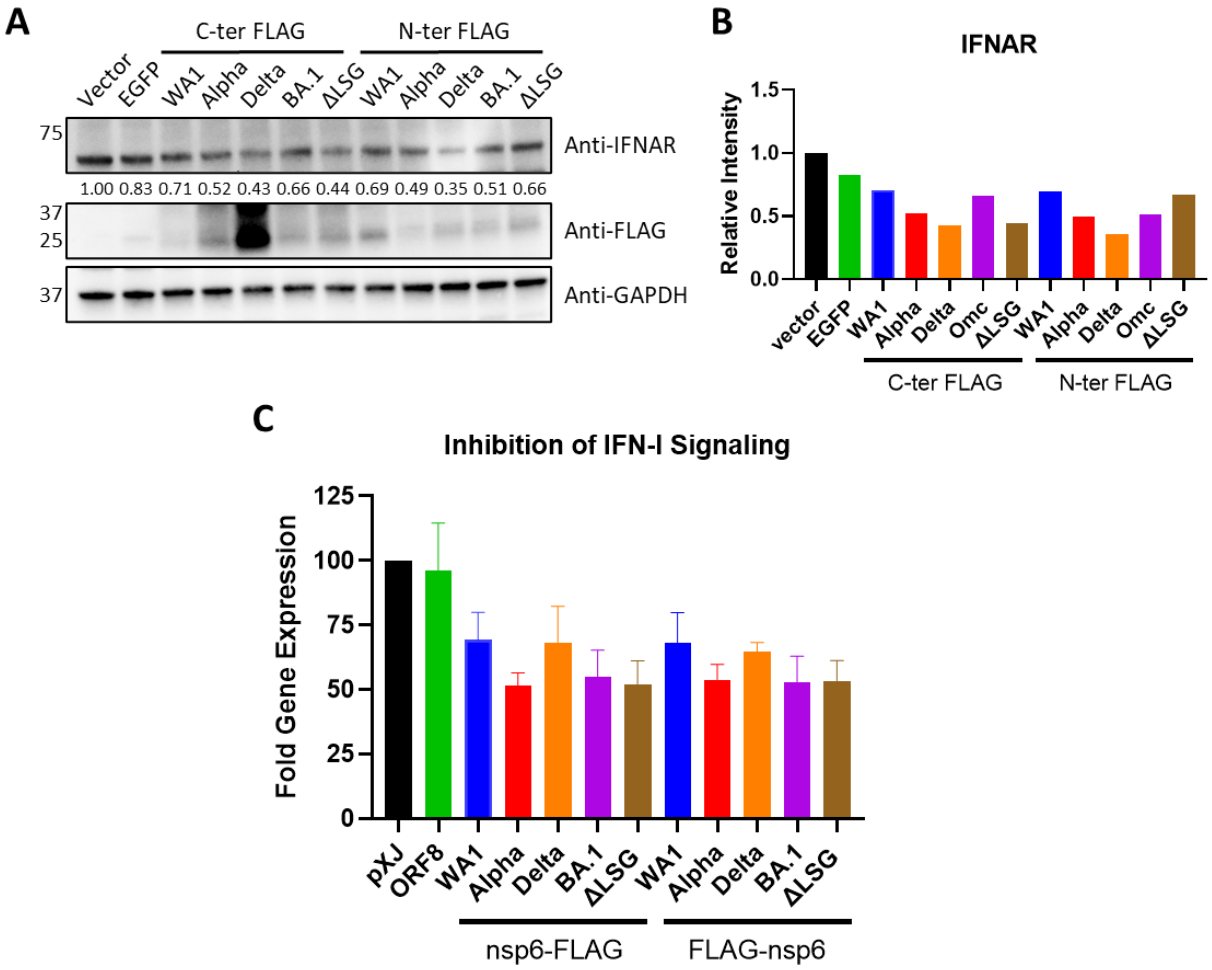

Figure 5.3 nsp6 expression reduces IFNAR expression

IFNAR expression from HEK293T cells transfected with 2 ug plasmid and harvested after 24 h. (A) Western blot showing expression levels of IFN alpha receptor (IFNAR), C-terminal (Ctr) and N-terminal (Ntr) Flag-tagged nsp6 protein, and housekeeping gene GAPDH. (B) IFNAR band intensities were normalized to GAPDH levels then normalized to the vector control. Band intensities were quantified using Image Lab software. (C) IFN-I signaling assay in HEK293T cells; specifically comparing variant nsp6 with C-terminal or N-terminal FLAG tags. Values represent measured luciferase signals from transfected cells treated with IFN-α; values are normalized to untreated cells.

Chapter 6: Discussion

The spike protein has been an important factor in viral evolution given its important role in binding cell receptors and entry into the intracellular space, but here I show that SARS-CoV-2 spike protein is not the only viral factor contributing to viral adaptation[14,15]. In summary, I demonstrated that various mutations found in the Alpha variant affect SARS-CoV-2 susceptibility to IFN-α treatment (Fig. 3.3). In particular, nsp6(ΔSGF) reduces SARS-CoV-2 sensitivity to IFN-I compared to WA1 in Vero E6-TMPRSS2 cells (Fig.3.3; Fig.4.1G-J). Alpha nsp6(ΔSGF), Omicron BA.1 nsp6(ΔLSG+I189V), and a mutant nsp6(ΔLSG), suppress phosphorylation of STAT1 and STAT2 to a greater degree compared to WA1 (Fig. 4.1M,N). Delta nsp6(V149A) which evolved without a triple deletion in the 105-108 region, also suppressed phosphorylation of STAT1 and STAT2, but the effect was minor compared to the more potent effect seen by nsp6 with a triple deletion (Fig. 4.1M,N). Additionally, all of the variant nsp6 genes repressed IFN-I induction but the effect was no greater than WA1 nsp6, suggesting that ΔSGF and ΔLSG mutations specifically influence antagonism of the IFN-I pathway (Fig. 4.1L). Importantly, ΔSGF-WA1 showed signs of greater viral fitness in primary airway cultures and produced more severe disease in mice (Fig. 4.2), possibly due to activation of a cytokine storm (Fig. 4.3). Increased levels of ΔSGF-WA1 viral RNA is not, however, the result of enhanced RNA replication, rather, it is likely the direct result of improved antagonism of IFN-I responses (Fig.5.1). Additionally, I demonstrate that like ΔSGF-WA1 (Alpha-nsp6), BA.1-nsp6 is also less susceptible to IFN-α treatment. Finally, I present additional preliminary data demonstrating that nsp6(ΔSGF) activates ER stress responses and may reduce IFNAR expression, but ER stress does not affect nsp6-mediated antagonism of IFN-I signaling pathways. Altogether these data suggest that ΔSGF and likely the ΔLSG deletions in the 105-108 region of nsp6 contribute to immune escape in the Alpha and Omicron variants and contribute to greater virulence *in vivo*.

It is important to note that significant attention has been given to studies such as the one research presented here due to concerns of gain-of-function experiments. It is important to first define what is classified as gain-of-function. A large amount of useful research has been generated from this laboratory that was based on infectious clones, many of which were based solely on the genomes of naturally present variants, and many others that contained only a portion of the mutations. The public wants to know what new mutations mean for viral pathogenicity and transmissibility. These experiments aimed to answer those questions by studying naturally occurring mutations that play a substantial role in pathogenesis of SARS-CoV-2 variants. In this case, the ΔSGF-WA1 virus was equally susceptible to IFN-α treatment as the full-length Alpha SARS-CoV-2; therefore, I do not consider this research to be a gain-of-function study, rather, it is an important investigation of the effects of a naturally occurring mutation common to past and contemporary SARS-CoV-2 variants, and that likely will occur in future variants. This type of research helps us better understand molecular pathogenesis of SARS-CoV-2 as well as provides additional understanding of future variants that acquire the same mutation.

6.1 Nsp6(ΔSGF)-mediated antagonism of IFN-I signaling

Mutations from different Alpha genes had various effects on viral replication kinetics and plaque morphologies. Surprisingly, the majority of Alpha mutations resulted in attenuation of SARS-CoV-2 replication. Alpha-N may be the exception, given that the growth curve was nearly identical to WA1, and plaque sizes were not significantly different. Importantly, Alpha-nsp6 growth curves more closely resembled the Alpha variant than WA1, suggesting that nsp6(ΔSGF) significantly impacts replication of SARS-CoV-2. Indeed, luciferase assays demonstrate that both ΔSGF and ΔLSG mutations enhance nsp6-mediated repression of IFN-I signaling, however, the exact mechanism for this effect is unclear. Antagonism of the IFN-I production pathway demonstrated a direct interaction with TBK1 to block phosphorylation of IRF3[6]; thus, direct interactions with components of the IFN-I signaling pathway are plausible. There are several ways in which nsp6 might directly block IFN-I signaling. First, (i) nsp6, as a transmembrane protein,

might interact with IFNAR to block maturation and trafficking to the plasma membrane, thus preventing reception of autocrine and paracrine signals; (ii) nsp6 might block IFNAR-mediated activation of JAK1 and TYK2; (iii) nsp6 could bind JAK1 or TYK2 to suppress the phosphorylation of STATs; or lastly (iv) nsp6 could bind directly to STAT1 and/or STAT2 to block phosphorylation or simply sequester them away kinase activators. Each possibility would achieve repression of STAT1 and STAT2 phosphorylation, as demonstrated above[8]. Future work should identify specific nsp6 interactions with components of the IFN-I signaling pathway.

The structure of the nsp6 protein remains unsolved, but predictions suggest that nsp6 has either 8 transmembrane domains, or nsp6 has six transmembrane domains and a seventh domain that is amphipathic and associates with the ER membrane rather than traversing the membrane (Fig. 1.2B-F, 2.1B)[16–18]. The N- and C-termini are predicted to reside in the cytoplasm, while the ΔSGF and ΔLSG deletions lie in an exposed lumenal loop (91-112) between transmembrane domains 3 and 4 (Fig. 1.2B-F, 2.1B). Various experiments support predictions of the 7 helix structure (Fig. 1)[10]. Not surprisingly, structural predictions using AlphaFold[16] and Protter[17] suggest that the ΔSGF and ΔLSG deletions in the long luminal loop have little impact on the nsp6 structure as a whole, but merely shorten the lumenal loop. How these deletions might enhance the repression of STAT1 and STAT2 phosphorylation is puzzling, and some critical questions remain. Does nsp6 interact directly with STAT1 and STAT2 to block phosphorylation, or is it an indirect interaction where perhaps nsp6 binds to another STAT1 and STAT2 binding partner? Do the ΔSGF and ΔLSG deletions cause significant conformational changes to the nsp6 structure that enhance protein-protein interactions? Other studies have shown that nsp6 localizes to the ER[10,19–22], but it is possible that nsp6 is transported to the plasma membrane where the lumenal loop is more accessible for STAT1 and STAT2 protein-protein interactions[23]. Additionally, it is possible that merely the deletion of two residues ΔSG (106-107), rather than three, is sufficient to increase IFN-I resistance in SARS-CoV-2. It would be interesting to investigate whether the deletion of these two amino acids alone would be sufficient to block phosphorylation of STAT1 and STAT2. The

105-108 region happens to be a consensus motif for *O*-glycosylation (LSGF). Ricciardi et al., suggest that *O*-glycosylation could form a spacer for lumenal bridges, and that ΔSGF and ΔLSG remove this spacer to augment ER zippering activity[10]. It would also be interesting to investigate whether altering the LSGF motif through point-mutagenesis, rather than deleting a portion of the motif, would still enhance antagonism IFN-I signaling. Alternatively, the deletion of three amino acids may be necessary to both shorten the long lumenal loop (91-112) and prevent *O*-glycosylation to sufficiently alter the structure and increase protein-protein interactions.

On the other hand, enhancement of nsp6 antagonism of IFN-I responses may be due to improved control over DMV formation as discussed above[10]. The IFNAR is heavily glycosylated so it is possible that extensive ER remodeling could cause ER stress that would prevent proper maturation of IFNAR in the ER/Golgi apparatus network[24–27]. Indeed, expression of mCherry-tagged nsp6 alone in HEK293T cells was highly cytotoxic, and nsp6 was similarly cytotoxic in an *in vivo Drosophila* model[22]. Cytotoxicity from nsp6 expression could interfere with IFNAR trafficking to the plasma membrane; therefore, the IFN-I signaling pathway would not be activated. Preliminary data presented in chapter 5 demonstrate an increase in ER stress markers and a slight reduction of IFNAR in nsp6-transfected HEK293T cells (Fig. 5.3, 5.4). Interestingly, the position of the FLAG tag on nsp6 affected the extent of ER stress. This is corroborated by a previous study that showed that the FLAG-tag on the C-terminus ablated formation of nsp6 compartments[10]. This did not, however, appear to impact the reduction of IFNAR in cells expressing IFNAR, suggesting that ER stress and reduction of IFNAR expression may be unrelated. Nsp6-induced ER stress is clear; however, further work is required to repeat the IFNAR experiment and determine whether reduced IFNAR levels are indeed impacted by nsp6 expression and nsp6-induced stress. Importantly, nsp6 mutations do not seem to affect the severity of ER stress, nor does ER stress seem to impact enhanced nsp6 antagonism of IFN-I signaling.

6.2 ΔSGF-WA1 AND CYTOKINE STORMS

Mice infected with ΔSGF-WA1 showed more severe signs of disease compared to WA1-infected mice and slightly higher levels of viral RNA in lung tissues (Fig. 4.2). This was to be expected given that various functions were improved by the ΔSGF deletion[8,10]. We were, however, surprised by the extent that disease worsened in mice, with just a 2.65-fold increase in viral RNA. This relatively small increase in viral RNA resulted in disease onset 1 day earlier, a disease period that was 2 days longer, and 25% reduction in survival rate. Results from the nCounter Analysis System proved insightful and demonstrated that in mice, ΔSGF-WA1 may antagonize early innate immune responses seen at day 2, resulting in upregulation of cytokine storm related pathways by day 4. (Fig. 4.2C,D).

These experiments possess some limitations. One limitation is that IFN-I responses would likely be seen by day 1 but samples were not taken until day 2, which may have been too late to see significant inhibition of IFN-I responses by ΔSGF-WA1. To effectively see differences in host responses from WA1- and ΔSGF-WA1 infected mice, future experiments may need to focus on daily observations between days 1-6. Additionally, previous papers showing a role for pyroptosis in pathology of lung epithelial cells and monocytes utilized multiplexing cytokine analysis to observe secretion of inflammatory markers in serum from mice or COVID-19 patients[28–30]. Cytokine analysis from blood and tissue samples is essential to corroborate these results and would be be a far more informative experimental technique. Furthermore, the nCounter system is an effective method for analyzing host responses by removing the reverse transcription step necessary for next-generation sequencing techniques and is limited to a specific geneset. Next-generation RNA-seq experiments may yield further insights regarding host responses.

Cases of severe COVID-19 are thought to be driven by a cytokine storm caused by hyperactivation of NF-κB signaling and the resulting overactive expression of inflammatory mediators[28–30]. Indeed, early on in the COVID-19 pandemic it was evident that SARS-CoV-2 infection was marked by a lower antiviral transcriptional state at the cellular level while higher

pro-inflammatory chemokine expression activated a stronger, more self-damaging immune response (Fig. 6.1)[31]. Sun et al. showed that SARS-CoV-2 nsp6 binds ATP6AP1, a component of

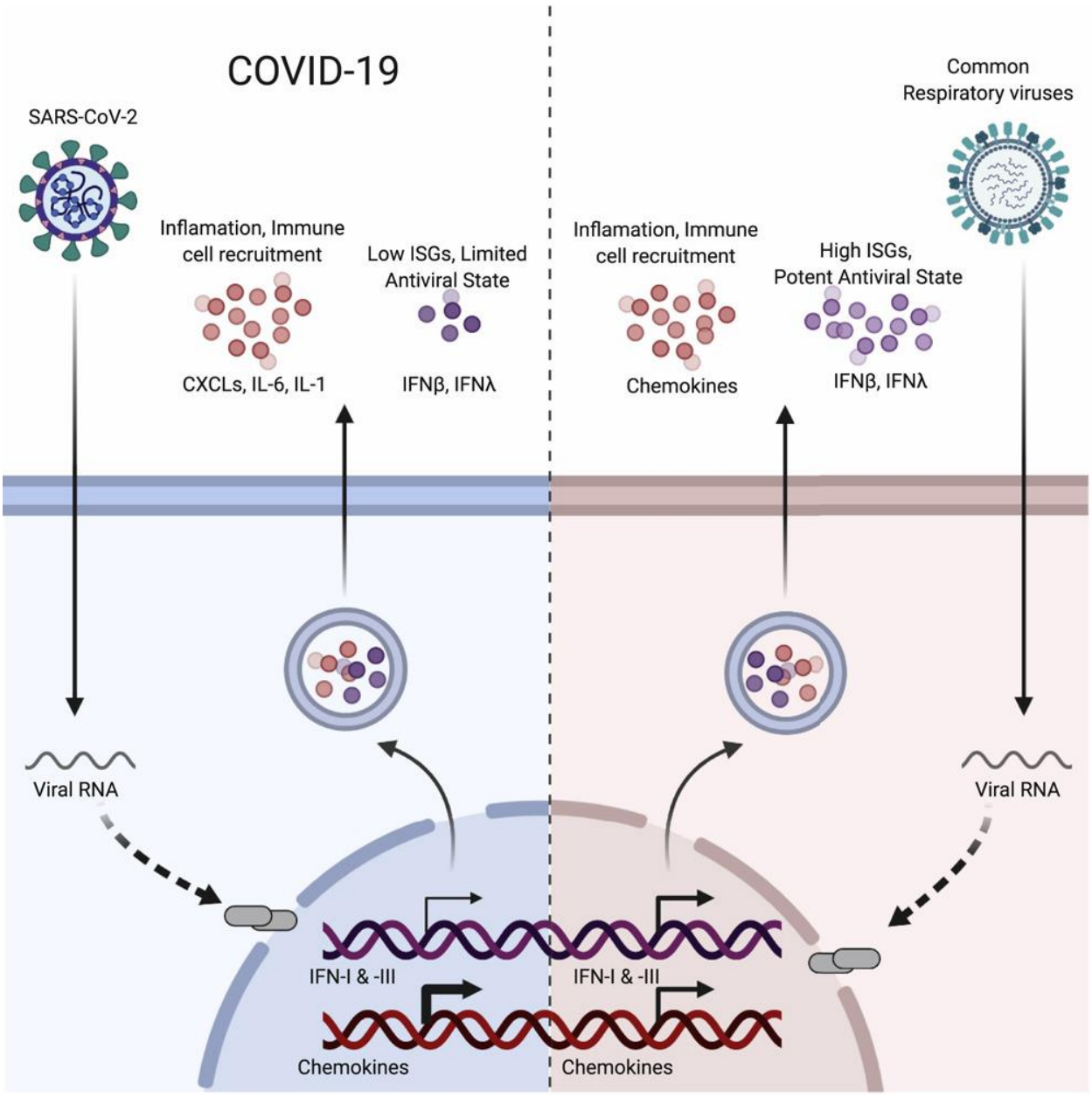

Figure 6.1 SARS-CoV-2 suppresses antiviral signals while activating pro-inflammatory signals

Typical responses to viral infection, such as influenza A virus, results in a balanced immune response of interferon expression and secretion of pro-inflammatory signals. SARS-CoV-2 suppresses IFN-I and IFN-III antiviral responses resulting in low ISG transcriptional activation, while activating robust inflammatory signals resulting in severe COVID-19. Blanco-Melo et al., 2020. Used with permission from Cell Press, MIT PRESS.

an ATPase proton pump, to block the acidification of lysosomes, which leads to the activation of NLRP3 inflammasomes and pyroptosis (Fig. 1.3)[29]. The nsp6 protein may be embedded in the lysosomal membrane where it can interact with the proton pump and prevent proteolytic activation. Whether the ΔSGF and ΔLSG deletions contribute to the inhibition of lysosomal acidification is unclear, but based on this study it seems plausible that deletions in nsp6 could be the source of higher pathogenicity in mice. The presence of ΔSGF in contemporary Omicron subvariants warrants further investigation, however, fewer patients identified as infected with Omicron subvariants are admitted for severe COVID-19 disease suggesting that ΔSGF does not increases disease severity of SARS-CoV-2[32,33]. Lower numbers of severe COVID-19 cases, however, is certainly attributable in part to the efficacy and prevalence of COVID-19 vaccines[34,35].

As part of an effort to identify genes that enhance Alpha variant resistance to IFN-I, I also developed a mutant virus consisting of the Alpha ORF3a gene in the WA1 backbone (Fig. 3.1, 3.2). Alpha ORF3a has a single amino acid change T223I that also emerged independently in Omicron BA.2, BA.4, and BA.5, which have caused epidemics in regions around the world[36–38]. Previous results from our group demonstrated that the ORF3a protein antagonizes IFN-I signaling by blocking phosphorylation of STAT1[6], although here I saw an increased sensitivity to IFN-α treatment (Fig.3.3). Future work by other members of the lab will investigate whether mutations in the ORF3a gene contribute to SARS-CoV-2 virulence.

6.3 CONCLUSION

The COVID-19 pandemic has ravaged the world and caused significant damage globally to individuals, nations, and economies[39]. The development and approval of vaccines in record time have changed the course of the pandemic, saving countless lives[40]. Waves of subvariants, however, are likely to remain a threat, as are other coronaviruses with pandemic potential [41]. Thus, it is vital to continue studying SARS-CoV-2 and other coronaviruses, especially the roles of nonstructural and accessory proteins. The nsp6 protein in particular, contributes to SARS-CoV-2 replication in a variety of ways, but several questions remain. Solving the molecular structure will provide

crucial insights into nsp6 interactions with both viral and host factors and how mutations, including ΔSGF and ΔLSG, might alter the secondary and/or tertiary structures to enhance or, in the case of L37F, hinder protein-protein interactions. Structural analyses will also improve our understanding of nsp6-mediated DMV formation and how drug candidates might inhibit interactions with nsp6. Identifying specific interacting partners will be vital to understanding nsp6 antagonism of IFN-I pathways and whether this contributes to increased virulence in mice.

Bibliography

1. Xie X, Lokugamage KG, Zhang X, et al. Engineering SARS-CoV-2 using a reverse genetic system. *Nat Protoc*. 2021;16(3):1761-1784. doi:10.1038/s41596-021-00491-8
2. Xie X, Muruato A, Lokugamage KG, et al. An Infectious cDNA Clone of SARS-CoV-2. *Cell Host Microbe*. 2020;27(5):841-848.e3. doi:10.1016/j.chom.2020.04.004
3. Ku Z, Xie X, Lin J, et al. Engineering SARS-CoV-2 specific cocktail antibodies into a bispecific format improves neutralizing potency and breadth. *Nat Commun*. 2022;13(1). doi:10.1038/s41467-022-33284-y
4. Echavarría-Consuegra L, Cook GM, Busnadiego I, et al. *Manipulation of the Unfolded Protein Response: A Pharmacological Strategy against Coronavirus Infection*. Vol 17.; 2021. doi:10.1371/journal.ppat.1009644
5. Guo K, Barrett BS, Morrison JH, et al. Interferon resistance of emerging SARS-CoV-2 variants. *Proc Natl Acad Sci U S A*. 2022;119(32):e2203760119. doi:10.1073/pnas.2203760119
6. Xia H, Cao Z, Xie X, et al. Evasion of Type I Interferon by SARS-CoV-2. *Cell Rep*. 2020;33(1):108234. doi:10.1016/j.celrep.2020.108234
7. Guo K, Barrett BS, Mickens KL, Hasenkrug KJ, Santiago ML. Interferon Resistance of Emerging SARS-CoV-2 Variants. *PLoS Biol*. Published online 2021.
8. Bills CJ, Xia H, Chen JYC, et al. Mutations in SARS-CoV-2 variant nsp6 enhance type-I interferon antagonism. *Submitted 21Feb2023*. Published online 2023.
9. Minakshi R, Padhan K, Rani M, Khan N, Ahmad F, Jameel S. The SARS coronavirus 3a protein causes endoplasmic reticulum stress and induces ligand-independent downregulation of the Type 1 interferon receptor. *PLoS One*. 2009;4(12):1-10. doi:10.1371/journal.pone.0008342
10. Ricciardi S, Guarino AM, Giaquinto L, et al. The role of NSP6 in the biogenesis of the SARS-CoV-2 replication organelle. *Nature*. 2022;606(7915):761-768. doi:10.1038/s41586-022-04835-6
11. Bills CJ, Xia X, Shi PY. The multiple roles of nsp6 in the molecular pathogenesis of SARS-CoV-2. *In Press*. Published online 2023.
12. Calfon M, Zeng H, Urano F, et al. IRE1 couples endoplasmic reticulum load to secretory capacity by processing the Xbp-1 mRNA. *Nature*. 2002;415(1):92-96.
13. Yoshida H, Matsui T, Yamamoto A, Okada T, Mori K. *XBP1 MRNA Is Induced by ATF6 and Spliced by IRE1 in Response to ER Stress to Produce a Highly Active Transcription Factor*. Vol 107.; 2001.
14. Patel R, Kaki M, Potluri VS, Kahar P, Khanna D. A comprehensive review of SARS-CoV-2 vaccines: Pfizer, Moderna & Johnson & Johnson. *Hum Vaccin Immunother*. 2022;18(1). doi:10.1080/21645515.2021.2002083
15. Abdolmaleki G, Taheri MA, Paridehpour S, et al. A comparison between SARS-CoV-1 and SARS-CoV2: an update on current COVID-19 vaccines. *DARU, Journal of Pharmaceutical Sciences*. 2022;Sep(2):1-28. doi:10.1007/s40199-022-00446-8
16. Jumper J, Evans R, Pritzel A, et al. Highly accurate protein structure prediction with AlphaFold. *Nature*. 2021;596(7873):583-589. doi:10.1038/s41586-021-03819-2

17. Omasits U, Ahrens CH, Müller S, Wollscheid B. Protter: Interactive protein feature visualization and integration with experimental proteomic data. *Bioinformatics*. 2014;30(6):884-886. doi:10.1093/bioinformatics/btt607
18. Hallgren J, Tsirigos KD, Damgaard Pedersen M, et al. DeepTMHMM predicts alpha and beta transmembrane proteins using deep neural networks. *bioRxiv*. Published online 2022:2022.04.08.487609. https://www.biorxiv.org/content/10.1101/2022.04.08.487609v1%0Ahttps://www.biorxiv.org/content/10.1101/2022.04.08.487609v1.abstract
19. Cottam EM, Maier HJ, Manifava M, et al. Coronavirus nsp6 proteins generate autophagosomes from the endoplasmic reticulum via an omegasome intermediate. *Autophagy*. 2011;7(11):1335-1347. doi:10.4161/auto.7.11.16642
20. Angelini MM, Akhlaghpour M, Neuman BW, Buchmeier MJ. Severe acute respiratory syndrome coronavirus nonstructural proteins 3, 4, and 6 induce double-membrane vesicles. *mBio*. 2013;4(4). doi:10.1128/mBio.00524-13
21. Snijder EJ, Limpens RWAL, de Wilde AH, et al. A unifying structural and functional model of the coronavirus replication organelle: Tracking down RNA synthesis. *PLoS Biol*. 2020;18(6):1-25. doi:10.1371/journal.pbio.3000715
22. Lee JG, Huang W, Lee H, van de Leemput J, Kane MA, Han Z. Characterization of SARS-CoV-2 proteins reveals Orf6 pathogenicity, subcellular localization, host interactions and attenuation by Selinexor. *Cell Biosci*. 2021;11(1):1-12. doi:10.1186/s13578-021-00568-7
23. Ramachandran K, Maity S, Muthukumar AR, et al. SARS-CoV-2 infection enhances mitochondrial PTP complex activity to perturb cardiac energetics. *iScience*. 2022;25(1):103722. doi:10.1016/j.isci.2021.103722
24. Ling LE, Zafari M, Reardon D, Brickelmeier M, Goelz SE, Benjamin CD. Human Type I Interferon Receptor, IFNAR, Is a Heavily Glycosylated 120-130 kD Membrane Protein. *Journal of Interferon and Cytokine Research*. 1995;15(1):55-61. doi:10.1089/jir.1995.15.55
25. Sommereyns C, Michiels T. N-glycosylation of murine IFN-β in a putative receptor-binding region. *Journal of Interferon and Cytokine Research*. 2006;26(6):406-413. doi:10.1089/jir.2006.26.406
26. Smirle J, Au CE, Jain M, Dejgaard K, Nilsson T, Bergeron J. Cell Biology of the Endoplasmic Reticulum and the Golgi Apparatus through Proteomics. *Cold Spring Harb Perspect Biol*. 2013;5(1):a015073. doi:10.1101/CSHPERSPECT.A015073
27. Sprooten J, Garg AD. Type I interferons and endoplasmic reticulum stress in health and disease. *Int Rev Cell Mol Biol*. 2020;350(January):63-118. doi:10.1016/bs.ircmb.2019.10.004
28. Rodrigues TS, de Sá KSG, Ishimoto AY, et al. Inflammasomes are activated in response to SARS-cov-2 infection and are associated with COVID-19 severity in patients. *Journal of Experimental Medicine*. 2020;218(3). doi:10.1084/JEM.20201707
29. Sun X, Liu Y, Huang Z, et al. SARS-CoV-2 non-structural protein 6 triggers NLRP3-dependent pyroptosis by targeting ATP6AP1. *Cell Death Differ*. 2022;29(6):1240-1254. doi:10.1038/s41418-021-00916-7
30. Junqueira C, Crespo Â, Ranjbar S, et al. FcγR-mediated SARS-CoV-2 infection of monocytes activates inflammation. *Nature*. Published online 2022. doi:10.1038/s41586-022-04702-4

31. Blanco-Melo D, Nilsson-Payant BE, Liu WC, et al. Imbalanced Host Response to SARS-CoV-2 Drives Development of COVID-19. *Cell*. 2020;181(5):1036-1045.e9. doi:10.1016/j.cell.2020.04.026
32. Wise J. Covid-19: Symptomatic infection with omicron variant is milder and shorter than with delta, study reports. *BMJ*. 2022;377:o922. doi:10.1136/bmj.o922
33. Menni C, Valdes AM, Polidori L, et al. Symptom prevalence , duration , and risk of hospital admission in individuals infected with SARS-CoV-2 during periods of omicron and delta variant dominance : a prospective observational study from the ZOE COVID Study. *The Lancet*. 2022;399:1618-1624. doi:10.1016/S0140-6736(22)00327-0
34. Baden LR, el Sahly HM, Essink B, et al. Efficacy and Safety of the mRNA-1273 SARS-CoV-2 Vaccine. *New England Journal of Medicine*. 2021;384(5):403-416. doi:10.1056/NEJMOA2035389/SUPPL_FILE/NEJMOA2035389_DATA-SHARING.PDF
35. Polack FP, Thomas SJ, Kitchin N, et al. Safety and Efficacy of the BNT162b2 mRNA Covid-19 Vaccine. *New England Journal of Medicine*. 2020;383(27):2603-2615. doi:10.1056/NEJMOA2034577/SUPPL_FILE/NEJMOA2034577_PROTOCOL.PDF
36. Cao Y, Yisimayi A, Jian F, et al. BA.2.12.1, BA.4 and BA.5 escape antibodies elicited by Omicron infection. *Nature 2022 608:7923*. 2022;608(7923):593-602. doi:10.1038/s41586-022-04980-y
37. Hachmann NP, Miller J, Collier A ris Y, et al. Neutralization Escape by SARS-CoV-2 Omicron Subvariants BA.2.12.1, BA.4, and BA.5. *New England Journal of Medicine*. 2022;387(1):86-88. doi:10.1056/NEJMC2206576/SUPPL_FILE/NEJMC2206576_DISCLOSURES.PDF
38. Qu P, Faraone J, Evans JP, et al. Neutralization of the SARS-CoV-2 Omicron BA.4/5 and BA.2.12.1 Subvariants. *New England Journal of Medicine*. 2022;386(26):2526-2528. doi:10.1056/NEJMC2206725/SUPPL_FILE/NEJMC2206725_DISCLOSURES.PDF
39. Collaborators C 19 EM. Estimating excess mortality due to the COVID-19 pandemic: a systematic analysis of COVID-19-related mortality, 2020-21. *Lancet*. 2022;399(10334):1513-1536. doi:10.1016/S0140-6736(21)02796-3
40. Watson OJ, Barnsley G, Toor J, Hogan AB, Winskill P, Ghani AC. Global impact of the first year of COVID-19 vaccination: a mathematical modelling study. *Lancet Infect Dis*. 2022;22(9):1293-1302. doi:10.1016/S1473-3099(22)00320-6
41. Gralinski LE, Menachery VD. Return of the Coronavirus: 2019-nCoV. *Viruses*. 2020;12(135).

Vita

Cody Jay Bills

BIOGRAPHICAL

Date of Birth: April 28, 1993	Place of Birth: Murray, UT, USA
Mother: Trina Ericksen Bills	Father: Kevin lee Bills

EDUCATION

Doctor of Philosophy (Ph.D.); Biomedical Science
University of Texas, Medical Branch, Galveston, TX
- Currently enrolled; graduating May 2023
- GPA 3.73

Bachelor of Science in Cellular & Molecular Biology & Chemistry Minor
Utah State University, Logan UT
- Graduated September 2017

PUBLICATIONS

Bills, Cody J., John Yun-Chung Chen, Xuping Xie, Hongjie Xia, Pei-Yong Shi. "Mutations in SARS-CoV-2 Variant nsp6 Enhance Type-I Interferon Antagonism." Accepted 26Apr2023 to *Emerging Microbes and Infections*.

Bills, Cody, Xuping Xie, and Pei-Yong Shi. 2023. "The Multiple Roles of Nsp6 in the Molecular Pathogenesis of SARS-CoV-2." Antiviral Research 213 (May): 105590. https://doi.org/10.1016/J.ANTIVIRAL.2023.105590.

Xia, H., Yeung, J., Kalveram, B., Bills, C. J., Chen, J. Y. C., Kurhade, C., Zou, J., Widen, S. G., Mann, B. R., Kondor, R., Davis, C. T., Zhou, B., Wentworth, D. E., Xie, X., &; Shi, P. Y. (2023). Cross-neutralization and viral fitness of SARS-CoV-2 Omicron sublineages. Emerging Microbes and Infections, 12(1).

WORK and RESEARCH EXPERIENCE

Graduate Assistant
University of Texas, Medical Branch, Galveston TX
Mariano Garcia-Blanco Laboratory:
June 2019 – May 2021
- Studied human host factors involved in flavivirus replication
- Learned to ask effective research questions and write compelling research proposals

Pei-yong Shi Laboratory:
May, 2021 – Current

- Worked collaboratively to investigate interference of innate immunity by SARS-CoV-2
- Planned, prioritized, and managed multiple projects while maintaining detailed records of ongoing experiments

Laboratory Technician
Institute for Antiviral Research at Utah State University, Logan UT
April 2016 – July 2018
- Reliably conducted NIH funded testing in a timely manner for independently developed compounds against a variety of viruses in BSL2 and BSL3 settings

Undergraduate Student Research Assistant
Carol von Dohlen Laboratory at Utah State University, Logan UT
October 2014 – September 2017
- Worked in a lab to learn basic skills to build and annotate the genome for bacterial endosymbionts of adelgids
- Developed and independently pursued my own research project
- Presented my research at multiple local and national research conferences

Sales Representative
Vantage Marketing, Westborough, MA
May 2015 – August 2015
- Worked independently across Massachusetts selling pest control contracts door-to-door for Insight Pest Solutions
- Learned sales strategies to approach potential customers and match company services to customer needs, ultimately selling 97 contracts in my first summer with the company

AWARDS

- Mclaughlin Fellowship award
- Undergraduate Researcher of the Year, USU Department of Biology
- USU Dean's List
- Lillywhite Presidential Scholar
- Aggie Scholar Academic Scholarship for Academic Excellence
- Undergraduate Research and Creative Opportunities grant from USU
- Mini-grant from USU College of Science

SERVICE AND SKILLS

- Member of USU Science Council
- Mentor for Biotechnology Academy at USU
- Treasurer for Biochemistry Student Organization at UTMB
- Bishop for the Church of Jesus Christ of Latter-day Saints
  Galveston, TX; Jan 2020-Nov 2022
  - Responsibilities include finance management, managing welfare efforts, leadership training, teaching, regular public speaking, counseling individuals, and overseeing the youth program
- Served a 2-year religious mission in Santiago, Chile; 2012-2014
- Participated in a 4-week service-learning trip to Peru
  - Learned about fair trade business practices to enable crop producers
  - Taught and enabled youth in isolated disadvantaged communities

- Fluent in Spanish
- Familiar with Word, Excel, and PowerPoint
- Eagle Scout, Order of the Arrow

Permanent address: 710 Ferry Rd, Apt 208, Galveston, TX, USA, 77550

Email: cjbills@utmb.edu; codyjaybills@gmail.com

This thesis was typed by Cody Jay Bills.